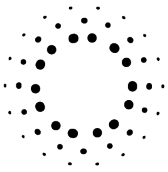

IFT - UNESP
INSTITUTO DE FÍSICA TEÓRICA

DISSERTAÇÃO DE MESTRADO IFT–D.009/24

Thermalization Dynamics of the Quark Condensate Under Strong Magnetic Fields

Arthur Almeida Frazon

Orientador

Prof. Dr. Gastão Inácio Krein

October 8, 2024

Frazon, Arthur Almeida
F848t Thermalization dynamics of the quark condensate under strong magnetic fields / Arthur Almeida Frazon. – São Paulo, 2024
120 f. : il. color.

Dissertação (mestrado) – Universidade Estadual Paulista (Unesp), Instituto de Física Teórica (IFT), São Paulo
Orientador: Gastão Inácio Krein

1. Cromodinâmica quântica. 2. Partículas (Física nuclear) - Quiralidade. 3. Transformações de fase – Física estatística. I. Título

Sistema de geração automática de fichas catalográficas da Unesp. Biblioteca do Instituto de Física Teórica (IFT), São Paulo. Dados fornecidos pelo autor(a).

THERMALIZATION DYNAMICS OF THE QUARK CONDENSATE UNDER STRONG MAGNETIC FIELDS

Dissertação de mestrado apresentada ao Instituto de Física Teórica do Câmpus de São Paulo, da Universidade Estadual Paulista "Júlio de Mesquita Filho", como parte dos requisitos para obtenção do título Mestre em Ciências, área de Física.

Comissão Examinadora:

Prof. Dr. GASTÃO INÁCIO KREIN (Orientador)
Instituto de Física Teórica/UNESP

Prof. Dr. RUDNEI DE OLIVEIRA RAMOS
Universidade Estadual do Rio de Janeiro/UERJ

Prof. Dr. RICARDO LUCIANO SONEGO FARIAS
Universidade Federal de Santa Maria/UFSM

Conceito: Aprovado

São Paulo, 13 de setembro de 2024.

O mundo tem mil coisas invisíveis
Nada é só concreto assim

- Tim Bernardes

Agradecimentos

Esta tese foi escrita graças a muitas pessoas e a 8 patas. As 8 patas são da Frida, um *Calico cat* e do Frevo, um gato rajado. Cada pessoa e gato doaram um pouquinho de forma única e especial para que este trabalho fosse concluído.

Uma vez que escrevemos "gostaria de agradecer primeiramente a..." estamos comparando contribuições igualmente importantes em aspectos diferentes, portanto, cada agradecimento não é ordem de importância, mas sim em ordem de inspiração no momento da escrita.

Inicialmente, agradeço ao CNPq pelo financiamento dos meus estudos e ao IFT-UNESP pela estrutura acadêmica que me fora ofertada durantes estes 2 anos de Mestrado.

Agradeço ao Professor Gastão Krein primeiramente por ter acreditado em mim e, segundamente, pelos inúmeros momentos de discussão, conselhos, de programação e de escrita deste texto que foram, e estão sendo fundamentais para o desenvolvimento deste trabalho e para o meu desenvolvimento como pesquisador. Também gostaria de agradecer imensamente pelas cartas de recomendação enviadas.

Aos meus muitos colegas de grupo de pesquisa também agradeço pela troca de experiências e pelos socorros nos (muitos) pedidos de ajuda que precisei, em especial, Professora Ana Mizher (muito obrigado pelas cartas de recomendação), David Rosa (muito obrigado pelas cartas de recomendação), João Caetano e a Isabela Maietto.

Gostaria também de agradecer a Letícia por muitas coisas: por estar sempre do meu lado na nossa caminhada, pelas nossas conversas sobre absolutamente tudo e por fim, por aguentar - bravamente - me escutar falando sobre quarks, gluons e outras coisas com nomes super divertidos. A recíproca não é verdadeira dado que conversar sobre Terry Eagleton, Fredric Jameson e Raymond Williams nos proporcionam longos momentos de conversa.

Também gostaria de agradecer ao seu Aroldo e a dona Marlene por estarem junto comigo desde 1995 -e eu com eles- nos incontáveis momentos bons e nos contáveis momentos ruins. Também gostaria de agradecer ao Joãozinho, meu irmão mais alto que eu, que veio ao mundo em 2010 num dia de um milagroso França 1 x 2 África do Sul.

Falando em futebol, gostaria de encerrar os agradecimentos citando um dos maiores treinadores de futebol de todos os tempos, Arrigo Sachi, que uma vez disse: *"O futebol é a coisa mais importante dentre as coisas menos importantes"*. De fato, não posso deixar de agradecer ao Corinthians pelos momentos bons (e de stress) que me proporcionou durante a escrita dessa dissertação.

"A poet once said, "The whole universe is in a glass of wine." We will probably never know in what sense he meant that, for poets do not write to be understood. But it is true that if we look at a glass of wine closely enough we see the entire universe. There are the things of physics: the twisting liquid which evaporates depending on the wind and weather, the reflections in the glass, and our imagination adds the atoms. The glass is a distillation of the earth's rocks, and in its composition we see the secrets of the universe's age, and the evolution of stars. What strange array of chemicals are in the wine? How did they come to be? There are the ferments, the enzymes, the substrates, and the products. There in wine is found the great generalization: all life is fermentation. Nobody can discover the chemistry of wine without discovering, as did Louis Pasteur, the cause of much disease. How vivid is the claret, pressing its existence into the consciousness that watches it! If our small minds, for some convenience, divide this glass of wine, this universe, into parts—physics, biology, geology, astronomy, psychology, and so on—remember that nature does not know it! So let us put it all back together, not forgetting ultimately what it is for. Let it give us one more final pleasure: drink it and forget it all!"

Richard P. Feynman

Resumo

Campos magnéticos fortes afetam propriedades da cromodinâmica quântica (QCD) em muitas situações, como no universo primitivo, magnetares e colisões de íons pesados. Uma propriedade da QCD afetada por campos magnéticos fortes é o condensado de quarks quiral, um parâmetro de ordem aproximado da transição da QCD entre uma fase quark-glúon a altas temperaturas e uma fase hadrônica a baixas temperaturas. Nesta dissertação, estudamos numericamente a dinâmica de termalização do condensado de quarks usando uma equação de campo de Langevin derivada por Krein e Miller em Symmetry 13, 551 (2021). O condensado é representado pelo campo escalar-isoescalar do modelo sigma linear com quarks. Usando o formalismo "closed-time path" da teoria quântica de campos de não-equilíbrio, a equação de campo de Langevin é obtida integrando os quarks em uma aproximação de campo médio. Resolvemos numericamente essa equação de Langevin dentro de um cenário de quench de temperatura, em que a temperatura do sistema muda repentinamente de uma temperatura alta, na qual o valor do condensado é muito pequeno, para temperaturas baixas para as ele é diferente de zero. Mostramos que as soluções apresentam um crescimento inicial explosivo e depois oscilações amortecidas em direção a um valor de equilíbrio. O amortecimento é determinado por um coeficiente de dissipação devido ao decaimento do condensado em pares de quark-antiquark. O campo magnético tem um efeito dramático no coeficiente de dissipação, produzindo um cenário de termalização consideravelmente diferente da termalização na ausência do campo.

Palavras Chaves: Cromodinâmica Quântica (QCD); Simetria Quiral; Condensado de Quarks; Transições de Fase na QCD; Campos Magnéticos na QCD.

Áreas do conhecimento: Física de Partículas e Campos; Física Nuclear

Abstract

Strong magnetic fields affect quantum chromodynamics (QCD) properties in many situations, such as the early universe, magnetars, and heavy-ion collisions. A QCD property affected by strong magnetic fields is the chiral quark condensate, an approximate order parameter of the QCD transition between a high-temperature quark-gluon phase and a low-temperature hadronic phase. In this dissertation, we studied numerically the thermalization dynamics of the quark condensate using a Langevin field equation derived by Krein and Miller in Symmetry 13, 551 (2021). The condensate is represented by the scalar-isoscalar field of the linear sigma model with quarks. Using the closed-time path formalism of nonequilibrium quantum field theory, the Langevin field equation is obtained by integrating out the quarks in a mean-field approximation. We solved numerically this equation within a quench scenario, in that the temperature of the system suddenly changes from a high temperature, at which the vaue of the condensate is very small, to low temperatures for which its value is nonzero. We showed that the solutions display an explosive initial growth and then damped oscillations toward an equilibrium value. The damping is determined by a dissipation coefficient that is due to the decay of the condensate into quark-antiquark pairs. The magnetic field has a dramatic effect on the dissipation coefficient, producing a considerably different thermalization scenario than thermalization in the absence of the field.

Keywords: Quantum Chromodynamics (QCD); Chiral Symmetry; Quark Condensate; QCD Phase Transitions; Magnetic Fields in QCD.

Knowledge Area: Physics of Particles and Fields; Nuclear Physics.

Contents

1 Introduction **1**

2 QCD Symmetries and Linear Sigma Model **5**

2.1 Introductory Aspects of QCD 5

2.2 Λ_{QCD} and Quark Masses 7

2.3 Chiral Symmetry in QCD 10

2.3.1 Spontaneous Symmetry Breaking 12

2.3.2 Continuous Symmetries and Goldstone Bosons 15

2.3.3 Fermions: Axial and Vector Transformations 18

2.4 Linear-Sigma Model 22

2.4.1 Model Construction 22

2.4.2 Explicit Breaking of Chiral Symmetry 28

2.5 The Quark Condensate as an Order Parameter 31

3 Phases Transitions and Stochastic Models **34**

3.1 Phase Transitions and Order Parameters 34

3.2 Ginzburg-Landau Theory 41

3.2.1 Mean-Field Theory 41

3.2.2 Landau Theory 42

3.2.3 Phenomenological Langevin Equation 46

4 Non-Equilibrium Quantum Mechanics **50**

4.1 Closed-Time Path Formalism 51

4.2 Influence Functional Formalism 58

4.3 The Linear Bath Model 62

4.4 Microscopic Langevin Equation 67

5 Quark Condensate Dynamics under Magnetic Fields **72**

5.1 Mean-Field Langevin Equation for the Quark Condensate 73

5.2 Relativistic Heavy-Ion Collisions 79

6 Numerical Results **83**

6.1 Discretization of the Stochastic GLL Equation 83

6.2 Numerical Results 86
6.2.1 Dissipation Coefficient, Sigma, and Quark Masses. 86
6.2.2 Time Evolution of Chiral Quark Condensate 88
6.2.3 Late-time Behavior 97

7 Conclusions and Future Prospects **101**

A Quantum Mechanics and Path Integrals **103**
A.1 Quantum Mechanics Elements 103
A.2 Path Integrals in Quantum Mechanics 106

B Partially Conserved Axial Current **112**

Bibliography **114**

Chapter 1

Introduction

In nature, one may find many examples of systems that are subject to the presence of a magnetic field. In the macroscopic scale of the universe, neutron stars and magnetars carry significantly large magnetic fields, for instance. It is possible that primal magnetic fields, such as those generated during the Big Bang, have survived until today, albeit with much weaker strengths. Furthermore, many relevant processes that occurred in the early universe, such as the QCD phase transition that gave the origin to the proton and neutrons, which make up most of the visible matter in the universe, were affected by the presence of these fields [1]. This phase transition occurred 10^{-5} seconds after the Big Bang at temperatures of around 10^{12} K. A similar transition may also occur in the core of neutron stars and magnetars [1], which contains QCD matter at very large densities but close to zero temperature. Nowadays, it is possible to reproduce the existing conditions in the early universe in laboratory conditions through collisions of two heavy ions accelerated to energies of several hundreds of GeV.

Noncentral heavy-ion collisions produce magnetic fields [2] that are, possibly, the highest ever produced in the universe, reaching values as high as $B \approx 10^{19}$ G ($eB \approx 6m_{\pi}^2$) for collisions at the Relativistic Heavy-Ion Collider (RHIC), and even higher at the Large Hadron Collider (LHC), where noncentral Pb-Pb collisions are predicted to produce fields of strengths as large as $eB = 15m_{\pi}^2$ [3, 4, 5, 6]. Such field strengths are of the order of the QCD intrinsic scale $\Lambda_{\rm QCD} \simeq 300$ MeV, the scale at which QCD becomes a strongly-coupled theory, and as such can be expected to interfere with QCD phenomena. Such an expectation was confirmed by lattice QCD simulations some time ago—references [7] are reviews on the subject and provide extensive lists of references. Most notably, strong magnetic fields affect QCD phenomena associated with the approximate chiral symmetry in the light-quark sector, in particular on the chiral condensate, which is an approximate order parameter for the QCD transition from a high-temperature quark-gluon phase (QGP) and a low-temperature hadronic phase.

The QGP is a high-temperature state of matter comprised of deconfined quarks

and gluons. It existed in the early universe and is produced in heavy-ion collisions at very high energies. In a heavy-ion experiment, the QGP lasts less than 10^{-23} seconds before it hadronizes into more than 5000 particles (in the case of Au+Au at 200 GeV) which arrive in the detectors and can be measured and analyzed [8, 9]. One of the major objectives of the experiments is to understand this QGP to hadronic transition. Theoretically, the transition from a high-temperature QGP phase to a hadron-dominant one is not a usual phase transition, but a crossover [10], in that the (approximate) order parameters characterizing the transition change smoothly as a function of the temperature. One of the order parameters characterizing the QGP-hadron transition is the chiral condensate $\langle \bar{q}q \rangle$, in which $q = (u, d)$. In the hypothetical limit that the u and d quarks are taken massless, chiral symmetry is spontaneously broken for temperatures below a critical temperature resulting in a nonzero value for the condensate while it vanishes at high temperatures. The u and d quarks are not massless and as such chiral symmetry is only an approximate symmetry at the hadron scale and the chiral condensate in only an approximate order parameter. Lattice simulations have shown the chiral condensate is nearly zero in the QGP phase, and nonzero in the hadronic phase, with a rapid change around the temperature $T_{\rm pc} \simeq 150$ MeV [10]; $T_{\rm pc}$ is known as the pseudo-critical temperature. Understanding such a rapid change in the value of the condensate will lead us to understand how precisely hadrons, protons, and neutrons in particular, are formed and why they have the masses they have given that the quarks and gluons comprising them are almost massless [11, 12].

The magnetic fields produced in peripheral heavy-ion collisions are produced at the early stages of the collision and may dissipate very fast as the QGP evolves in time [4, 5] but while it evolves, it might generate electric currents intense enough to produce feedback fields that can be sustained in time with considerable strength until the system breaks into hadrons [13, 14, 15]. The real experimental situation is very a complex one and a definite conclusion has not yet been achieved regarding the lifetime and strength of magnetic fields in the QGP time evolution. To study the problem theoretically involves a complex many-body problem that we are far from being able to tackle. While one does not have such a capability, one can abstract from some of the complicated aspects of the problem and concentrate on some features involving either static or dynamical effects magnetic fields might have on QCD properties, like on the quark condensate and hadron spectrum. The insight gained in such studies will be useful in more thorough studies of the full, complex problem. Most of the vast literature on the subject concerns static properties. To

the best of our knowledge, reference [16] was the first one that took the challenge of studying the effects of a magnetic field on the time evolution of the quark condensate. Specifically, reference [16] investigated how the dynamics, i.e. the time evolution, of quark condensate, $\langle\bar{q}q\rangle$ is affected by the presence of a constant, strong magnetic field. That reference addressed the condensate dynamics by deriving a mean-field Langevin equation from a one-loop effective action defined by the linear sigma model [17] with quarks (LSMq) [18]. In the LSMq, the condensate is modeled by a scalar-isoscalar field σ. The model also includes pseudoscalar-isovector $\boldsymbol{\pi}$ field representing the pseudo-Goldstone bosons of the spontaneous chiral symmetry breaking. It also includes spin-1/2 fermion fields representing the u and d constituent quarks which become massive due to the spontaneous symmetry breaking. The authors in [16] used the closed time path formalism of nonequilibrium quantum field theory to obtain the Langevin equation using a coarse-grained procedure that consisted of integrating out the quarks from the effective action. They based their study on earlier ones not related to magnetic fields but using the same procedure [19, 20, 21]. The Langevin equation derived in [16] contains damping and noise terms reflecting condensate's interactions with a magnetized quark background in local thermal equilibrium. The authors of that reference studied the impact of the magnetic field change of the dissipation coefficient on the short-time dynamics in a quench scenario, i.e. in a scenario that the system's temperature changes suddenly from a high value to a lower value. In this dissertation, we give continuity to that initial study.

Specifically, in this dissertation we study the condensate (σ-field) dynamics by solving numerically the Langevin field equation over a large time interval. In a high-to-low temperature quench scenario, the condensate evolves from an initial value close to zero until it reaches a new equilibrium value. For short times $t \gtrsim 0$, when σ is small, the Langevin equation can be linearized and solved analytically [16], but for $t \gg 0$, it cannot be linearized and then a full numerical simulation is required. Our original contribution is to set up an algorithm to solve numerically the Langevin equation and discuss the impact of a strong magnetic field on the thermalization of the condensate. Specifically, we have set up an algorithm to discretize the Langevin equation in time and space. Discrete-time evolution is based on a leapfrog algorithm and the discretization of spatial derivatives is based on finite-differences. Although we build on the references [22, 23] to construct the algorithm, our code was written from scratch and all results are original.

This work is organized as follows. We start in Chapter 2 with material related to some aspects of QCD relevant to this dissertation. We review some general aspects

of the theory, giving special attention to a discussion of the quark masses. In the sequence, we explore the chiral symmetry in QCD; this will allow us to introduce the effective model on which we will rely our studies, the linear sigma model with quarks (LSMq). Finally, we discuss how the quark condensate emerges as the order parameter for the chiral phase transition. In the sequence, in Chapter 3, we discuss the Ginzburg-Landau theory of phase transitions. The motivation for discussing this theory is to make contact with phenomenological ideas regarding dissipation and fluctuation in the context of Model A in the classification of Hohemberg and Halperin of dynamical phase transitions [24]. Many properties of phase transitions may be investigated by employing Ginzburg-Landau's framework. The latter will serve as a motivation to derive the coarse-grained Langevin equation through the method of closed-time-path (CTP) formalism of finite temperature field theory. This formalism is an approach to writing path integrals for general density matrices thus, enabling the tackling of non-equilibrium problems. We present the discussion of the CTP formalism in the context of quantum mechanics, not field theory. We do so because the most relevant issues and subtleties of the formalism already appear in this much simpler setting and serve as a more didactic introduction to the subject for future students and researchers interested in getting acquainted with the formalism. In Chapter 5, we present the mean-field Langevin equation derived in [16]. Since we study the solutions of that Langevin for a situation resembling time evolution in a heavy-ion collision, we discuss very briefly at the end of this chapter how magnetic fields emerge in the context of a relativistic heavy-ion collision. Subsequently, in Chapter 6, we discuss the discretization method of the Langevin field equation and introduce the numerical methods employed to simulate the mean-field Langevin Equation for the quark condensate. Original results for the time evolution of chiral quark condensate for a long time regime are presented and discussed. Finally, in the chapter 7 we summarize the obtained results and discuss the many prospects for the present work. We provide appendixes that present some material which were left out of the main text.

Chapter 2

QCD Symmetries and Linear Sigma Model

"... although the symmetries are hidden from us, we can sense that they are latent in nature, governing everything about us. That's the most exciting idea I know: that nature is much simpler than it looks. Nothing makes me more hopeful that our generation of human beings may actually hold the key to the universe in our hands–that perhaps in our lifetimes we may be able to tell why all of what we see in this immense universe of galaxies and particles is logically inevitable."

Steven Weinberg

In this section, we discuss aspects of QCD and symmetries relevant to our objectives in this work. We discuss chiral symmetry in QCD and how it leads us to introduce the effective model upon which we will base our studies on: the linear sigma model with quarks (LSMq).

2.1 Introductory Aspects of QCD

In the Standard Model of Particle Physics, QCD is the theory responsible for explaining the strong interactions. Until now there are four known forces: the gravitational without a known mediator, the electromagnetic whose mediator is the photon; the weak force with the bosons W and Z as mediators of the interactions, and the strong force with the gluons acting as mediators. Regarding QCD, the fundamental particles of the theory are quarks and gluons that possess color charge.

This trait leads to not just a coupling between quarks and gluons but an auto-coupling between gluons as well. This phenomenon does not occur in QED, for example, since there's no auto-coupling between photons. Furthermore, quarks and gluons are confined within the hadrons, the colorless bound states of quarks. Evidence of this phenomenon is that there's no observation yet of free quarks and gluons. This mechanism is under intense investigation by the community [25, 26]. Finally, the coupling constant of the theory shows a property known as asymptotic freedom: the coupling of the theory increases with decreasing energy. This means that the coupling becomes large at low energies [26]. We will discuss further this subject later in this section.

Before we introduce the Lagrangian of QCD, it's important to remark that QCD is based on the gauge group $SU(3)$, the special unitary group of degree 3 in color space, a mathematical group describing symmetry operations on a 3-dimensional complex vector space. In QCD, $SU(3)$ refers to color symmetry, the symmetry governing the strong interaction, in which quarks come in three color charges of the fundamental representation and gluon in the eight charges in the adjoint representation. The associated algebra has eight independent generators, which can be taken as being the Gell-Mann matrices λ^a [27].

The QCD Lagrangian is given by:

$$\mathcal{L}_{QCD} = \sum_f \bar{q}_f (i\gamma^\mu D_\mu - m_f) q_f - \frac{1}{4} G^a_{\mu\nu} G^{\mu\nu}_a \ , \tag{2.1}$$

in which iD_μ Is the covariant derivative that introduces the interaction between quarks and gluons by replacing the usual derivative with a gauge-covariant derivative. This term is given by:

$$iD_\mu = i\partial\!\!\!/ + g\gamma_\mu T^c A^c_\mu \ , \tag{2.2}$$

with g being the strong coupling constant, T^c the generators of the SU(3) color group, and A^c_μ are the gluon fields. The term $G^a_{\mu\nu} G^{\mu\nu}_a$ describes the self-interactions of the gluon fields:

$$G^a_{\mu\nu} = \partial_\mu A^a_\nu - \partial_\nu A^a_\mu - g f^{abc} A^b_\mu A^c_\nu \ , \tag{2.3}$$

in which g is a dimensionless coupling constant. The sum over a runs over the eight members of the color octet and the sum over f runs over the six QCD flavors. Furthermore, m is a diagonal matrix of the masses in the flavor space. This matrix

refers to the current (or free) mass of the quarks. In short, we will discuss how this mass is different from the constituent mass that takes into account the mass generated due to quark's interactions. In the QCD Lagrangian, g is an adimensional coupling constant whose value is obtained from numerical calculations, γ^μ are the Dirac matrices that express the vector nature of the strong interaction, with μ being a Lorentz vector index.

Unlike leptons, such as electrons and neutrinos, quarks are confined inside hadrons and are not observed as physical particles, hence, their masses can't be measured directly, but must be determined through their influence on the other hadronic properties. The quarks are divided into different types known as flavors. There are 6 quark flavors: up (u), down (d), strange (s), charm (c), bottom (b), and top (u). Each one of these flavors comes with its own antiparticle. As mentioned before, each quark or anti-quark also has a color number accounting for the charge of the particle. Since the quarks are fermions, they have spin half-integer and are represented by Dirac spinors: $\psi_\alpha^{f,c}(x)$, in which $f = 1, 2, ..., N_f$ is the flavor index and N_f is the number of flavors; $c = 1, 2, 3..., N_c$ is the color index and N_c is the number of colors; finally, $\alpha = 1, 2, 3, 4$ are the Dirac indexes. We already mentioned that hadrons are colorless bound states of quarks and anti-quarks which are divided into two categories: those with spin half-integer, the baryons formed by three quarks/anti-quarks, and, the mesons with spin integer and composed by a pair quark-antiquark. As mentioned, the quarks have fractional charge, thus the observed physical states possess integer electric charge due to the different quark combinations. Gluons also carry color charge leading to the aforementioned quark-gluon coupling or the auto-coupling gluon-gluon but, differently from the quarks, gluons don't have flavor [28, 27].

2.2 Λ_{QCD} and Quark Masses

Due to the fact that there's no observation of free quarks in nature, one can't directly measure their masses, thus one must define a theoretical framework in order to define the masses' values [29, 28]. Thus, the values of the quark masses and the coupling constant α_s both depend on the scheme, hence these are running quantities, for instance, $m_q = m_q(\mu)$ and $\alpha_s = \alpha_s(\mu)$, in which μ is a mass scale introduced by the scheme and $\alpha_s(\mu)$ gives the strength of the strong interaction. The most used framework is the so-called $\overline{\text{MS}}$ scheme [29]. In this framework, the equation for a

running quark mass $m_q(\mu)$, is given by:

$$\mu^2 \frac{dm_q(\mu)}{d\mu^2} = \left[-\frac{\alpha_s(\mu)}{\pi} + \mathcal{O}(\alpha_s^2) \right] m_q(\mu), \tag{2.4}$$

while the equation for $\alpha_s(\mu)$ is:

$$\mu^2 \frac{d\alpha_s(\mu)}{d\mu^2} = \beta(\alpha_s) = -b_0\, \alpha_s^2 + \mathcal{O}(\alpha_s^3), \tag{2.5}$$

in which b_0 is a term given in terms of the number of flavors N_f:

$$b_0 = \frac{33 - 2N_f}{12\pi}, \tag{2.6}$$

where N_f is the number of light flavors with masses less than the scale μ. By integrating Eq. (2.5) from μ_0 to μ for $\alpha_s(\mu)$ sufficiently small one obtains that:

$$\frac{1}{\alpha_s(\mu)} = \frac{1}{\alpha_s(\mu_0)} + b_0 \ln\left(\frac{\mu^2}{\mu_0^2}\right), \tag{2.7}$$

which can be rewritten in terms of a mass scale, Λ_{QCD}, which is independent of the term μ:

$$\frac{1}{\alpha_s(\mu)} - b_0 \ln\left(\frac{\mu^2}{\Lambda_{\text{QCD}}^2}\right) = \frac{1}{\alpha_s(\mu_0)} - b_0 \ln\left(\frac{\mu_0^2}{\Lambda_{\text{QCD}}^2}\right). \tag{2.8}$$

Rearranging it as:

$$\Lambda_{\text{QCD}} = \mu\, e^{-1/[2b_0\alpha_s(\mu)]}, \tag{2.9}$$

one can rewrite it in the following equivalent manner:

$$\alpha_s(\mu) = \frac{1}{b_0 \ln(\mu^2/\Lambda_{\text{QCD}}^2)} = \frac{12\pi}{(33 - 2N_f)\, \ln(\mu^2/\Lambda_{\text{QCD}}^2)}. \tag{2.10}$$

From this last expression, one may see that as μ increases, $\alpha_s(\mu)$ decreases, being the regime of weakly coupled QCD. This feature is the already-mentioned phenomenon of asymptotic freedom. Furthermore, this development allowed us to introduce a mass scale, Λ_{QCD}, the value that divides the theory into the two already mentioned regimes, strongly or weakly coupled, in which the former scenario occurs for energies below 1 GeV. The quantity Λ_{QCD} is obtained by solving the scheme equations for

$\alpha_s = \frac{g^2}{4\pi}$, the theory's equivalent of the fine-structure constant. The present values for Λ_{QCD} in the $\overline{MS}$ scheme for different flavor numbers N_f are [29]:

$$\Lambda_{\text{QCD}} = \begin{cases} 332 & \text{for } N_f = 3 \\ 292 & = 4 \\ 210 & = 5 \\ 89 & = 6 \end{cases} \tag{2.11}$$

Knowing $\alpha_s(\mu)$, one can solve the RG equation for the quark masses $m_q(\mu)$. The quarks are classified in terms of their masses: the light quarks (u, d, and s) are those that possess masses below $\Lambda_{QCD} = 1$ GeV, while the heavy quarks (c, b, and t) are those with masses heavier than this scale. The following table (2.1), shows the masses values renormalized in the $\overline{MS}$ scheme:

Quark	up (u)	down (d)	strange (s)	charm (c)	bottom (b)	top (t)
Mass (MeV)	2.2	4.7	93	1270	4180	172,760

Table 2.1: Approximate quark masses extracted from [29].

From this table, the (u, d, s) quarks are much lighter than the (c, b, t) quarks even if we take into account that the s quark is much heavier than the (u, d) quarks, it still is an order of magnitude lighter than the lightest of the heavy quarks, the c quark. Due to the celebrated Appelquist's and Carazzone's Decoupling Theorem [30], this huge difference in the quark masses scale allows one to decouple the dynamics of the light sector from the heavy sector such that the heavy quarks aren't relevant to determine the properties of Hadrons containing only light quarks.

It's important to differentiate two types of masses that emerge in QCD: bare quark masses are the fundamental parameters in the QCD Lagrangian, representing the intrinsic mass of quarks without any contributions from interactions or symmetry-breaking effects (such as those that we will investigate in short), while constituent quark masses arise from the quark's interactions with the QCD vacuum, where the spontaneous breaking of chiral symmetry generates an effective mass for quarks. These masses are significantly larger than the bare masses due to the dynamical generation of mass from the quark condensate [26, 28]. The constituent quark masses, which are of order 350 MeV for the u and d quarks, model the effects of dynamical chiral symmetry breaking and are not related to the quark mass parameters of the QCD Lagrangian [31, 26] thus, to explain the large discrepancies between the sum of bare quark masses and the baryon mass that they form as shown in the table (2.2),

$m_u \approx 2,2$ MeV	$m_d \approx 4,7$ MeV	$m_s \approx 93$ MeV
Hadron	**Quark Content**	**Mass**
p	uud	938
n	udd	939
ρ^+	ud	775
ω	$(u\bar{u} + d\bar{d})/\sqrt{2}$	782
ϕ	$s\bar{s}$	1020

Table 2.2: Bare quark masses in the first line and masses of some hadrons. One can see that the small quark masses do not add up to the masses of the hadrons. Masses extracted from[31].

we introduce the so-called constituent masses, which are significantly higher [8].

It is worth noting that Lattice QCD, LQCD for short, is a powerful tool to evaluate quark masses. The values of the quark masses obtained from the simulations are bare quark masses and, in order to employ these results in phenomenology, it is necessary to relate these masses to the renormalized masses in some standard renormalization scheme [32, 31, 26]. Shortly, to determine the quark masses through LQCD calculations, firstly one must compute a set of physical quantities, for instance, hadronic masses, by employing many input values of the quark masses. The physical values of the quark masses are those that correctly reproduce the set of adopted physical quantities [31].

QCD also possesses additional approximate flavor symmetries, i.e. internal symmetries, closely related to the values of masses of the three lightest quarks. In the next section, we will devote our attention to exploring these approximate symmetries which will lead us to develop an effective model displaying this trait.

2.3 Chiral Symmetry in QCD

Symmetries are one of the Physics cornerstones: it is a concept that arises in many different physical situations and one may easily point out an example of symmetry. In Physics, by knowing a symmetry one may ease the description and the manipulation of a system or an object. This idea is contained in the already discussed Noether's Theorem, which establishes a connection between symmetries and conserved quantities.

Despite the richness of symmetries, one of the subliminal goals of this section is to show that Physics is richer when symmetries are broken rather than they are when conserved.

In field theory, symmetry is a transformation applied on the fields that leaves the equations of motion unchanged, equivalently, under such transformation, a solution of the equations of motion remains a solution [33]. One of the fundamental transformations in Physics can be obtained if we imagine the reflection of a given coordinate system $\boldsymbol{r} = (x, y, z)$ through its mirrored picture, for instance, $P : \boldsymbol{r} \to -\boldsymbol{r}$, the Parity Transformation. In a certain way, one can think of it as turning right into left and vice-versa. The property of an object not being invariant under these transformations is called chirality.[1]

The chiral objects that we are going to be interested in are fermions, specifically the already discussed quarks and some of their bound states. These structures are represented by a spinor field which can be divided into left-handed and right-handed parts, namely ψ_R and ψ_L such that $\psi_R = 1/2(1+\gamma_5)\psi$ and $\psi_L(x) = 1/2(1-\gamma_5)\psi$ as [31, 29]. Thus the Lagrangian (2.1) may be expressed as:

$$\mathcal{L}_q = \overline{q}(x)\, i\not{D}\, q(x) = \overline{q}_R(x)\, i\not{D}\, q_R(x) + \overline{q}_L(x)\, i\not{D}\, q_L(x)\ . \tag{2.12}$$

This Lagrangian is invariant under the transformations:

$$q_R(x) \to q'_R = R\, q_R(x), \qquad q_L(x) \to q'_L = L\, q_L(x), \tag{2.13}$$

with $R \in SU_R(3)$ and $L \in SU_L(3)$. To show that, we will decompose the quark field $q(x)$ into its right-handed and left-handed components $q(x) = q_R(x) + q_L(x)$, in which q_R and q_L are given above and the conjugate fields are $\overline{q}_R(x) = \overline{q}(x)\frac{1-\gamma^5}{2}$, and $\overline{q}_L(x) = \overline{q}(x)\frac{1+\gamma^5}{2}$. Substituting these into the Lagrangian, we get equation (2.12). Applying the transformed fields the Lagrangian becomes:

$$\mathcal{L}'_q = \overline{q}_R R^\dagger\, i\not{D}\, R q_R + \overline{q}_L L^\dagger\, i\not{D}\, L q_L \tag{2.14}$$

In order to check the invariance we will use the fact that R and L are elements of $SU(3)$, thus they are unitary, which means that $R^\dagger R = I$ and $L^\dagger L = I$. Thus:

$$\overline{q}_R R^\dagger\, i\not{D}\, R q_R = \overline{q}_R\, i\not{D}\, q_R\ , \tag{2.15}$$

and

$$\overline{q}_L L^\dagger\, i\not{D}\, L q_L = \overline{q}_L\, i\not{D}\, q_L\ . \tag{2.16}$$

[1] This term is coined after the Greek word for hand: $\xi\epsilon\lambda\rho$.

Therefore, we have:

$$\mathcal{L}'_q = \overline{q}_R \, i\not{D} \, q_R + \overline{q}_L \, i\not{D} \, q_L = \mathcal{L}_q \, . \tag{2.17}$$

The breaking of this symmetry is usually discussed in terms of the quark condensate, the vacuum expectation value (VEV) of quark bilinears $\overline{q}^f(x)q^{f'}(x) = \overline{q}^f_R q^{f'}_L(x) + \overline{q}^f_L q^{f'}_R(x)$ [29]:

$$\left\langle \overline{q}^f_R(x) q^{f'}_L(x) \right\rangle = B \, \delta^{ff'}, \tag{2.18}$$

in which $B \sim \Lambda^3_{\mathrm{QCD}}$ and f and f' are flavor indices [29]. The VEV's existence tells us that the space-time vacuum is filled with quark-anti-quark pairs. When the condensate's value is zero, there will be no coupling between the quarks with left and right chirality. On the other hand, a non-zero condensate's value happens due to the spontaneous chiral symmetry breaking as we will discuss in this section. This discussion will motivate the interpretation of the quark condensate as an order parameter for spontaneous chiral symmetry breaking.

Note that the expression (2.18) only allows for equal flavor condensates, this is due to the fact that this VEV is a measure of how the quark fields condense in the vacuum. For the condensate to break the chiral symmetry in a consistent way, it must respect the underlying symmetries of QCD. The simplest and most natural way for this to happen is for the condensates to be diagonal in flavor space, for instance, $\langle \bar{u}u \rangle$, $\langle \bar{d}d \rangle$ and $\langle \bar{s}s \rangle$. These condensates indicate that quark-antiquark pairs of the same flavor are forming in the vacuum.

The main focus of this dissertation is to investigate the dynamics of chiral symmetry breaking and its restoration in a system with the presence of strong magnetic fields. Our present knowledge does not allow us to tackle the problem analytically using the QCD Lagrangian and models are required to make progress. In this work, we will use the Gell-Mann-Levy linear sigma model [17]. To motivate the model, we must review some central concepts. We will start with two classical examples of spontaneous symmetry breaking, and then we will discuss the model.

2.3.1 Spontaneous Symmetry Breaking

Consider a classical real $\lambda\varphi^4$ theory with Lagrangian given by:

$$\mathcal{L} = \frac{1}{2}(\partial_\mu \varphi)^2 - \frac{1}{2!} m^2 \varphi^2 - \frac{\lambda}{4} \varphi^4 \, . \tag{2.19}$$

This Lagrangian is invariant under the discrete transformation $\varphi \to -\varphi$. In the following, we argue that this symmetry is broken by the minimum energy state (the vacuum). At the classical level, the minimum energy state is determined by the potential term (since the square of the derivative term only increases the energy):

$$V(\varphi) = \frac{1}{2!}m^2\varphi^2 + \frac{\lambda}{4}\varphi^4 \,, \tag{2.20}$$

in which we will consider $\lambda > 0$ (due to the stability of the system) and two different cases, the first $m^2 = \mu^2 > 0$ and the other $m^2 = -\mu^2 < 0$. Starting with the former, it has only one trivial minimum at $\varphi_0 = 0$:

$$V'(\varphi) = +\mu^2\varphi + \lambda\varphi^3 = \varphi\big(\mu^2 + \lambda\varphi^2\big) = 0 \,. \tag{2.21}$$

The only real solution for this expression is at $\varphi_0 = 0$. The potential plot for this case is given as follows in the picture (2.1).

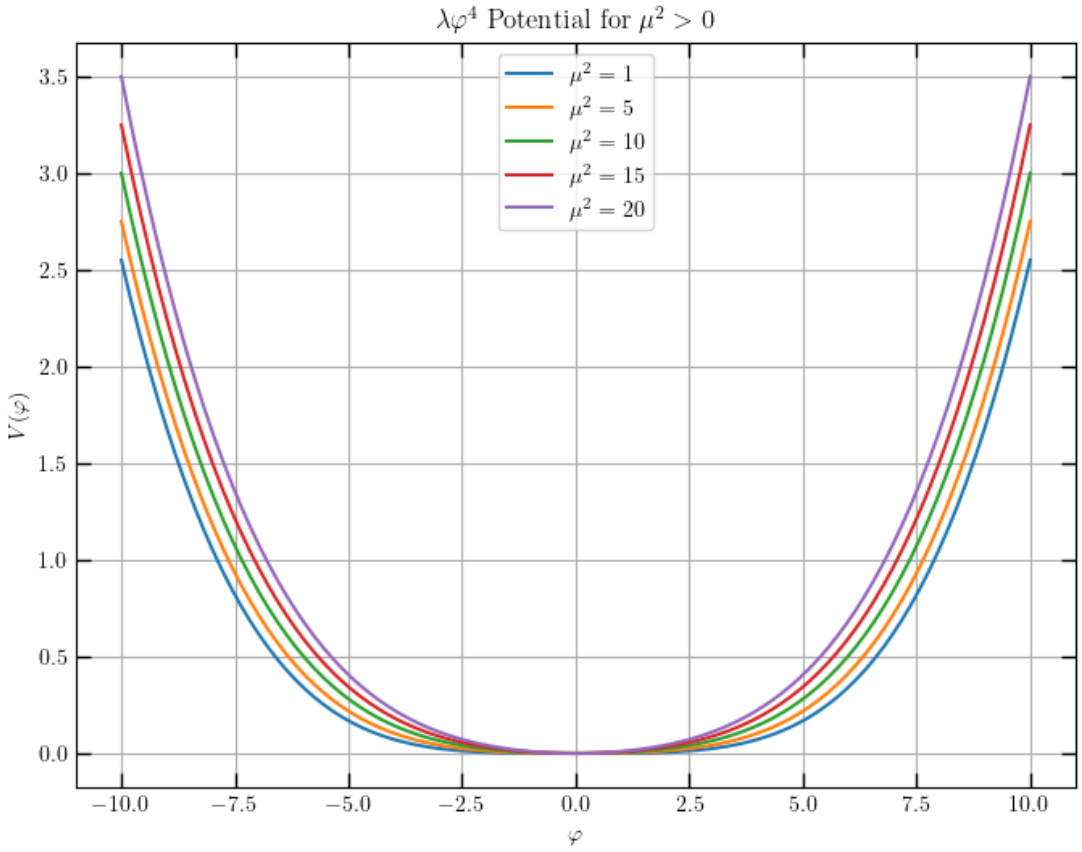

Figure 2.1: Plot of $\lambda\phi^4$ potential for different values of $m^2 = \mu^2 > 0$ as depicted in the plot legend. Note the emergence of one global minimum.

The latter case, $m^2 = -\mu^2 < 0$, is more subtle:

$$V'(\varphi) = \big(-\frac{1}{2}\mu^2\varphi^2 + \frac{\lambda}{4}\varphi^4 \big)' = 0$$

$$\varphi_0 = \pm\sqrt{\frac{\mu^2}{\lambda}} \,, \tag{2.22}$$

$$\varphi_0 = 0 \,. \tag{2.23}$$

The second derivative test determines whether these points are minima or maxima:

$$\frac{d^2V}{d\varphi^2} = -\mu^2 + 3\lambda\varphi^2 \,, \tag{2.24}$$

at $\varphi = 0 \implies \frac{d^2V}{d\varphi^2} = -\mu^2 < 0$ is a local maximum and at $\varphi = \pm\sqrt{\frac{\mu^2}{\lambda}} \implies \frac{d^2V}{d\varphi^2} = 2\mu^2 > 0$, a local minimum. Therefore, the potential has a double-well shape, with two degenerate minima as depicted in the picture (2.2).

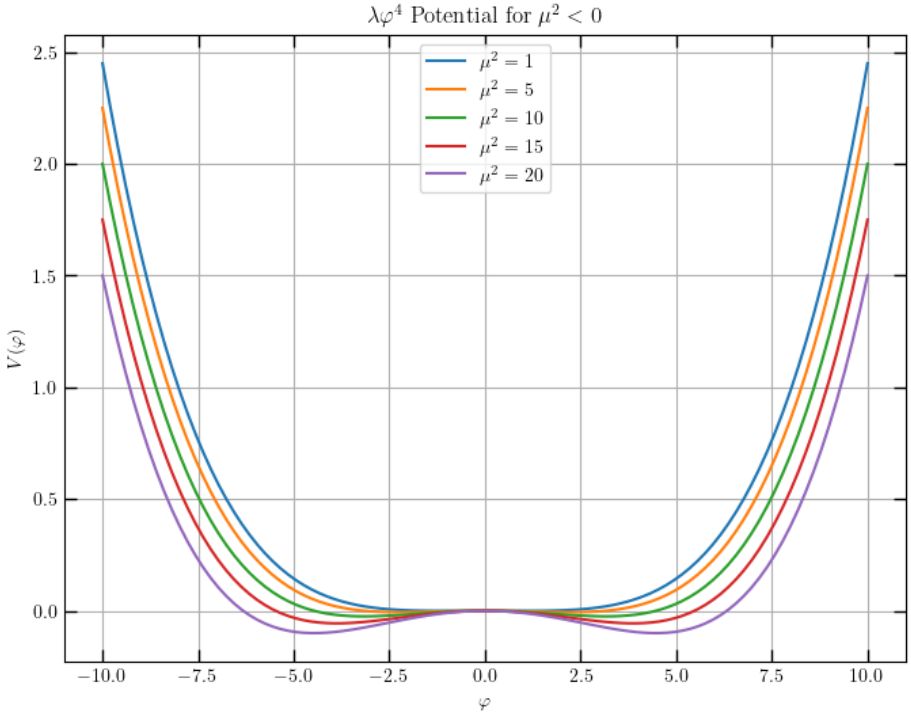

Figure 2.2: Plot of $\lambda\phi^4$ potential for different values of $m^2 = -\mu^2 < 0$ as depicted in the plot legend. Note the emergence of two global minima.

The energy's value at these minima is smaller than the minimum of the previous

case. At the minimum, the field φ is non-zero:

$$\varphi_0 = \pm\sqrt{\frac{\mu^2}{\lambda}} \,. \tag{2.25}$$

Therefore, the minimum energy states are characterized by these values (a.k.a. as vacuum expectation value, VEV, in the jargon of quantum field theory, in which case φ_0 is denoted $\varphi_0 = \langle\varphi\rangle$.). The system can then settle in either of the two minima. One may think of the field as "spontaneously choosing" one of the ground states, as it has no reason to prefer one over the other. Once it has settled in one of these two, say in the one with $\varphi_0 = +\sqrt{\mu^2/\lambda}$ the symmetry is broken, since the system cannot cross to the other minimum, $\varphi_0 = -\sqrt{\mu^2/\lambda}$, which is the $\varphi \to -\varphi$ state. But this is not physically attainable, since to "cross the barrier" costs an infinite amount of energy; it would have to cross the barrier at each space point, and since the volume is infinite, the energy cost is infinite. That is, the discrete symmetry of the Lagrangian under $\varphi \to -\varphi$ is not reflected in the ground state (vacuum state). This is an example of spontaneous symmetry breaking via a classical argument. Quantum and or thermal fluctuations can change this picture in the sense that the ground state is not determined by the minimum of the classical potential. When taking thermal and or quantum fluctuations into account, the above argument is then made by analyzing the minimum energy state determined by the minimum of the effective action.

From this example involving a discrete symmetry, we have shown how the phenomena of spontaneous symmetry breaking emerge. However, the classes of symmetries that will be relevant for this work, are the continuous symmetries which we will focus on in the next section.

2.3.2 Continuous Symmetries and Goldstone Bosons

Now, we will discuss the spontaneous breaking of continuous symmetries. This will lead us to the introduction of one of the central concepts of this dissertation. Based on the Lagrangian (2.19), we will consider the following Lagrangian first investigated by Goldstone:

$$\mathcal{L} = \frac{1}{2}\left[(\partial_\mu\varphi_1)\,(\partial^\mu\varphi_1) + (\partial_\mu\varphi_2)\,(\partial^\mu\varphi_2) - \frac{1}{2}\mu^2\varphi^2 + \frac{1}{4}\lambda(\varphi^2)^2\right] \,, \tag{2.26}$$

in which $\varphi^2 = \varphi_1^2 + \varphi_2^2$. This Lagrangian is invariant under the group $SO(2)$ of rotations in the plane:

$$\varphi \equiv \begin{pmatrix} \varphi_1 \\ \varphi_2 \end{pmatrix} \implies \varphi' = \begin{pmatrix} \varphi_1' \\ \varphi_2' \end{pmatrix} = \begin{pmatrix} \cos(\theta) & -\sin(\theta) \\ \sin(\theta) & \cos(\theta) \end{pmatrix} \begin{pmatrix} \varphi_1 \\ \varphi_2 \end{pmatrix} . \tag{2.27}$$

Recall that the special orthogonal group $SO(2)$ corresponds to all real 2x2 rotation matrices. As before, the potential term leads to different Physics if one considers $\mu^2 > 0$ and $\mu^2 < 0$: while the former leads to the case of exact symmetry, the latter will allow us to explore further the Physics of the problem.

As done for the preceding case, to find the vacuum expectation value, we will consider the potential part of the Lagrangian and look for the minimum of this potential. For $\varphi^2 = \varphi_1^2 + \varphi_2^2$, this gives:

$$\mu^2 = \lambda(\varphi_1^2 + \varphi_2^2) , \tag{2.28}$$

hence, the magnitude of the vacuum expectation value φ_0 is:

$$\varphi_0^2 = \frac{\mu^2}{\lambda} . \tag{2.29}$$

This means that since we have two degrees of freedom, the vacuum can be any point on a circle of radius $\sqrt{\frac{\mu^2}{\lambda}}$ in the (φ_1, φ_2) plane. Now, we may ask for the mass values of the particles φ_1 and φ_2. For this, we need to study the fluctuations around the vacuum. For this, we will choose the vacuum expectation value in the φ_1 direction:

$$\langle \varphi_1 \rangle = v = \sqrt{\frac{\mu^2}{\lambda}}, \quad \langle \varphi_2 \rangle = 0 \tag{2.30}$$

Let's parameterize the fields as:

$$\varphi_1 = v + \eta, \quad \varphi_2 = \nu , \tag{2.31}$$

in which η and ν are the fluctuations around the vacuum. Hence, $\varphi^2 = (v+\eta)^2 + \nu^2$. Substituting this into the Lagrangian, the kinetic terms become:

$$\frac{1}{2}\left[(\partial_\mu(v+\eta))^2 + (\partial_\mu \nu)^2\right] = \frac{1}{2}\left[(\partial_\mu \eta)^2 + (\partial_\mu \nu)^2\right] , \tag{2.32}$$

since v is constant. The potential term becomes:

$$V(\varphi) = \frac{1}{2}\mu^2\left[(v+\eta)^2+\nu^2\right] - \frac{1}{4}\lambda\left[(v+\eta)^2+\nu^2\right]^2 \ . \tag{2.33}$$

Expanding this and keeping terms up to second order in η and ν:

$$V(\varphi) \approx \frac{1}{2}\mu^2(v^2+2v\eta+\eta^2+\nu^2) - \frac{1}{4}\lambda(v^4+4v^3\eta+6v^2\eta^2+4v^2\nu^2) \ , \tag{2.34}$$

and using $v^2 = \frac{\mu^2}{\lambda}$ in different places, we find that the constant and linear terms cancel, leaving:

$$V(\varphi) \approx \frac{1}{2}(2\lambda v^2)\eta^2 + \frac{1}{2}(0)\nu^2 \ . \tag{2.35}$$

This shows an important result: The η particle has mass $m_\eta = \sqrt{2\mu^2} > 0$, whereas the ν particle is massless.

The emergence of massless particles is a general consequence of the spontaneous breakdown of a continuous symmetry, this is Goldstone's Theorem. In summary, this theorem states that there is one scalar particle called Nambu–Goldstone Boson, for each generator of the continuous symmetry that is spontaneously broken, in other words, that does not preserve the ground state. As we have shown, these particles are massless if the symmetry is exact, or light if the symmetry is not exact.

Later in this chapter, we will investigate how the pions emerge as the pseudo-Goldstone bosons of the theory since they are light, but not massless, and how this emergence impacts the theory. The smallness of the pion mass, $m_\pi \approx 135$ MeV, refers to its mass being significantly smaller than the typical hadron masses.

Another prominent characteristic in the context of continuous symmetries is Noether's theorem, which states that symmetries of the Lagrangian lead to conserved quantities, the currents. Let us consider a many-component scalar field theory, $\varphi = (\varphi_1, \varphi_2, \cdots)$ and $\delta\varphi_i$ the change of each component under an infinitesimal transformation that leaves the action of the theory invariant:

$$\varphi_i \to \varphi_i' = \varphi + \delta\varphi_i, \tag{2.36}$$

Specifically, let us consider the following transformation:

$$\varphi \to e^{-i\theta^a T^a}\varphi \ . \tag{2.37}$$

in which θ corresponds to the rotation angle and T^a is the generator of the transformation; the number of indices a depends on transformation considered. The corresponding infinitesimal transformation is given by:

$$\varphi_i \to \varphi_i - i\theta^a (T^a)_{ij}\varphi_j \equiv \varphi_i + \delta\varphi_i \ . \tag{2.38}$$

The associated Noether current is given by:

$$J^a_\mu = -i\frac{\partial \mathcal{L}}{\partial(\partial^\mu \varphi_i)} T^a_{ij}\varphi_j \ . \tag{2.39}$$

For the case of the Lagrangian in (2.26) and the transformation in (2.27), there is only one generator:

$$T^a \to i\tau = \begin{pmatrix} 0 & -1 \\ 1 & 0 \end{pmatrix} \quad \text{and} \quad U = e^{\theta\tau} = \cos\theta + \tau\sin\theta = \begin{pmatrix} \cos\theta & -\sin\theta \\ \sin\theta & \cos\theta \end{pmatrix} \tag{2.40}$$

which, as said above, is the orthogonal transformation $SO(2)$. The variations of the Lagrangian with regards to the fields are given by:

$$\frac{\partial \mathcal{L}}{\partial(\partial^\mu \varphi_1)} = \partial_\mu \varphi_1, \quad \frac{\partial \mathcal{L}}{\partial(\partial^\mu \varphi_2)} = \partial_\mu \varphi_2 \ , \tag{2.41}$$

the conserved current is:

$$J_\mu = \varphi_1 \partial_\mu \varphi_2 - \varphi_2 \partial_\mu \varphi_1 \ . \tag{2.42}$$

After this short review of symmetries and their breaking, we are ready to focus on how these concepts arise in the context of QCD.

2.3.3 Fermions: Axial and Vector Transformations

We will explore the physics of chiral symmetry in the context of QCD. This requires a discussion of currents associated with symmetries involving fermion fields (in QCD, quark fields). For this and the subsequent subsections, we will closely follow [18].

Let's start by considering the Lagrangian of two flavors of massless fermions:

$$\mathcal{L} = i\bar{\psi}^j_\alpha (\gamma^\mu)_{\alpha\beta}\partial_\mu \psi^j_\beta = i\bar{\psi}\,\partial\!\!\!/\,\psi \ , \tag{2.43}$$

in which, as usual, we used the convention of an implicit sum over repeated indices and $\not{\partial} = \gamma^\mu \partial_\mu$, the index j refers to the two different flavors, that we will consider as up (u) and down (d) and the indices $\alpha, \beta = (1, 2, 3, 4)$ are the Dirac spinorial indexes. Consider the following (infinitesimal) transformations acting on the fields ψ^j_α:

$$\begin{aligned}\Lambda_V: \ \psi^j_\alpha \to \psi'^j_\alpha &= \left(e^{-i\frac{1}{2}\boldsymbol{\tau}\cdot\boldsymbol{\theta}}\right)^{jk} \psi^k_\alpha \approx \left(1 - i\,\frac{1}{2}\boldsymbol{\tau}\cdot\boldsymbol{\theta}\right)^{jk} \psi^k_\alpha = \psi^j_\alpha - i\,\frac{1}{2}(\boldsymbol{\tau})^{jk}\cdot\boldsymbol{\theta}\,\psi^k_\alpha \\ &= \psi^j_\alpha - i\,\frac{1}{2}(\tau^a)^{jk}\theta^a\,\psi^k_\alpha \qquad (2.44)\\ \bar\psi^j_\alpha \to \bar\psi'^j_\alpha &= \bar\psi^k_\alpha \left(e^{i\frac{1}{2}\boldsymbol{\tau}\cdot\boldsymbol{\theta}}\right)^{jk} \approx \bar\psi^k_\alpha \left(1 + i\,\frac{1}{2}\boldsymbol{\tau}\cdot\boldsymbol{\theta}\right)^{jk} \\ &= \bar\psi^j_\alpha + \bar\psi^k_\alpha i\frac{1}{2}(\tau^a)^{jk}\theta^a\,, \qquad (2.45)\end{aligned}$$

where $\boldsymbol{\tau} = (\tau^1, \tau^2, \tau^3)$ are the Pauli matrices. From now on, for the sake of clarity, we will drop the flavor and spinorial indexes.

Let's check if the Lagrangian given by equation (2.43) is invariant under the transformations given by the set of equations (2.45):

$$\begin{aligned}\mathcal{L}' = \bar\psi' i\not{\partial}\psi' &= \bar\psi(1 + \frac{i\boldsymbol{\tau}\cdot\boldsymbol{\theta}}{2}) i\not{\partial}(1 - \frac{-i\boldsymbol{\tau}\cdot\boldsymbol{\theta}}{2})\psi \\ &= \bar\psi i\not{\partial}\psi + i\bar\psi\frac{\boldsymbol{\tau}\cdot\boldsymbol{\theta}}{2} i\not{\partial}\psi - \bar\psi i\not{\partial}\frac{i\boldsymbol{\tau}\cdot\boldsymbol{\theta}}{2}\psi - i\bar\psi\frac{\boldsymbol{\tau}\cdot\boldsymbol{\theta}}{2} i\not{\partial}\frac{i\boldsymbol{\tau}\cdot\boldsymbol{\theta}}{2} \\ &= i\bar\psi\not{\partial}\psi - i\boldsymbol{\theta}(\bar\psi i\frac{\boldsymbol{\tau}}{2}\not{\partial}\psi - \bar\psi i\not{\partial}\frac{\boldsymbol{\tau}}{2}\psi) \\ &= i\bar\psi\not{\partial}\psi = \mathcal{L}\,, \qquad (2.46)\end{aligned}$$

in the second line, we have used the fact that $\mathcal{O}(\boldsymbol{\theta}^2)$ terms are not considered in the expansion and, in the third line we have used that Pauli Matrices and Gamma matrices operate on different spaces: while the former acts on the isospin indices that take the values (1,2), the latter acts on the four Dirac spinor indices, hence, the two types of indices live in distinct vector spaces allowing us to rearrange the terms containing these matrices without obstruction.

To evaluate the conserved current we employ Noether's Theorem (2.39)

$$J^a_\mu = -i\frac{\partial\mathcal{L}}{\partial(\partial^\mu\phi_j)} T^a_{jk}\phi_k \to \boldsymbol{V}_\mu = \bar\psi\gamma_\mu\frac{\boldsymbol{\tau}}{2}\psi\,, \qquad (2.47)$$

in which we have performed the partial derivatives in the Lagrangian (2.43). The symbol $\mathbf{V}_\mu$ stands for a Lorentz vector current, associated with the vector symmetry transformation Λ_V.

Now, we will turn our attention to a different set of transformations given by:

$$\begin{aligned}\Lambda_A : &\psi \to \psi' \approx e^{-i\gamma^5 \frac{\boldsymbol{\tau}\cdot\boldsymbol{\theta}}{2}}\psi \approx (1 - i\gamma^5 \frac{\boldsymbol{\tau}\cdot\boldsymbol{\theta}}{2})\psi \\ &\bar{\psi} \to \bar{\psi}' \approx \bar{\psi} e^{-i\gamma^5 \frac{\boldsymbol{\tau}\cdot\boldsymbol{\theta}}{2}} \approx \bar{\psi}(1 - i\gamma^5 \frac{\boldsymbol{\tau}\cdot\boldsymbol{\theta}}{2}) \ ,\end{aligned} \tag{2.48}$$

in which $\gamma^5 = i\gamma^0\gamma^1\gamma^2\gamma^3$. To obtain the transformation for the adjoint field, we have used the transformation rule for ψ on the adjoint transformation altogether with the fact that $\gamma^0\gamma^5 = -\gamma^5\gamma^0$. As before, we may investigate how $\mathcal{L}$ transforms under Λ_A:

$$\begin{aligned}\mathcal{L}' = \bar{\psi} i\partial\!\!\!/ \psi &= \bar{\psi}(1 - i\gamma_5 \frac{\boldsymbol{\tau}\cdot\boldsymbol{\theta}}{2}) i\partial\!\!\!/ (1 - i\gamma^5 \frac{\boldsymbol{\tau}\cdot\boldsymbol{\theta}}{2})\psi \\ &= i\bar{\psi}\partial\!\!\!/\psi + i\boldsymbol{\theta}(-i\bar{\psi}\partial_\mu\gamma^\mu\gamma^5 \frac{\boldsymbol{\tau}}{2}\psi - i\bar{\psi}\gamma^5 \frac{\boldsymbol{\tau}}{2}\partial_\mu\gamma^\mu\psi) \\ &= i\bar{\psi}\partial\!\!\!/\psi + i\boldsymbol{\theta}(-i\bar{\psi}\partial_\mu\gamma^\mu\gamma^5 \frac{\boldsymbol{\tau}}{2}\psi + i\bar{\psi}\partial_\mu\gamma^5\gamma^\mu \frac{\boldsymbol{\tau}}{2}\psi) \\ &= i\bar{\psi}\partial\!\!\!/\psi = \mathcal{L} \ ,\end{aligned} \tag{2.49}$$

Hence the Lagrangian is invariant under Λ_A with the conserved axial current given by:

$$J^a_\mu = -i\frac{\partial\mathcal{L}}{\partial(\partial^\mu\phi_j)} T^a_{jk}\phi_k \to \boldsymbol{A}_\mu = \bar{\psi}\gamma_\mu\gamma^5 \frac{\boldsymbol{\tau}}{2}\psi \ . \tag{2.50}$$

The symbol $\mathbf{A}_\mu$ stands for a Lorentz axial vector current, associated with the axial vector symmetry transformation Λ_A.

We have shown that the Lagrangian for massless fermions is invariant under the transformations Λ_A and Λ_V. Now we may ask the following question: What if we don't consider the mass term in the Lagrangian (2.43) as absent? In this case, we can show that the $\mathcal{L}$ would be invariant under Λ_V but not under Λ_A. Since we have already performed the calculations for the free part, let's apply the transformations just on the massive term:

$$\Lambda_V : m(\bar{\psi}\psi) \to m(\bar{\psi}'\psi') \tag{2.51}$$

$$\begin{aligned}&= m\bar{\psi}\left(1 - i\frac{\boldsymbol{\tau}\cdot\boldsymbol{\theta}}{2}\right)\left(1 + i\frac{\boldsymbol{\tau}\cdot\boldsymbol{\theta}}{2}\right)\psi \\ &= m\bar{\psi}\left(1 + i\frac{\boldsymbol{\tau}\cdot\boldsymbol{\theta}}{2} - i\frac{\boldsymbol{\tau}\cdot\boldsymbol{\theta}}{2} + \frac{\boldsymbol{\tau}^2\boldsymbol{\theta}^2}{4}\right)\psi \\ &= m(\bar{\psi}\psi) \ .\end{aligned} \tag{2.52}$$

Hence the massive Lagrangian for free fermions is invariant under the vector transformations leading to a conservation of the Lagrangian. Proceeding to the axial transformations:

$$\begin{aligned}\Lambda_A : m(\bar{\psi}\psi) &\to m(\bar{\psi}'\psi') \\ &= m\left[(1 - i\gamma^5\frac{\boldsymbol{\tau}\cdot\boldsymbol{\theta}}{2})\bar{\psi}(1 - i\gamma^5\frac{\boldsymbol{\tau}\cdot\boldsymbol{\theta}}{2})\psi\right] \\ &= m\bar{\psi}\psi - 2im\boldsymbol{\theta}\left(\bar{\psi}\frac{\boldsymbol{\tau}}{2}\gamma^5\psi\right) \ , \end{aligned} \tag{2.53}$$

which is not invariant due to the presence of the subtracting extra terms. Therefore, Λ_A is not a good symmetry if the quarks have masses. On the other hand, as long as $m \approx 0$ one may treat Λ_A as an approximate symmetry of QCD. We will return to this matter later in this subsection and throughout this chapter. In the appendix B.1 we investigate the argument of partially conserved axial current (PCAC) and Goldberger-Treiman relations which provide us strong evidence in favor of the approximate chiral symmetry.

Before this section conclusion, we will discuss how the QCD Lagrangian transforms under Λ_V and Λ_A. One can see that there are no differences in comparison with the already considered Lagrangian. We have shown how the massive part of the Lagrangian acts subject to these transformations. We have two novelties: first is the term iD_μ but, since it only contains γ matrices and Gell-Mann Matrices, it will behave exactly as we have shown before under both transformations. The term that accounts for the self-interaction of the gluon fields is also left-invariant because these transformations do not act on the gluon fields. In short, under these transformations, $\mathcal{L}_{QCD}$ behaves in the same fashion as the Lagrangian in (2.43).

As a final word that will motivate the next sections, let us briefly mention why Λ_V and Λ_A are approximate symmetries for QCD: light quark masses are of the order $m_{ud} = \ 5 \approx 10$ MeV, whereas the hadronic energy scale is $\Lambda_\chi \approx 1000$ MeV. Even the strange quark, not considered here, whose mass is $m_s \approx 150$ MeV, can be considered in most cases as being light; in this case, the symmetry is $SU_V(3) \times SU_A(3)$. In the next section, we will make use of the above transformations to motivate an effective model realizing these approximate symmetries in terms of effective degrees of freedom, the linear-σ model.

2.4 Linear-Sigma Model

In the last subsection, we have discussed how fermion fields transform when subjected to the two transformations that we have defined, the vectorial transformation (Λ_V), and axial transformation (Λ_A). We are now, starting from these transformations, ready to motivate the introduction of an effective model that displays these approximate symmetries.

This model is the Linear-σ Model, which Gell-Mann and Levy introduced in 1960 [17]. Originally, it was constructed to investigate the chiral symmetry in the pion-nucleon system[17]. The model is based on a chiral invariant Lagrangian whose degrees of freedom are mesons and nucleons. In the QCD era, the model has been extended by replacing the nucleons with constituent quarks. In this case, the degrees of freedom are quark combinations σ and $\boldsymbol{\pi}$.

In order to introduce the model, we will need to recast concepts developed earlier in this chapter such as spontaneous symmetry breaking and the Goldstone Theorem. We will see that the $\boldsymbol{\pi}$ fields will emerge as the pseudo-Goldstone boson of the theory, thus we will need to discuss how to include the effect of the finite quark masses, which will lead to a discussion regarding the explicit breaking of chiral symmetry. For instance, this explicit breaking will be responsible for recovering the pions as massive particles. The model will allow us to identify the VEV of the symmetry-breaking terms in QCD as equal to the symmetry-breaking VEV from the linear-sigma model.

To construct the model, we will closely follow the steps done in [18]. We will first investigate how the quark field combinations, $\boldsymbol{\pi}$ and σ transform under Λ_V and Λ_A.

2.4.1 Model Construction

Consider the following quark field combinations:

$$\boldsymbol{\pi} = i\bar{\psi}\boldsymbol{\tau}\gamma^5\psi \ , \quad \sigma = \bar{\psi}\psi \ ,$$

in which $\psi = (u, d)^T$ is a fermionic field representing the light u and d quarks. Next, we show how these combinations are affected by Λ_V and Λ_A transformations. Firstly,

$\boldsymbol{\pi}$ fields transform under Λ_V as:

$$\begin{aligned}\boldsymbol{\pi} = i\bar{\psi}\boldsymbol{\tau}_i\gamma^5\psi \rightarrow i\bar{\psi}'\boldsymbol{\tau}_i\gamma^5\psi' \\ &= i\bar{\psi}\boldsymbol{\tau}_i\gamma^5\psi + \boldsymbol{\theta}_j(\bar{\psi}\boldsymbol{\tau}_i\gamma^5\frac{\boldsymbol{\tau}_j}{2}\psi - \bar{\psi}\frac{\boldsymbol{\tau}_j}{2}\boldsymbol{\tau}_i\gamma^5\psi) \\ &= i\bar{\psi}\boldsymbol{\tau}_i\gamma^5\psi + i\boldsymbol{\theta}_j(\epsilon_{ijk}\bar{\psi}\gamma^5\boldsymbol{\tau}_k\psi)\ , \end{aligned} \tag{2.54}$$

in which we have used the fact that $[\boldsymbol{\tau}_i, \boldsymbol{\tau}_j] = \boldsymbol{\tau}_i\boldsymbol{\tau}_j - \boldsymbol{\tau}_j\boldsymbol{\tau}_i = 2i\epsilon_{ijk}\boldsymbol{\tau}_k$. Using the cross product definition $(A \times B)_i = \epsilon_{ijk}A_jB_K$, one may rewrite the last expression above as:

$$\boldsymbol{\pi} \rightarrow \boldsymbol{\pi} + (\boldsymbol{\theta} \times \boldsymbol{\pi})\ . \tag{2.55}$$

This is an isospin rotation in which the isospin direction of $\boldsymbol{\pi}$ is rotated by an angle $\boldsymbol{\theta}$.

Hence Λ_V is identified with isospin rotations, in other words, just like a rotation in ordinary space changes the orientation of a vector, Λ_V changes the orientation of an isospin state. Finally, we turn our attention to the axial transformations of the fields. As done for the Λ_V, we will start with $\boldsymbol{\pi}$ field:

$$\begin{aligned}\boldsymbol{\pi} &= i\bar{\psi}\boldsymbol{\tau}_i\gamma^5\psi + \boldsymbol{\theta}_j(\bar{\psi}\boldsymbol{\tau}_i\gamma^5\gamma^5\frac{\boldsymbol{\tau}_j}{2}\psi + \bar{\psi}\gamma^5\frac{\boldsymbol{\tau}_j}{2}\boldsymbol{\tau}_i\gamma^5\psi) \\ &= i\bar{\psi}\boldsymbol{\tau}_i\gamma^5\psi + \boldsymbol{\theta}_j(\bar{\psi}\psi)\ , \end{aligned} \tag{2.56}$$

in which we have used that $\{\ \boldsymbol{\tau}_i, \boldsymbol{\tau}_j\ \} = 2\delta_{ij}$ and $\gamma^5\gamma^5 = 1$. This leads to:

$$\boldsymbol{\pi} \rightarrow \boldsymbol{\pi} + \boldsymbol{\theta}\sigma\ . \tag{2.57}$$

Similarly for σ field:

$$\sigma \rightarrow \sigma - \boldsymbol{\theta} \cdot \boldsymbol{\pi}\ . \tag{2.58}$$

Thus, the axial transformation mixes the sigma and pion particles.

To construct a Lagrangian, we must take into account that it must be a Lorentz scalar and invariant under the transformations Λ_A and Λ_V. Also, the model is constructed by requiring renormalizability, so that the number of terms satisfying these requirements is limited; each term in the Lagrangian must have a mass dimension equal to four, and coupling constants must be dimensionless. We start by

investigating how the square of the fields is affected under Λ_V:

$$\Lambda_V : \boldsymbol{\pi}^2 \to \boldsymbol{\pi}^2 \tag{2.59}$$

$$: \sigma^2 \to \sigma^2 \ , \tag{2.60}$$

whereas under Λ_A:

$$\Lambda_A : \boldsymbol{\pi}^2 \to \boldsymbol{\pi}^2 - 2\sigma\boldsymbol{\theta}_i\boldsymbol{\pi}_i \tag{2.61}$$

$$: \sigma^2 \to \sigma^2 + 2\sigma\boldsymbol{\theta}_i\boldsymbol{\pi}_i \ . \tag{2.62}$$

Hence, the quantity $(\boldsymbol{\pi}^2 + \sigma^2)$ is invariant under both transformations and is a Lorentz scalar. A quark-pion interaction involves the quark fields ψ and $\bar{\psi}$ and the pion field:

$$g_\pi i\bar{\psi}\gamma^5(\boldsymbol{\tau}\cdot\boldsymbol{\pi})\psi \ , \tag{2.63}$$

in which g_π is the quark-pion coupling constant. To obtain an invariant expression, one needs to include the quark-sigma interaction, $\bar{\psi}\sigma\psi$, so that the invariant interaction Lagrangian is given by:

$$\delta\mathcal{L} = -g_\pi[i\bar{\psi}\gamma^5(\boldsymbol{\tau}\cdot\boldsymbol{\pi})\psi + \bar{\psi}\sigma\psi] \ . \tag{2.64}$$

We will turn our attention to the construction of the nucleon mass term. We have shown that an explicit nucleon mass term breaks chiral symmetry. Thus, there is the need to develop a term that gives mass to the nucleon and at the same time, does not break chiral symmetry. For this sake, we will exploit the term $g_\pi(\bar{\psi}\psi)\sigma$ from the expression (2.64) since it has the structure of a nucleon mass term. However, we must impose that σ possess a finite VEV:

$$\langle\sigma\rangle = \sigma_0 = f_\pi \ , \tag{2.65}$$

in which the choice of $\sigma_0 = f_\pi$ is from the Goldberger-Treiman relation [34] in the limit of $g_a \to 1$ (because we are here at the quark level; at the nucleon level $g_a \simeq 1.25$ and g_π is the pion-nucleon coupling constant).

A finite VEV implies that chiral symmetry will be broken spontaneously. To generate such VEV, one must introduce a potential for the σ field with a minimum

at $\sigma = f_\pi$. For the potential to be chirally invariant, we will choose it as:

$$V(\boldsymbol{\pi}^2 + \sigma^2) = \frac{\lambda}{4}\left([\boldsymbol{\pi}^2 + \sigma^2] - f_\pi^2\right)^2 \tag{2.66}$$

This potential has the shape depicted in (2.3).

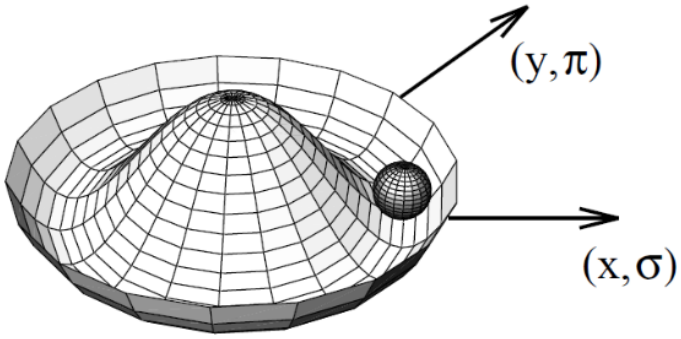

Figure 2.3: Plot of the potential (2.66): note that the x-y axis are exchanged by σ $\boldsymbol{\pi}$ axis. Extracted from [18].

Before we proceed, it's important to stress some QFT concepts: what we understand as particles are excitations on some background. This background corresponds to a minimum of the effective potential,[2] hence, the masses of the particles are given by the potential's second derivative. For instance, consider a scalar field with an effective potential $V_{eff}(\varphi)$. If the field acquires a non-zero vacuum expectation value then, $\langle\varphi\rangle = v$ it means that the symmetry of the potential is spontaneously broken. The value v is determined by minimizing the effective potential:

$$\left.\frac{dV_{eff}(\varphi)}{d\varphi}\right|_{\varphi=v} = 0\ , \tag{2.67}$$

Hence, the mass of a particle associated with a scalar field is related to the curvature of the effective potential at the minimum, the second derivative of the effective potential evaluated at the VEV:

$$\left.\frac{d^2V_{eff}(\varphi)}{d\varphi^2}\right|_{\varphi=v} = m_\sigma^2\ . \tag{2.68}$$

This second derivative measures how steeply the potential increases near its minimum,

[2] One can think of the effective potential as adding quantum corrections to the classical potential.

corresponding to the particle's mass [35].

Returning to the central discussion, by finding the extremal points of the effective potential concerning σ and evaluating at $\boldsymbol{\pi} = 0$ one obtains that:

$$\begin{aligned}\frac{\partial\ V(\boldsymbol{\pi}^2+\sigma^2)}{\partial\sigma}\bigg|_{\boldsymbol{\pi}=0} &= \frac{\lambda}{2}\big([\boldsymbol{\pi}^2+\sigma^2]-f_\pi^2\big)2\sigma = 0 \\ &= \lambda\sigma\big(\sigma^2-f_\pi^2\big) = 0 \rightarrow \sigma_0 = f_\pi\ . \end{aligned} \tag{2.69}$$

To check if it is indeed a minimum of the potential, one must derivate one more time and evaluate the expression at $\sigma_0 = f_\pi$:

$$\begin{aligned}\frac{\partial^2\ V(\boldsymbol{\pi}^2+\sigma^2)}{\partial\sigma^2}\bigg|_{\boldsymbol{\pi}=0} &= \lambda\Big[\big(\sigma^2-f_\pi^2\big)+2\sigma^2\Big] = \lambda\Big[\big(f_\pi^2-f_\pi^2\big)+2f_\pi^2\Big] \\ &= 2\lambda f_\pi^2 > 0\ , \end{aligned} \tag{2.70}$$

so $\sigma_0 = f_\pi$ indeed is the minimum of the potential and later we will see that this term is indeed related to the σ mass.

The final elements of the Linear-σ Model are the presence of kinetic terms for the ψ fields and for the mesons $\boldsymbol{\pi}$ and σ. For the former, the choice is $i\bar{\psi}\partial\!\!\!/\psi$ while for the later, $\frac{1}{2}(\partial_\mu\boldsymbol{\pi}\partial^\mu\boldsymbol{\pi}+\partial_\mu\sigma\partial^\mu\sigma)$. Both terms are chirally invariant if we follow the calculations done before: while the first term is the Lagrangian of the free massless fermions, which we have shown is invariant, the second term has the invariant structure $(\sigma^2+\boldsymbol{\pi}^2)$.

Putting the expressions for the nucleons and mesons kinetic terms,(2.64) and (2.66) together we obtain the Linear-σ Model Lagrangian:

$$\begin{aligned}\mathcal{L}_{SM} &= i\bar{\psi}\partial\!\!\!/\psi - g_\pi\left(\bar{\psi}\gamma^5(\boldsymbol{\tau}\cdot\boldsymbol{\pi})\psi+\bar{\psi}\sigma\psi\right) \\ &- \frac{\lambda}{4}\big[(\boldsymbol{\pi}^2+\sigma^2)-f_\pi^2\big]^2 + i\bar{\psi}\partial\!\!\!/\psi\frac{1}{2}\left(\partial_\mu\boldsymbol{\pi}\cdot\partial^\mu\boldsymbol{\pi}+\partial_\mu\sigma\cdot\partial^\mu\sigma\right)\end{aligned} \tag{2.71}$$

In the next subsection, we will show that we must add a term that explicitly breaks the chiral symmetry in order to give the $\boldsymbol{\pi}$ field mass. Before we discuss it, let us develop some relevant properties from this model.

Firstly, in the ground state, σ has a finite VEV, whereas $\boldsymbol{\pi}$ has none. The nucleon term obtains its mass by interacting with the σ field. Now we will turn our attention to the following question: what are the σ and $\boldsymbol{\pi}$ mesons masses? As one can see from equation (2.71), there are no explicit mass terms for these fields but, as for the nucleon case, there could be some coupling to the VEV of σ field which gives rise to

mass terms. From the potential shape plotted in figure (2.66), one may expect the $\boldsymbol{\pi}$ field to be massless and the σ field to become massive. To see it, we will start by expanding the σ field around its minimum by introducing a new fluctuating field σ' leading to $\sigma = f_\pi + \sigma'$. Starting with the kinetic terms:

$$\begin{aligned}\frac{1}{2}\big((\partial_\mu\sigma)^2 + (\partial_\mu\boldsymbol{\pi})^2\big) &= \frac{1}{2}\big(\partial_\mu(\sigma' + f_\pi)\big)^2 + \big((\partial_\mu\boldsymbol{\pi}\big)^2\big) \\ &= \frac{1}{2}\big(\partial_\mu\sigma'\big)^2 + \big(\partial_\mu\boldsymbol{\pi}^2\big)\ , \end{aligned} \tag{2.72}$$

and the free fermion and interaction parts:

$$i\bar{\psi}\partial\!\!\!/\psi - g_\pi(\bar{\psi}\gamma^5(\boldsymbol{\tau}\cdot\boldsymbol{\pi})\psi) + \bar{\psi}\sigma\psi) = i\bar{\psi}\partial\!\!\!/\psi - g_\pi(\bar{\psi}\gamma^5\boldsymbol{\tau}\cdot\boldsymbol{\pi}\psi) - g_\pi\bar{\psi}\psi(\sigma' + f_\pi)\ . \tag{2.73}$$

Finally, the potential term changes as:

$$\begin{aligned}-\frac{\lambda}{4}\left[(\boldsymbol{\pi}^2 + \sigma^2) - f_\pi^2\right]^2 &= -\frac{\lambda}{4}\left[(\boldsymbol{\pi}^2 + (\sigma' + f_\pi)^2) - f_\pi^2\right]^2 \\ &= -\frac{\lambda}{4}\left[\boldsymbol{\pi}^2 + \sigma'^2 + 2\sigma' f_\pi + f_\pi^2 - f_\pi^2\right]^2 \\ &= -\frac{\lambda}{4}\left[\boldsymbol{\pi}^2 + \sigma'^2 + 2\sigma' f_\pi\right]^2\ . \end{aligned} \tag{2.74}$$

Merging these results together, the changed Lagrangian is given by:

$$\begin{aligned}\mathcal{L} = &\frac{1}{2}\big(\partial_\mu\sigma'\big)^2 + \big(\partial_\mu\boldsymbol{\pi}^2\big) + i\bar{\psi}\partial\!\!\!/\psi - g_\pi(\bar{\psi}\gamma^5(\boldsymbol{\tau}\cdot\boldsymbol{\pi})\psi) \\ &- g_\pi\bar{\psi}\psi(\sigma' + f_\pi) - \frac{\lambda}{4}\big(4f_\pi^2\sigma^2\big)\ , \end{aligned} \tag{2.75}$$

rewriting it, we obtain the following:

$$\begin{aligned}\mathcal{L} = &\bar{\psi}(i\gamma^\mu\partial_\mu - gf_\pi)\psi - ig\bar{\psi}\gamma^5(\boldsymbol{\tau}\cdot\boldsymbol{\pi})\psi + \big(\partial_\mu\sigma'\big)^2 \\ &+ \big(\partial_\mu\boldsymbol{\pi}^2\big) - \frac{\lambda}{4}\big(4f_\pi^2\sigma^2\big) \end{aligned} \tag{2.76}$$

From this expression we are able to identify the mass spectrum of the Lagrangian after the spontaneous symmetry breaking: the nucleon mass is given by $M_N = gf_\pi$ and, in agreement with what we have discussed, we see that $m_\pi = 0$, implying that indeed the three $\boldsymbol{\pi}$ states are the massless Goldstone boson of the theory. The meson masses agree qualitatively with what is seen in nature where the $\boldsymbol{\pi}$ is the lightest hadron and the σ-meson is located at a few hundred MeV. In this case, the

symmetry is 'hidden', however, we have shown that the ground state is not invariant thus, the symmetry is spontaneously broken. We stress that the $\boldsymbol{\pi}$ are actually the pseudo-goldstone bosons of the theory since they possess a finite non-zero mass. In short, we will show how to reconcile this fact with the model.

The mass of the σ-meson in the Goldstone mode is directly related to the restoring force for small oscillations about the minimum $\sigma = f_\pi$ and $\boldsymbol{\pi} = 0$. By performing a Taylor expansion in the potential $\mathrm{V}(\sigma, \boldsymbol{\pi})$ around the minimum one obtains that:

$$\begin{aligned} V(\sigma, 0) &= const. + \frac{1}{2}\frac{\partial^2 V}{\partial \sigma^2}\bigg|_f (\sigma - f)^2 + \mathcal{O}(\sigma'^3) \\ &= const. + 2\lambda f_\pi^2 \sigma'^2 + \mathcal{O}(\sigma'^3) \ . \end{aligned} \tag{2.77}$$

In outline, we obtained the following properties of the ground state of the Linear-Sigma Model :

$$\langle \sigma \rangle = \sigma_0 = f_\pi \ , \quad \langle \boldsymbol{\pi} \rangle = 0 \ , \tag{2.78}$$

$$m_\sigma^2 = 2\lambda f_\pi^2 \neq 0 \ , \quad m_\pi = 0 \ , \tag{2.79}$$

$$m = g_\pi \, \sigma_0 \, , . \tag{2.80}$$

However, we have obtained the result that the pion mass is zero, which is inconsistent with nature. Hence, we will show in the sequence how to reconcile the construction of the Linear Sigma Model with reality by introducing the concept of explicit breaking of chiral symmetry.

2.4.2 Explicit Breaking of Chiral Symmetry

So far we have assumed that Λ_A is an exact symmetry of QCD. However, we discussed that the small, finite quark masses of the u and d quarks explicitly break the axial-vector symmetry.

To proceed with the discussion, let us recall the pion-sigma potential plot given in figure (2.66) but this time we will slightly tilt one of the minima in the σ-direction as depicted in the picture (2.4).

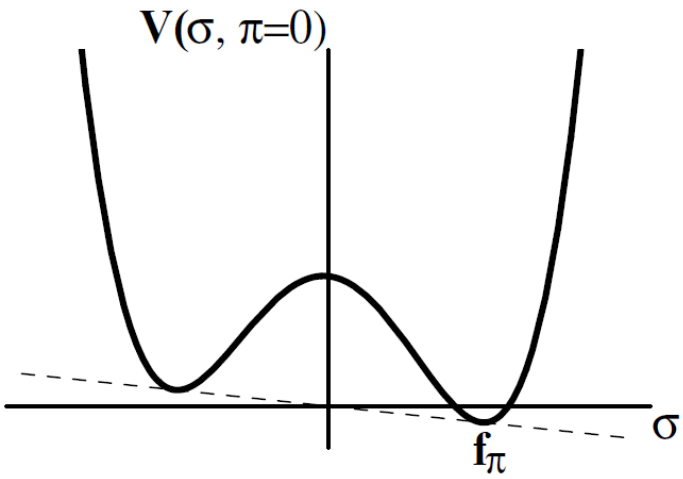

Figure 2.4: Linear Sigma Model Potential with a tilt in one of the minima in the σ direction to account for explicit symmetry breaking. Extracted from [18].

We are assuming that this tilt is small, if compared to that due to the spontaneous symmetry breaking. An χ_{SB} would imply that both potentials are not invariant under rotations for instance. A consequence of this tilt is that the ground state of the potential is away from the center. Furthermore, rotational excitations generated by $\boldsymbol{\pi}$ are still considerably softer than the radial ones generated by σ fields. Hence, we expect the effect due to the spontaneous breaking of chiral symmetry to dominate the dynamics, as long as the χ_{SB} is small [18].

Now we are in a position to justify the introduction of an extra term in Linear σ-Model that explicitly breaks symmetry. The mass scale due to spontaneous symmetry breaking is the nucleon mass, whereas that generated by χ_{SB} is the $\boldsymbol{\pi}$ mass as we will show in short. The imposition of a small explicit breaking and perfect Λ_A, will survive after the introduction of the extra term to a very good approximation. In QCD, the symmetry is explicitly broken by a quark mass term given by $\delta_{X\chi SB} = -m\bar{q}q$ and a spontaneously broken symmetry term given by $\delta_{SB} = \epsilon\sigma$, in which ϵ is an explicit spontaneous symmetry breaking parameter. This last term is not invariant under Λ_A but preserves Λ_V since:

$$\Lambda_V : \sigma \to \sigma \tag{2.81}$$

$$\Lambda_A : \sigma \to \sigma - \boldsymbol{\theta} \cdot \boldsymbol{\pi} \ . \tag{2.82}$$

Hence, the full potential of the Linear Sigma Model is given by:

$$V(\sigma, \boldsymbol{\pi}) = \frac{\lambda}{4}[(\boldsymbol{\pi}^2 + \sigma^2) - v^2]^2 - \epsilon\sigma \; . \tag{2.83}$$

The term v must go to f_π in the limit of $\epsilon \to 0$. The first consequence of this additional term is that the potential minimum is slightly shifted as drawn in the picture (2.4), thus breaking the symmetry. The minimum of the potential w.r.t. σ is now given by:

$$\lambda\sigma_0(\sigma_0^2 - v^2) - \epsilon = 0 \; . \tag{2.84}$$

Due to the Goldberger-Treiman relation, we have that $\sigma_0 = f_\pi$ so that

$$v^2 = f_\pi^2 - \frac{\epsilon}{\lambda f_\pi} \to v \simeq f_\pi^2 - \frac{\epsilon}{2\lambda f_\pi^2} \, . \tag{2.85}$$

The π and σ masses are readily found to be:

$$m_\pi^2 = \frac{\epsilon}{f_\pi} \, , \tag{2.86}$$

$$m_\sigma^2 = 2\lambda f_\pi^2 + \frac{\epsilon}{f_\pi} = 2\lambda f_\pi^2 + m_\pi^2 \, . \tag{2.87}$$

$$\tag{2.88}$$

The first expression also fixes the symmetry-breaking term ϵ and so v^2 in (2.85), namely:

$$v^2 = f_\pi^2 - \frac{m_\pi^2}{\lambda} \to v \simeq f_\pi - \frac{m_\pi^2}{2\lambda} \, . \tag{2.89}$$

Hence, the complete Lagrangian of the Linear-Sigma Model is given by:

$$\begin{aligned} \mathcal{L} = \bar{q}[i\partial\!\!\!/ - g(\sigma + i\gamma^5 \tau \cdot \boldsymbol{\pi})]q + \frac{1}{2}\left[\partial_\mu\sigma\partial^\mu\sigma + \partial_\mu\boldsymbol{\pi}\cdot\partial^\mu\boldsymbol{\pi}\right] \\ - \left[\frac{\lambda}{4}\left(\sigma^2 + \boldsymbol{\pi}^2 - f_\pi^2 + \frac{m_\pi^2}{\lambda}\right) - f_\pi m_\pi^2 \, \sigma\right] \, . \end{aligned} \tag{2.90}$$

Before we conclude this section, we can proceed even further and discuss relations between the expectation values of the scalar quark operator $\bar{q}q$ and measurable quantities such as f_π and m_π. When the symmetry-breaking term was introduced, the requirement was that it had the same transformation properties under the chiral transformations as the QCD-symmetry-breaking term. From that, it was possible to set the value of the symmetry-breaking strength ϵ to reproduce the ground state properties, the pion mass. Hence, it is reasonable to expect that the VEV

of the symmetry-breaking terms in QCD, $\delta\mathcal{L}_{\chi SB} = -m\bar{q}q$ and in the sigma-model $\delta\mathcal{L}_{SB} = \epsilon\sigma$, are the same:

$$\langle 0|\, \epsilon\sigma\, |0\rangle = -m\, \langle 0|\, \bar{q}q\, |0\rangle \ . \tag{2.91}$$

If we insert $\epsilon = m_\pi^2 f_\pi$ and use $\langle 0|\, \sigma\, |0\rangle = f_\pi$ we arrive at the Gell-Mann-Oakes-Renner (GOR) relation:

$$m_\pi^2 f_\pi^2 = -\frac{m_u + m_d}{2}\, \langle 0|\, \bar{u}u + \bar{d}d\, |0\rangle \ , \tag{2.92}$$

in which we have written out explicitly the average quark mass and the $\bar{q}q$ term. The GOR relation is useful since it relates the quark condensate with f_π, a measurable quantity. For a rigorous proof of this expression see [36].

In the following section, the last of the present chapter, we are going to discuss how the chiral quark condensate can be interpreted as an order parameter for the phase transition from the high-temperature QGP phase to a low-temperature hadron dominant phase.

2.5 The Quark Condensate as an Order Parameter

In this section, we are going to discuss the order parameter that describes the chiral phase transition which is also related to the transition from a quark-gluon plasma (QGP), a high-temperature phase, to a hadron dominant one in a lower temperature than the QGP: the chiral quark condensate, $\langle\bar{\psi}\psi\rangle$, discussed at the beginning of this chapter. As we have discussed, in the QCD's case the σ field with the quantum numbers of the vacuum acquires a finite expectation value by the spontaneous breaking of chiral symmetry, thus, one may choose to represent the chiral condensate as $\langle\sigma\rangle$ or as $\langle\bar{\psi}\psi\rangle$. The massless pseudo-Goldstone particles of the theory are the pions and their finite, but small mass comes from explicit symmetry breaking by the finite quark masses.

Chiral symmetry breaking is seen to occur in LQCD in a critical temperature $T_c \approx 155$ MeV. According to LQCD, this pseudo-critical temperature is found as a maximum in the susceptibility of the chiral condensate as depicted in the picture (2.5). The susceptibility of the chiral condensate, $\chi_m = \frac{\partial\langle\bar{q}q\rangle}{\partial m_q}$, measures the response of the quark condensate to changes in the quark mass.

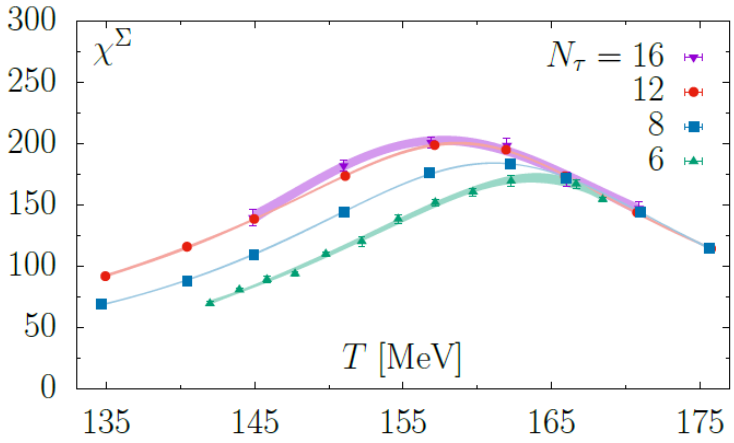

Figure 2.5: Susceptibility of the chiral quark condensate as a function of temperature. Extracted from [26].

The peak at $T_{pc} = 150$ MeV reflects the enhanced fluctuations of the quark condensate near the transition, signaling critical behavior in the QCD medium since, near this temperature, the system undergoes large fluctuations in the order parameter. These fluctuations are strongest near the phase transition, as the system is more sensitive to changes in external parameters. In QCD with light but non-zero quark masses, like those we are interested in the up and down quarks, the chiral transition is a smooth crossover rather than a sharp phase transition. In a crossover, the quark condensate and its susceptibility, show a peak near T_{pc}.

Below the T_c the regime of chiral symmetry breaking starts, leading to the existence of hadronic matter as we know it. As the temperature rises, the entropy effects are not negligible, and the restoration of the spontaneously broken symmetries is expected. This restoration is what is known as the chiral phase transition of QCD. Hence, the chiral quark condensate can be understood as an order parameter for the dynamic of the breaking of the chiral symmetry above a certain critical temperature and its further restoration for lower temperatures.

It is expected that at high temperatures or densities, the quark condensates $\langle \bar{q}q \rangle$ melts leading to a system where chiral symmetry is not spontaneously broken anymore: this is the chirally restored phase.

Nowadays, one of the biggest challenges in relativistic heavy-ion collision experiments is to recreate the conditions to observe the emergence of the chiral restoration [25, 26].

Finally, we will present without discussing further, how and which are the evidences of the formation of the chiral condensate. There are two compelling

arguments: one comes from numerical simulations on the lattice, for instance, [37], however, a full analytic calculation of the condensate is not yet possible. The other argument is that the condensate must form whenever a theory confines, which is the case of QCD. A complete discussion regarding the second argument is given in [38].

In the next chapter, we will study some models that display dynamic phase transitions, such as the Ising model. We will see that these phase transitions are characterized by order parameters that are responsible for distinguishing the different phases that a system can assume.

Chapter 3

Phases Transitions and Stochastic Models

"Landau had a logarithmic scale with which he ranked theoretical physicists, with Einstein on top, and that after working out the Landau-Ginzburg theory, he moved himself up by half a notch."

Anthony Zee

In this chapter, we will briefly discuss the theory of phase transitions. We start with static phase transitions. The Ising Model will be the basic model we use to discuss this physics and then discuss Landau's theory. Then, we discuss how fluctuations are included heuristically in the study of dynamical phase transitions; this will lead to a Langevin equation for the order parameter.

3.1 Phase Transitions and Order Parameters

Let us start considering a familiar system featuring phase transitions, water. The phase diagram of water in the pressure-temperature $(P-T)$ plane is depicted in the figure (3.1). One may identify the standard water phases separated by the solid black lines known as phase coexistence lines. At each point of these lines, we have a coexistence of the phases that the line divides and at the intersections between these curves, the equality between the chemical potentials is achieved, implying that in the temperatures in which equality occurs, the coexistence of the two phases at equilibrium occurs. At temperatures other than the coexistence temperature, only the phase with the lowest μ is stable. At equilibrium, μ must be identical throughout the system as well as when multiple phases are present in equilibrium [39]. For instance, for the melting line, solid and liquid coexist, implying that the chemical potential of these two phases is equal, $\mu_s(P,T) = \mu_l(P,T)$ since this quantity is a

measure of the chemical energy of a substance, and at equilibrium, the chemical potential must be the same in all coexisting phases to ensure no net transfer of particles from one phase to another. Note that we have one equation, and two variables, T and P. Hence, the coexistence of two phases is described by $T(p)$ or $p(T)$, for instance, a line in the (P, T) water phase diagram. The black dots in the diagram represent the triple point, where the solid, liquid, and gas phases coexist, implying that the chemical potentials of all three phases are the same.

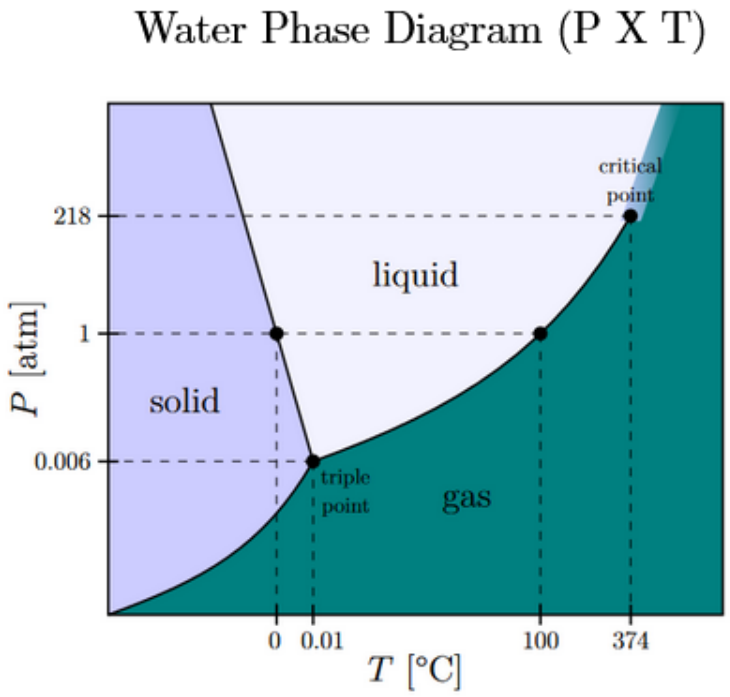

Figure 3.1: The water phase diagram: drawn in function of Temperature (°C) by Pressure (atm). The three familiar phases: gaseous, solid, and liquid are colored green, blue, and white, respectively. Relevant points are highlighted in the plot and further discussed in the text.

Phase transitions from one state of matter to another are generically classified as first-order and second-order phase transitions. First-order transitions are characterized by a discontinuous change in the first derivative of an appropriate free energy (e.g. Helmholtz or Gibbs), whereas second-order transitions are characterized by a continuous change in the appropriate free energy.

Another category of phase transition, which will be central to this work, is *crossover*. In this case, it is hard to identify a clear phase separation, subsequently, it's rather a rapid phase change rather than a real phase transition. Unlike first-order or second-order phase transitions, which are characterized by abrupt changes and

critical points, crossovers do not exhibit a sharp distinction between phases. Instead, they involve a gradual change in the properties of the system.

The concept of phase transitions and symmetry are intertwined. Recasting the previous example of the water phase diagram, at high temperatures, water is in the gaseous phase, and at lower temperatures, it is crystallized. It's usual to identify the former state as a "higher symmetry" phase and the latter as a "lower symmetry" phase since in the gaseous phase, the particle density is homogenous, implying that the gas has the property of translational invariance and in the solid state, the density is no longer homogenous, thus exhibiting a broken translational invariance. In this context, the quantity called order parameter is a measure that indicates the degree of order across a given transition. We will consider the Ising model to illustrate this connection between symmetry breaking and phase transition [39, 40].

Consider an isotropic lattice of size $N \times N$ in which N is the number of sites in a given direction. We will focus on the 2D case. On each lattice's site i, one defines a classical variable S_i that can take two values: $+1$ ("spin up") and -1 ("spin down"). The Hamiltonian of the Ising model in the presence of an external uniform magnetic field B is given by [39]:

$$H = -J \sum_{\langle ij \rangle} S_i S_j - B \sum_{i=1}^{N \times N} S_i \,, \tag{3.1}$$

with $\langle ij \rangle$ meaning first-neighbor, J is a positive number accounting for the ferromagnetic interaction between neighboring spins in the lattice, and B accounts for an external magnetic field acting on the lattice. [39]. The quantity of interest is the average magnetization $\mathcal{M}$, which characterizes the "ordering" of the system defined by:

$$\mathcal{M} = \sum_{i=1}^{N \times N} \langle S_i \rangle \,, \tag{3.2}$$

where $\langle S_i \rangle$ is the thermodynamic average of the variable S_i at site i:

$$\langle S_i \rangle = \frac{1}{\mathcal{Z}} \sum_{\{S_i\}} S_i \, e^{-\beta \hat{H}} \quad \text{where} \quad \mathcal{Z} = \sum_{\{S_i\}} e^{-\beta \hat{H}} \,, \tag{3.3}$$

in which $\beta = 1/k_B T$, with k_B being Boltzmann's constant, and $\{\cdots\}$ indicates sum over configurations of the variables S_i over the lattice. $\mathcal{Z}$ is the partition function (and in the quantum case, the sum $\{\cdots\}$ is the trace over a complete set of states).

The magnetization per spin, $\langle m \rangle = \mathcal{M}/N^2$, which vanishes in the symmetric

phase but acquires a nonzero value in the phase with broken symmetry, is called an order parameter. It distinguishes an ordered from a disordered phase. Additional examples of order parameters in nature are the difference in the densities in the liquid-gas transitions, and, later in this text, we will introduce the QCD's order parameter that we will be interested in this dissertation: the chiral quark condensate.

We simulate the Model in a square lattice with dimensions 10×10 and temperature 10 temperature points. We have performed the simulation using the celebrated Metropolis Algorithm [39]. The initial setup was taken with the spins randomly displaced on the lattice, a procedure known as *hot start* [1]as illustrated in Fig. (3.2). After generating the lattice, the algorithm selects a spin at random from the lattice. In the sequence, one computes the change in energy that would result from flipping the value of the chosen spin. In the sequence, the Metropolis criterion decides whether to flip the spin: if $\Delta E \leq 0$ the spin is flipped, otherwise, if $\Delta E > 0$, flip the spin with probability $e^{-\Delta E/k_B T}$, in which k_B is the Boltzmann constant and T is the temperature. After the criterion, one must perform the above steps a given number of times to allow the system to reach equilibrium. In the following simulations, we have sampled 100-point lattice points. Finally, after the system has reached equilibrium, one may measure properties such as magnetization, susceptibility, and specific heat [39]. Below we also present results for magnetization in Fig. (3.3) using the above algorithm.

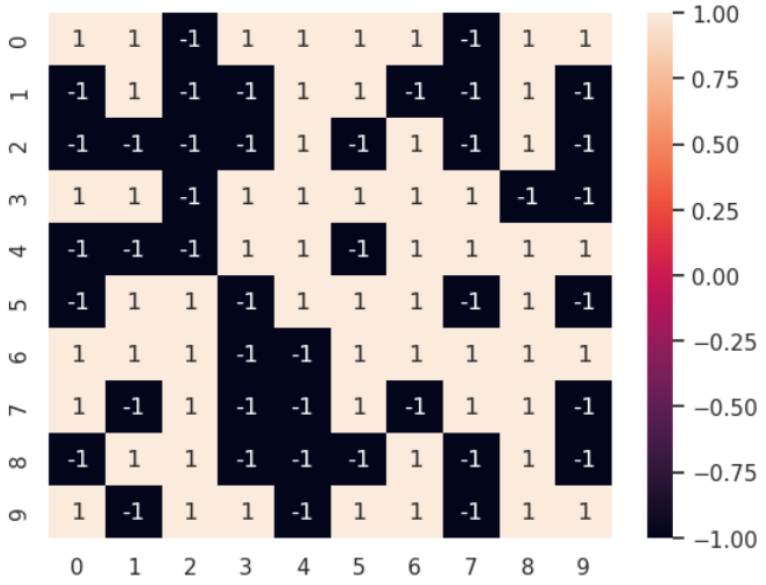

Figure 3.2: Initial setup of the lattice. The values -1 and 1 refer to the possible spin values that each site may assume. Note that the lattice has 100 sites.

[1]In contrast, *cold start* is when the lattice is initialized in a thermalized state.

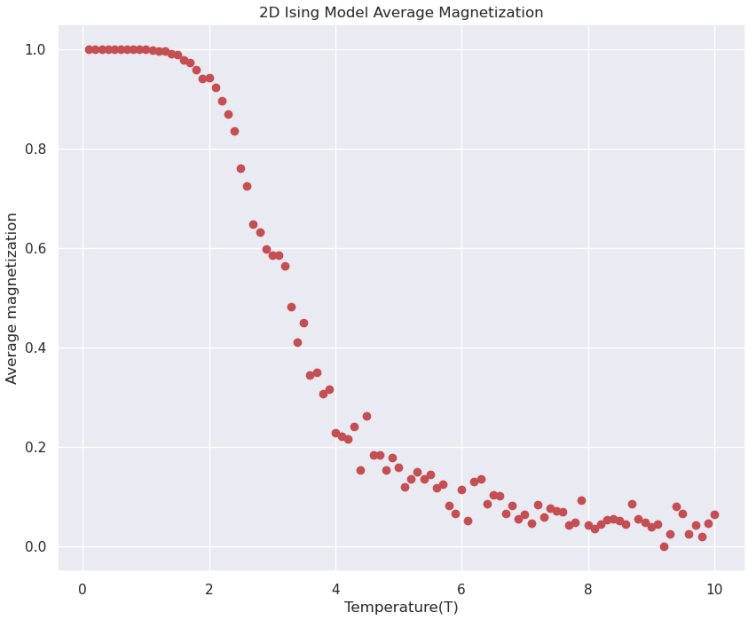

Figure 3.3: Magnetization per spin $\langle m \rangle$ in function of temperature for the 2D Ising model with a cold start.

Finally, for the same simulation, in the figure (3.4) we present the occurrence of the spin domains in the lattice as a function of the adimensional computational time step and the number of lattice sites.

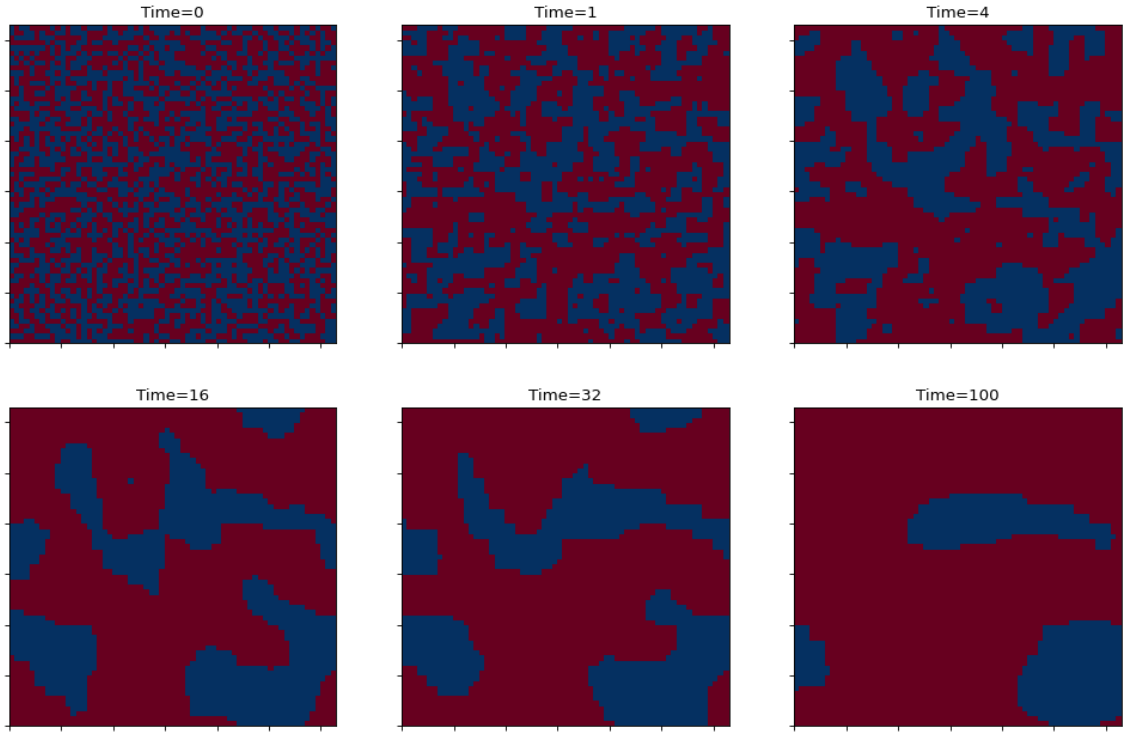

Figure 3.4: Occurrence of spin domains in the simulation for the Ising Model with the conditions discussed in the text. The red and blue regions are the spin-up and spin-down domains, respectively. Time is the computational step number to reach the depicted state.

At the beginning of the simulation, the lattice is filled with spins randomly orientated. As the simulation evolves, we notice the occurrence of regions in which the spins are clustering with non-zero magnetization, on average. Note that the temperature direction of the simulation is from a high temperature to a low temperature. Below a critical temperature, for the Ising model being the Curie Temperature T_c, the magnetic moment of the lattice disappears. If one includes an external field, it may still show residual magnetization. This high-temperature phase is known as the disordered state [40, 39]. This is a continuous phase transition: the magnetization rises continuously from zero as the temperature is reduced below T_c, as sketched in figure (3.3) in the magnetization plot. In other words, for low temperatures the system tends to stay in an ordered phase, meaning that on average over the ensemble, most of the spins will point to one of the possible directions, thus the magnetization average, $\langle m \rangle$ is non-zero. In this phase, the system's symmetry is broken. In the disordered phase, if a given spin is pointing up in a site of the lattice, it's more probable that its neighbors are pointing upwards than downwards. In this phase we have the emergence of a symmetric phase [40, 39]. These symmetry concepts will be

further developed in the context of QCD in the next chapter.

The measure of ordering in a system is contained in the correlation function, which describes how microscopic variables at different positions, such as the spins in the Ising model, are related. It is defined as the average of the scalar product of two variables at different positions [41, 39]:

$$\Delta(i-j) = \langle S_i S_j \rangle \ . \tag{3.4}$$

Thus, by picking arbitrary points i and j on the lattice and considering the expectation value $\langle S_i S_j \rangle$, this quantity gives how strongly correlated the observable at i and the observable at j are. In a broken symmetry phase, a relevant quantity is the connected correlation function, which describes the fluctuations of the deviations of a variable from its expectation value:

$$\Delta_c(i-j) = \langle S_i S_j \rangle - \langle S_i \rangle \langle S_j \rangle \ , \tag{3.5}$$

in which the subscript c in Δ_c, stands for connected. If the variables are independent, we obtain that $\langle S_i S_j \rangle = \langle S_i \rangle \langle S_j \rangle$ then $\Delta_c(i-j) = 0$ [41].

Before this section's conclusion, it's important to remark that the Ising Model phenomenology is part of a larger class of dynamical phenomena, in which one is interested in time-dependent processes, thus one must understand how the system configurations develop in time. For this, it is necessary to investigate how the physical quantities change under external time-dependent perturbations, for example, magnetic fields, temperature, mechanical dampings, and so on in the heat bath, and how the system reaches the equilibrium distribution subjected to the action of these perturbations [41, 42].

In the next section of this chapter, we will introduce a concept that underlies the Ising Model and we have neglected its discussion so far: unfortunately, one can't exactly solve the Ising model on a 3D lattice. However, one may perform an approximation to this model in any number of dimensions in a relatively simple manner by employing mean-field theory. We will discuss the idea behind it and introduce one of the many theories in this scope: the Ginzburg-Landau Theory, which will lead us to develop a phenomenological Langevin Equation.

3.2 Ginzburg-Landau Theory

In condensed matter physics, one of the goals is to understand the nature of the phase transitions by adopting methods of statistical mechanics and field theory. As we have discussed in the appendix (A), all of the thermodynamic information is contained in the partition function $\mathcal{Z} = \mathrm{Tr}_{\sigma_i}(e^{-\beta H(\sigma_i)})$, a Boltzmann-weighted trace over microscopic degrees of freedom, however, even for idealized systems, the exact trace can't be directly carried out requiring approximations. Nevertheless, properties of condensed matter phases and transitions exhibit the concept of universality discussed which is independent of the details of microscopic models. This allows one to introduce the central concept of coarse-grained fields, which we will explore more later, that allows us to build an effective theory for a given system.

A common approximation that allows one to investigate various systems further is Landau's mean-field theory, which treats these fields as nonfluctuating and usually uniform in space. In this section, we will discuss the construction of this theory and how it leads to a phenomenological Langevin Equation.

3.2.1 Mean-Field Theory

As discussed in the introduction of this section, generally, calculations of relevant thermodynamic quantities of a statistical mechanics model may be a very challenging task: while one usually solves such problems by employing Monte-Carlo simulations, such as we have done in the Ising Model simulation, analytic solutions allow one to deeply understand the physical mechanisms that are underlying the theory or phenomenology.

One of the reasons why statistical mechanics models are often hard to solve exactly is due to the already discussed fact: the existence of correlations in the system due to the interactions between the particles. Hence, if one approximates the full model by a non-interacting counterpart, solving this part of the theory will be much easier. Let's exemplify by recalling the Ising Model: we can express the spin variable S_i in terms of its mean value $\langle S_i \rangle$ and its fluctuations as $\delta S_{ij} = S_{ij} - \langle S_{ij} \rangle$. Hence, recalling the interaction part of the Ising Hamiltonian we may express it as:

$$\begin{aligned} S_i S_j &= (\delta S_i + \langle S_i \rangle)\,(\delta S_j + \langle S_j \rangle) \\ &= \langle S_i \rangle \langle S_j \rangle + \langle S_i \rangle \delta S_j + \delta S_i \langle S_j \rangle + \delta S_i \delta S_j \\ &\approx -\langle S_i \rangle \langle S_j \rangle + S_i \langle S_j \rangle + S_j \langle S_i \rangle \ , \end{aligned} \tag{3.6}$$

in the third line, we have used a mean-field approximation neglecting the quadratic fluctuations around the mean value. Hence, from this assumption, we may treat a system of interacting particles as a system of non-interacting particles in which each particle only interacts with a "mean field" that captures the average behavior of the particles around it [43].

Therefore, the mean-field theory is consisted by assuming that the system's fluctuations are negligible. This is a widely employed method in physics to explore the behavior of complicated many-body systems that cannot be solved exactly, allowing for the calculation of analytical solutions for a plethora of statistical mechanics models [43, 41].

Finally, it's important to remark without discussing it further, that in general, the system's number of dimensions is a relevant factor in determining whether a mean-field procedure will work for a given problem: it's possible that above a certain number of the system's dimension, namely the critical dimension, the approach is not valid anymore. For a discussion regarding this, see [43].

3.2.2 Landau Theory

Landau's theory is a mean-field theory in the sense discussed in the last subsection: a physical variable, such as magnetization, is replaced by its average value, and fluctuations about that value are ignored. It is also possible to use Landau's theory to estimate the importance of fluctuations, in other words, to check on the self-consistency of the theory. However, it is found that near a critical point, fluctuations are not negligible, thus the theory is not self-consistent. For a broader discussion regarding this issue, we refer the reader to [43].

In the previous sections, we discussed types of phase ordering that can occur in nature, especially in the context of the Ising Model, and how the introduction of order parameters can quantify this ordering process. In this section, we will elaborate further on the concept of mean-field theory to study phase transitions and the properties of the different phases in a system. For this, we closely follow references [41] and [43]. Mean-field theory is an approximation for the thermodynamic properties of a system based on treating the order parameter spatially constant.

There are many formulations of mean-field theory, beginning with the Van der Waals equation of state (*Van der Waals, 1873*) for the liquid-gas transition and the molecular field theory for ferromagnetism (*Weiss, 1906*) [41]. In this section, we will introduce mean-field theory with the Landau phenomenological mean-field

theory (*Landau, 1937*). These kinds of theories are the simplest treatment of an interacting statistical mechanical system, apart from the approximation of ignoring the interactions altogether [43].

Landau's theory postulates that one can write down a functional F known as the Landau Free Energy, or sometimes the Landau functional, which depends on the coupling constants k_i, temperature, pressure, the order parameter φ and any other relevant external parameter (for instance, electric or magnetic field, stress, etc.). The Landau Free Energy has the property that the state of the system is specified by the absolute minimum, or global minima with respect to the order parameter φ. The Landau Free Energy describes the system's energy in the vicinity of a phase transition. This functional has dimensions of energy and is related to, but, is not identical to the Gibbs free energy of the system introduced in the appendix (A). We assume that thermodynamic functions of state may be computed by differentiating F as if it were indeed the Gibbs free energy [41]. In the Landau theory, one assumes the existence of a high-symmetry phase, somewhere in the phase diagram, most likely at high temperatures. In this state, all the order parameters are zero. One may decompose F as:

$$F = F_0 + \delta F \ ,$$

in which F_0 does not depend on the order parameter, and δF is small in the vicinity of the phase transition depending on the order parameter.

The starting point to construct the Landau Theory is that for any value of the order parameters, δF is invariant by any element from the symmetry group of the disordered phase. For example, the Ising Model Hamiltonian already discussed is invariant under spin inversion $\sigma \to -\sigma$ and the free energy is a function of the temperature and magnetization. In the Landau Free Energy, this implies that F can only be a function of combinations of the order parameter that don't change, for example, scalars, under all operations in this group. In addition, δF may possess the additional symmetries of free space: parity and time reversal, provided that the external fields are transformed as well. For a complete discussion regarding these arguments, see reference [41] and [43].

Assuming that δF is small near the phase transition, in which all the order parameters are zero, the next step to construct the theory is to perform a Taylor expansion of $\delta F(\varphi)$ in powers of φ. For example, in the case of a simple real,

one-dimensional order parameter, the expansion is given by:

$$\delta F = -\varphi(r)B + \frac{a}{2}\varphi(r)^2 + \frac{c}{3}\varphi(r)^3 + \frac{b}{4}\varphi(r)^4 + \mathcal{O}\left(\varphi(r)^5\right) \ , \tag{3.7}$$

by integrating this expression over d dimensions with respect to the position r one obtains:

$$F = \int d^d r \left[-B\varphi(r) + \frac{a}{2}\varphi^2(r) + \frac{c}{3}\varphi^3(r) + \frac{b}{4}\varphi^4(r) + \mathcal{O}(\varphi^5(r)) \right] \ , \tag{3.8}$$

in which, we have used that the coefficient of the coupling term, φB to the external field B is equal to -1. By symmetry arguments, for instance, if the Hamiltonian of the system is invariant under the $m \to -m$ transformation, then no odd-power terms can appear. Another argument is that the Landau free-energy would be ill-conditioned if the Taylor expansion were to stop at an odd order term because it would be unbound from below [41].To find the stable states one must minimize the free energy F as a function of the order parameters.

The term $-B\varphi(r)$ is not always present: this term is the value of the Lagrangian in the high-temperature phase representing the degrees of freedom in the system which are not described by the order parameter, hence it may be thought of as a smooth background term [43]. Finally, φ must be transformed by rotation such that the coupling term is kept invariant. If these conditions are met, the phase transition is of the ferromagnetic type. In contrast with the linear term, the second order term is always allowed: In the Landau theory, phase transitions occur when one of the coefficients of the quadratic term in the order parameter expansion changes sign, from positive to negative, for instance, as a function of temperature, whilst all the other coefficients remain positive. If the driving parameter is temperature, the sign-changing term is usually written as $a(T - T_c)\varphi^2$, in which T_c is the transition or critical temperature. Finally, the quartic term is essential in producing a well-conditioned free energy, with the requirement that the free energy goes to infinity as the order parameter goes to infinity [43, 41].

Considering the case without an external magnetic field, by minimizing the free energy with respect to the order parameter, one obtains:

$$a(T - T_c)\varphi + b\varphi^3 = 0 \ . \tag{3.9}$$

This equation has the following solutions:

$$\varphi_1 = 0 \ , \tag{3.10}$$

$$\varphi_2 = \pm\sqrt{\frac{a}{b}}(T_c - T)^{\frac{1}{2}} \ , \tag{3.11}$$

note that the qualitative behavior near T_c is $\varphi \propto (T_c - T)^{\frac{1}{2}}$ which is the familiar mean-field result for magnetization. The zero solutions of the second line are present only below T_c. For $T > T_c$, $\varphi = 0$ is a global minimum, while for $T < T_c$ is a local maximum. The free energy behavior is depicted in the picture (3.5).

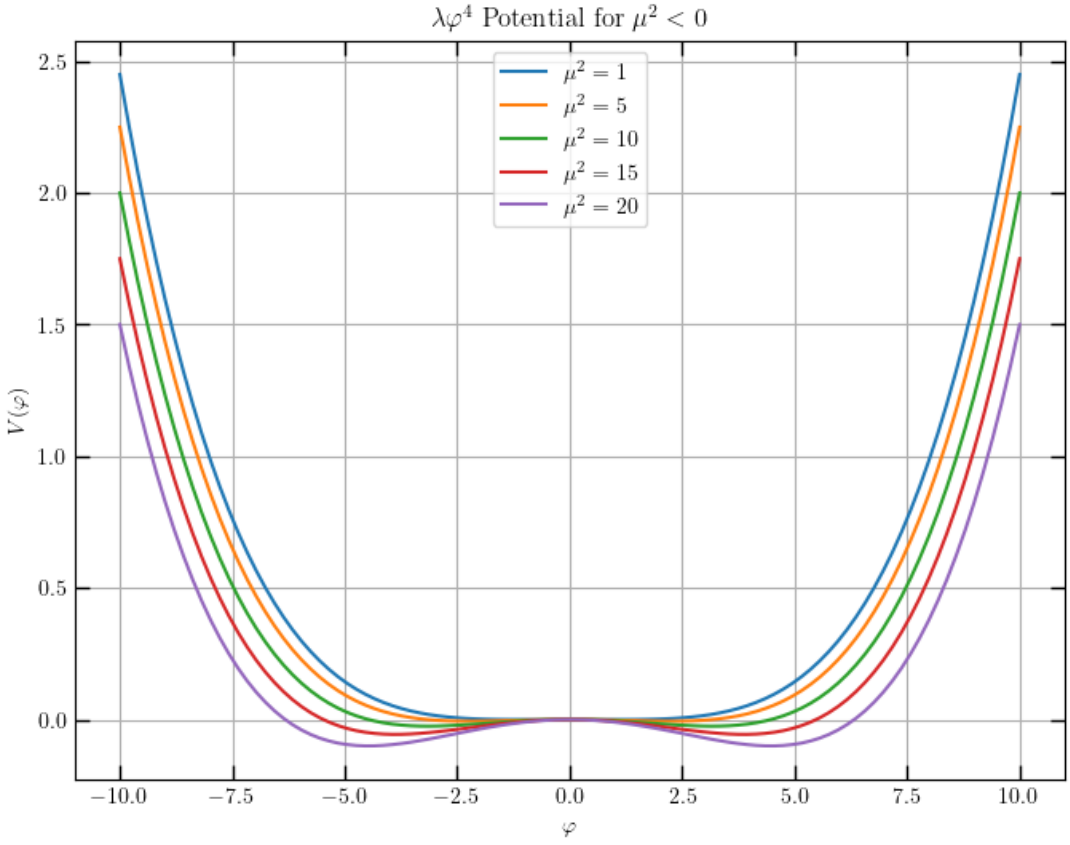

Figure 3.5: Landau Free Energy Plot in function of the order parameter φ for $a = 1$ and different temperatures: we have considered $T = [100, 200, 300]$ and $T_c = [100, 1500, 400]$ in K units. More details in the text.

Note that for $T > T_c$, for instance, the pink, grey, and red curves, $\varphi = 0$ is a global minimum of the potential. Also, the nontrivial zero solutions of the potential line are present only for T below T_c, for example, the brown, yellow, and orange curves of the graphic above. The case T=T_C yields another trivial solution as one

can check in the blue curve of the plot above.

The Landau mean field theory can easily be derived for models such as Model A developed by Hohenberg and Halperin in 1977 [24]. With this intent, we will obtain a phenomenological Langevin Equation from the Landau mean-field theory.

3.2.3 Phenomenological Langevin Equation

To derive the Langevin equation one can proceed via two methods: the first is derived from phenomenological postulates while the second is derived from a microscopic model through a coarse-graining procedure. Later in the text, we will obtain a Langevin Equation via the second method. In this subsection, we will derive the Langevin Equation by the former procedure, since it introduces many stochastic concepts that will be relevant throughout the text.

As we have presented, we are interested in the time fluctuations of a system in relation to the equilibrium state. For this, we must specify the dynamics of the system. The level of description to deal with static critical phenomena is that of Landau theory and its associated order parameter φ, hence, if we want to preserve this level of description, we must investigate the dynamics of the order parameter. In general, it is an impossible task to derive this from the dynamics of the microscopic dynamical variables of the system [43], however, by using the ideas developed in the scope of the Landau theory, we may suppose the form of the result that would be obtained if we were to derive the dynamics from microscopic physics.

Recall that the Landau free energy is given by:

$$F = \int d^d r \left[\frac{1}{2}\gamma(\nabla\varphi)^2(r) + a\varphi^2(r) + \frac{1}{2}b\varphi^4(r) - H\varphi(r) \right] . \tag{3.12}$$

In equilibrium, the spatial configuration of the order parameter is given by:

$$\frac{\delta F}{\delta \varphi(r)} = 0 , \tag{3.13}$$

It is not a stretch to assume that the rate at which the system relaxes back to equilibrium is proportional to the deviation from the original equilibrium if the system is slightly out of equilibrium [43]. This assumption of linear response is phenomenological and leads to the following equation for the rate of change of the

order parameter:

$$\frac{\partial\varphi(r)}{\partial t} = -\Gamma\frac{\delta F}{\delta\varphi(r)} \ , \tag{3.14}$$

in which Γ is a phenomenological parameter that is independent of φ and temperature dependent. As we will see in the next section, when a stochastic term is included, this equation is known as the time-dependent Ginzburg-Landau Equation, or Model A in the context of the seminal work by Hohenberg and Halperin [24].

Note that this equation can't be a correct description of the approach to the equilibrium state, since this state is a global minimum of F: equation (3.14) will force φ to evolve towards one of the local minima that may not be the global minimum. We must remember that the order parameter dynamics is not purely relaxational but may exhibit thermal fluctuations, arising from the microscopic degrees of freedom [43]. These fluctuations may lead the order parameter to move further away from equilibrium during its evolution, hence preventing the system from falling in any metastable minima that may be present. To account for this effect, we may introduce a space and time-dependent noise term ξ into equation (3.14):

$$\frac{\partial\varphi(r)}{\partial t} = -\Gamma\frac{\delta F}{\delta\varphi(r)} + \xi(r,t) \ , \tag{3.15}$$

this noise is assumed to be a Gaussian random function with average zero:

$$\langle\xi(r,t)\rangle = 0 \ , \tag{3.16}$$

and the variance is equal to unity. It ensures that the equilibrium distribution is maintained and that the Fluctuation-Dissipation Theorem is satisfied. This theorem predicts the behavior of systems that satisfy the principle of detailed balance: at equilibrium, each elementary process - steps of a given process or collisions, for instance - from a kinetic system is in equilibrium with its reverse process. Given that a system obeys detailed balance, the FDT theorem quantifies the thermodynamic fluctuations in a physical variable and the system's response due to applied perturbations. For a broader discussion regarding this subject see [39]. Since the force due to the stochastic effects, on average, is zero, and by adopting Einstein's relation $D = Tk\Gamma$:

$$\langle\xi(r,t)\xi(r',t')\rangle = D\delta(r-r')\delta(t-t') \ , \tag{3.17}$$

implying that the sampled stochastic noises are independent of each other. The noise amplitudes are related to the temperature of the system since the origins of the noise term are the microscopic degrees of freedom whose interaction with the order parameter is responsible for equilibration. The equation (3.15) together with the conditions (3.16) and (3.17) constitute the Langevin Equation derived from phenomenological grounds.

This equation is the basis for Model A, also known as the Glauber-Ginzburg-Landau Model. One of the first employments of this model was done by *Landau* and *Khalatnikov* in 1954 to explain the anomalous attenuation of sound propagation in Helium near the λ-point.[2] It provides a good description of spins in an Ising Model lattice with a thermal conductivity very large compared to that of the spins alone. The energy of the spins in such a system is transferred quickly to the lattice implying that it's not conserved. We may rewrite the equation (3.15) in terms of a total and phenomenological Hamiltonian by noting that the Landau free energy and the Hamiltonian share conceptual similarities in their roles in describing the equilibrium state of a system, the principle of minimization, and their functional forms:

$$\begin{aligned}\frac{\partial\varphi}{\partial t} &= -\Gamma\frac{\delta\mathcal{H}_T}{\delta\varphi} + \zeta(x,t) \\ &= -\Gamma\frac{\delta\mathcal{H}}{\partial\varphi} + \Gamma h(x,t) + \xi(x,t)\ ,\end{aligned} \tag{3.18}$$

in which $\mathcal{H}_T$ and $\mathcal{H}$ are different: the first, is the total Hamiltonian while the latter is a phenomenological Hamiltonian. The total Hamiltonian contains all potential energy and kinetic energy contributions and is derived from the fundamental principles and laws governing the system. For example, in classical mechanics, it is derived from the Lagrangian. It aims to be as complete and accurate as possible, taking into account all known interactions and components of the system. The phenomenological Hamiltonian is an effective Hamiltonian that describes a system based on observed phenomena and empirical information rather than derived from first principles. It is often constructed to match experimental results and can include empirical parameters that are fitted to data. Usually, its components are terms that approximate the behavior of the system without necessarily representing the underlying fundamental interactions and parameters that are adjusted to fit experimental observations.

Model A describes the slow dynamics of a non-conserved variable, in this case, the field φ but not that of a conserved variable. A purely dissipative dynamics

[2] λ-point is the temperature at which normal fluid helium (helium I) makes the transition to superfluid helium II at approximately 2.17 K at 1 atm.

for a conserved variable can be obtained by replacing Γ by $-\Lambda\Delta^2$: this is Model B described in detail in [24, 44]. One may also consider the coupling between a conserved and a non-conserved order parameter: this is Model C with detailed discussion in [24, 42]. Many other universality classes are thoroughly investigated in the references [24, 41], for instance.

In this section, we argued a phenomenological Langevin equation from the Ginzburg Landau theory. Further ahead, we will discuss how a Langevin equation can be obtained using non-equilibrium techniques. The latter approach was used in [16] to address the dynamics of the quark condensate under the effect of strong magnetic fields.

Chapter 4

Non-Equilibrium Quantum Mechanics

"A method is more important than a discovery, since the right method will lead to new and even more important discoveries."

Lev Landau

This work is interested in investigating the behavior of the chiral quark condensate under the effect of strong magnetic fields evolving through a crossover, in this specific case, the crossover from a high-temperature QGP phase to a low-temperature hadron dominant one. Due to the explosive dynamics in a heavy-ion collision, nonequilibrium effects are important at the phase transition, which occurs at finite temperatures. For instance, the possibility of spontaneous symmetry breaking and restoration implies that one needs to describe relativistic many-body systems at finite temperatures. As we have discussed, this evolution is a non-equilibrium process, henceforth, we must employ techniques to address these dynamics. At first sight, one may have two options to tackle this evolution: while the imaginary time formalism is not well suited to study ou-of-equilibrium systems since it gives up time variable in favor of introducing temperature, the Schwinger-Keldysh formalism, or closed real time-path CTP formalism, is constructed to facilitate studying the evolution of observables in quantum systems usually adopting the Heisenberg picture [45]. This formalism is applied in many branches of Physics, for example, for studying the dynamics of phase transitions; investigating the dynamical matter-antimatter creation; in heavy ion collisions, is used to describe the many non-trivial out-of-equilibrium steps involved in the evolution of the system after the collision and, the study of chiral symmetry breaking [16]. We will develop this formalism in order to write an equation of motion that displays dissipation and fluctuation. As we have discussed in this chapter, a good candidate that displays this trait is the Langevin equation. At the classical level, the motion of a particle is fully deterministic given full knowledge of the position

and momentum of all particles involved and by keeping track of every single one of them during the time evolution. This scenario is almost impossible, even for the simplest cases, furthermore, it does not display dissipative behavior. Classically, the Langevin equation focuses only on the evolution of the relevant degrees of freedom, for instance, the movement of a given particle in a medium. In this scenario, the medium acts as a heat bath, or environment, and we only consider its average effect plus stochastic fluctuations on the relevant part of the system. Thus, we will need to develop a tool that allows us to average over these irrelevant degrees of freedom in order to obtain a Langevin-like equation of motion for the relevant part of the system. As we shall show, in order to do so, we will need to introduce the influence functional formalism, which will allow us to derive a microscopic Langevin equation.

This procedure will be done in the scope of quantum mechanics since the relevant traits may be easily generalized to a QFT description. Furthermore, by performing the calculations using quantum mechanics techniques, we allow a more didactic introduction to the subject for future students and researchers interested in the subject. Once the subject is understood in quantum mechanics, its transcription to QFT becomes easier to follow. For this section discussion, we will mainly follow [46, 47].

4.1 Closed-Time Path Formalism

In general terms, the CTP formalism, invented by Schwinger [48] and Keldysh [49] in the 1960s, is based on considering a quantum state which is first evolving in the forward time direction then, after this evolution, consider the backward system's evolution, in other words, one considers the reverse evolution. The crucial step in the procedure is to consider the final state to be the same as the initial one then, no matter what the final state of the evolution (which in the out-of-equilibrium case, is an unpredictable state), let's say at a given time $t = \infty$, after the backward evolution, the system will return to the initial state, which is known. With this procedure, one may avoid the lack of information regarding the $t = \infty$ state [45].

The CTP formalism is an approach to writing path integrals for general density matrices, for example, describing the quantum mechanical evolution of a system in a nonequilibrium state or systems subject to time-varying external fields. In the following, we present a short review of this approach, since it is used in Ref. [16] to derive the Langevin equation on which we base our work in this dissertation. Instead of discussing it in the context of a field theory, we have chosen to review the subject

using a quantum mechanical model since all the essential concepts are present in this case. We follow very closely the presentation in the book [46]. The contour is usually represented in the literature as depicted in the figure (4.1): one of the history branches goes forward in time until a final time t and, after that, the other goes backward. The time variables τ and τ' refer to the first and second branches histories, respectively, hence, we are reserving the notation in which primed variables refer to the second branch, while the not primed refers to the first branch history. These two histories are the cost to employ this formalism since in comparison with the usual path integral representation of the evolution operator has just one history [47].

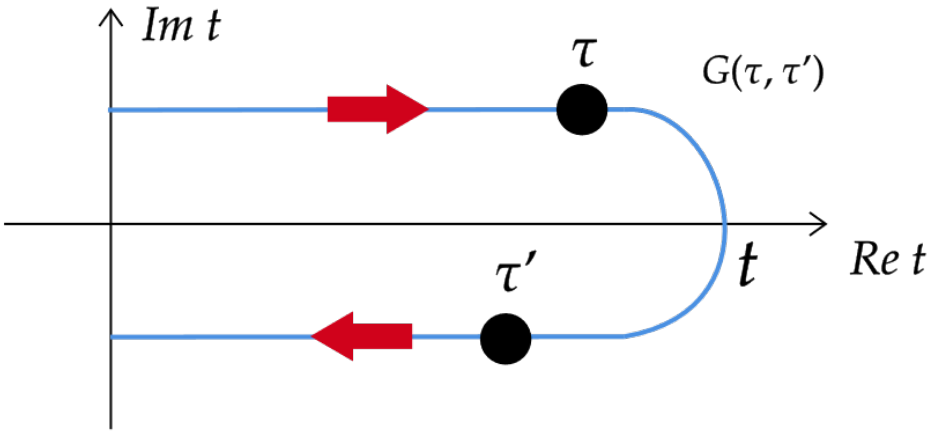

Figure 4.1: Closed-Time Path Contour explicitly showing both branches. More details in the text.

We start from the time evolution of a quantum mechanical state specified at time $t = 0$ in the coordinate representation, $\psi(q_0, 0) = \langle q_0|\psi(t = 0)\rangle$. Since states evolve according to equation (A.2), we may use the path integral representation of the matrix elements of the evolution operator to write:

$$\psi(q,t) = \int dq_0\, U(q, q_0, t)\, \psi(q_0, 0) = \int_{q(t)=q} \mathcal{D}q\, e^{i/\hbar\, S[q]}\, \psi(q_0, 0), \tag{4.1}$$

in which $U(q, q_0, t) = \langle q|\hat{U}(t)|q_0\rangle$, and $S[q]$ is the action of the system, given in terms of the Lagrangian $L(q, \dot{q}, t)$ as:

$$S[q] = \int_0^t dt'\, L(q, \dot{q}, t'), \tag{4.2}$$

Next, we show how to derive the nonequilibrium Green's functions (or propagators)

from the time evolution of the density matrix in this representation. The nonequilibrium Green's functions are the basic objects to compute physical quantities. Recall that $\hat{\rho}(t) = \sum_i |\alpha_i(t)\rangle\, \rho_i\, \langle\alpha_i(t)|$ such that:

$$\begin{aligned}\rho(q,q',t) &= \langle q|\hat{\rho}(t)|q'\rangle = \sum_i \langle q|\alpha_i(t)\rangle\, \rho_i\, \langle\alpha_i(t)|q'\rangle \\ &= \sum_i \langle q|\hat{U}|\alpha_i\rangle\, \rho_i\, \langle\alpha_i|\hat{U}^\dagger|q'\rangle = \langle q|\hat{U}\sum_i \rho_i|\alpha_i\rangle\, \langle\alpha_i|\hat{U}^\dagger|q'\rangle \\ &= \langle q|\hat{U}(t)\hat{\rho}(0)\hat{U}^\dagger(t)|q'\rangle\ , \end{aligned} \tag{4.3}$$

in which, in the second line, we have used that $\sum_i |\alpha_i\rangle\, \rho_i\, \langle\alpha_i| = \hat{\rho}(0)$. Hence, $\rho(q,q',t)$ may be written in the path integral representation for the evolution of the density matrix as follows:

$$\begin{aligned}\rho(q,q,t) &= \langle q|\hat{U}(t)\hat{\rho}(0)\hat{U}^\dagger(t)|q'\rangle \\ &= \int dq_0 dq_0'\ \langle q|\hat{U}(t)|q(0)\rangle\, \rho(q(0),q'(0),0)\, \langle q'(0)|\hat{U}^\dagger|q'\rangle \\ &= \int dq_0 dq_0'\ \langle q|\hat{U}(t)|q(0)\rangle\, \rho(q(0),q'(0),0)\, \langle q'|\hat{U}(t)|q'(0)\rangle^*\ , \end{aligned} \tag{4.4}$$

in which we have used that $\sum_i \rho(q(0),q'(0),0)\, |q(0)\rangle\, \langle q'(0)| = \hat{\rho}(0)$. Therefore, from the developed path integral formalism in the appendix (A), we may write:

$$\begin{aligned}\rho(q,q',t) &= \langle q|\hat{U}(t)\hat{\rho}(0)\hat{U}^\dagger(t)|q'\rangle \\ &= \int_{q(t)=q} \mathcal{D}q \int_{q'(t)=q'} \mathcal{D}q'\ \exp\left(\frac{i}{\hbar}S[q] - \frac{i}{\hbar}S[q']\right)\rho(q(0),q'(0),0)\,. \end{aligned} \tag{4.5}$$

Using the cyclic permutation property of the trace, it's not hard to show that $\mathrm{Tr}\,\hat{\rho}(t) = 1$ if $\mathrm{Tr}\,\hat{\rho}(0) = 1$:

$$\begin{aligned}\mathrm{Tr}\,\hat{\rho}(t) &= \int dq\ \langle q|\hat{U}(t)\hat{\rho}(0)\hat{U}^\dagger(t)|q'\rangle \\ &= \int dq dq_0 dq_0'\ \langle q|\hat{U}(t)|q'\rangle\, \langle q(0)|\hat{\rho}(0)|q'(0)\rangle\, \langle q'(0)|\hat{U}^\dagger(t)|q\rangle \\ &= \int dq dq_0 dq_0'\ \langle q(0)|\hat{\rho}(0)|q'(0)\rangle\, \langle q'(0)|\hat{U}^\dagger|q\rangle\ \langle q|\hat{U}(t)|q(0)\rangle\, \langle q(0)|\hat{\rho}(0)|q'(0)\rangle \\ &= \int dq dq_0 dq_0'\ \langle q'(0)|\hat{U}^\dagger U|q(0)\rangle\, \langle q(0)|\hat{\rho}(0)|q'(0)\rangle \\ &= \int dq dq_0 dq_0'\ \langle q'(0)|\hat{\rho}(0)|q'(0)\rangle = \mathrm{Tr}\,\hat{\rho}(0)\,. \end{aligned} \tag{4.6}$$

In terms of the path integral, by integrating (4.5) in terms of dq we obtain that:

$$\begin{aligned}\int dq\rho(q,q,t) &= \int dq \int_{q(t)=q} \mathcal{D}q \int_{q'(t)=q'} \mathcal{D}q' \ \exp\left(\frac{i}{\hbar}S[q] - \frac{i}{\hbar}S[q']\right)\rho(q(0),q'(0),0) \\ &= \int dq dq_0 ... dq_N dq'_0 ... dq'_N \ \exp\left(\frac{i}{\hbar}S[q] - \frac{i}{\hbar}S[q']\right)\rho(q(0),q'(0),0) \ . \quad (4.7)\end{aligned}$$

As previously anticipated, we see that the path integral representation of the density matrix involves two histories encapsulated by the two evolution operators, rather than a single history of the system as in equation (4.1). This observation is the starting point of the closed time path formalism, or CTP for short. To investigate further the meaning of these two histories represented via path integrals, consider the object $G^{ij}(\tau,\tau')$, in which the indices i and j take values in $\{1,2\}$ and correspond to the two branches of the contour in the figure (4.1) and τ,τ' are the already mentioned time variables on the contour. We will start with the term $G^{11}(\tau,\tau')$, describing correlations and propagation when both times are on the forward evolution part of the contour, the first branch on the figure (4.1). This object is given by:

$$G^{11}(\tau,\tau') = \int_{q(t)=q'(t)} \mathcal{D}q\mathcal{D}q' \ \exp\left(\frac{i}{\hbar}\left(S[q] - S[q']\right)\right)\rho(q(0),q'(0),0)\, q(\tau)q(\tau') \ , \quad (4.8)$$

in which the integrals $\mathcal{D}q$ and $\mathcal{D}q'$ includes dq_0 and dq'_0 and $\tau > \tau' \in [0,t]$. The upper limit for the paths $q(t)$ and $q'(t)$ is free, provided it is the same for both histories. We may describe this as an integral over single histories defined on a closed time path CTP. This time path has a first branch from 0 to t, where the history takes the values $q(t)$, and a second branch from t back to 0, where the history takes the values $q'(t)$. The CTP boundary condition $q(t) = q'(t)$ says that the history is continuous as a function of the time path.

To understand why we are describing both branches as going forward in time, let us write $G^{11}(\tau,\tau')$ in the canonical language by assuming that $\tau > \tau'$:

$$\begin{aligned}G^{11}(\tau,\tau') = \int dq_0 dq'_0 \left[\int_{0\leq t\leq\tau'} \mathcal{D}q \exp\left(\frac{i}{\hbar}S[q]\right)\right] dq_{\tau'} q(\tau') \left[\int_{\tau'\leq t\leq\tau} \mathcal{D}q \exp\left(\frac{i}{\hbar}S[q]\right)\right] dq_\tau q(\tau) \\ \times \left[\int_{\tau\leq t\leq t} \mathcal{D}q \exp\left(\frac{i}{\hbar}S[q]\right)\right] dq(t) \left[\int_{q'(t)=q(t)} \mathcal{D}q' \exp\left(-\frac{i}{\hbar}S[q']\right)\right] \rho(q(0),q'(0),0) \ . \quad (4.9)\end{aligned}$$

Each term inside the brackets is a matrix element of some evolution operator, hence:

$$G^{11}(\tau,\tau') = \int dq_0 dq_0' dq_{\tau'} dq_\tau dq(t)\ \langle q(\tau')|\hat{U}(\tau',0)|q(0)\rangle\, q(\tau')\, \langle q(\tau)|\hat{U}(\tau,\tau')|q(\tau')\rangle \\ \times \langle q(t)|\hat{U}(t,\tau)|q(\tau)\rangle\, \langle q'(0)|\hat{U}(0,t)|q(t)\rangle\, \langle q(0)|\hat{\rho}(0)|q'(0)\rangle\,. \tag{4.10}$$

Next, we perform the following operation for each matrix element:

$$\langle q'(t)|\hat{U}(t,0)|q'(0)\rangle = \langle q(t)|\hat{U}(t,0)|q'(0)\rangle = \langle q(t)|\hat{U}(t,0)|q'(0)\rangle^* \\ = \langle q'(0)|\hat{U}^\dagger(t,0)|q(t)\rangle = \langle q'(0)|\hat{U}(0,t)|q(t)\rangle\ . \tag{4.11}$$

Hence, we have obtained that:

$$G^{11}(\tau,\tau') = \int dq_0 dq_0' dq_{\tau'} dq_\tau dq(t)\, \langle q(t)|\hat{U}(t,\tau)|q(\tau)\rangle\, q(\tau) \\ \times \langle q(\tau)|\hat{U}(\tau,\tau')|q(\tau')\rangle\, q(\tau')\, \langle q(\tau')|\hat{U}(\tau',0)|q(0)\rangle \\ = \langle q(0)|\hat{\rho}(0)|q'(0)\rangle\, \langle q'(0)|\hat{U}(0,t)|q(t)\rangle\ . \tag{4.12}$$

To perform the integrals over the variables, we must employ the Spectral Theorem developed in the appendix (A), leading to:

$$G^{11}(\tau,\tau') = \int dq(t)\, \langle q(t)|\hat{U}(t,\tau)\hat{q}\hat{U}(\tau,\tau')\hat{q}\hat{U}(\tau',0)\hat{\rho}(0)\hat{U}(0,t)|q(t)\rangle \\ = \mathrm{Tr}\left[\hat{U}(t,\tau)\hat{q}\hat{U}(\tau,\tau')\hat{q}\hat{U}(\tau',0)\hat{\rho}(0)\hat{U}(0,t)\right]\ . \tag{4.13}$$

This expression, as it stands, is in the Schrodinger representation since the state vectors evolve in time, while the operators are time-independent. It is convenient to express it in the Heisenberg representation, in which the operators depend on time. This can be done by using the evolution operator to change representation, namely:

$$G^{11}(\tau,\tau') = \mathrm{Tr}\left[\hat{U}(t,\tau)\hat{q}\hat{U}(\tau,\tau')\hat{q}\hat{U}(\tau',0)\hat{\rho}(0)\hat{U}(0,t)\right] \\ = \mathrm{Tr}\Big[\exp\left(-\frac{i}{\hbar}\hat{H}t\right)\exp\left(\frac{i}{\hbar}\hat{H}\tau\right)\hat{q}\exp\left(-\frac{i}{\hbar}\hat{H}\tau\right)\exp\left(\frac{i}{\hbar}\hat{H}\tau'\right)\hat{q} \\ \times \exp\left(-\frac{i}{\hbar}\hat{H}\tau'\right)\hat{\rho}(0)\exp\left(\frac{i}{\hbar}\hat{H}t\right)\Big] \\ = \mathrm{Tr}\left[\hat{q(\tau)}\hat{q(\tau')}\rho\right] = \langle\hat{q}(\tau)\hat{q}(\tau')\rangle\,, \tag{4.14}$$

in which, we have used the statistical expectation values defined as:

$$\langle \hat{A}(t,q)\hat{A}(t',q')...\rangle = \mathrm{Tr}\left[\hat{\rho}(t)\hat{A}(t,q)\hat{A}(t',q')\right] \ . \tag{4.15}$$

We note that the path integral has automatically set the largest (τ) to the left of the smallest (τ'). This is due to the fact that the time integral in the action $S[q]$ is from 0 to t, in which one breaks the interval from an initial time $0 \to t_1$, $t_1 \to t_2$ and so on, such that t_1 is always smaller than t_2. Had we started with the $\tau' > \tau$ ordering, we would have obtained the opposite ordering, in that $q(\tau')$ would have come to the left of $q(\tau)$ in the expectation value. Hence, one can write for any ordering of τ and τ' :

$$G^{11}(\tau,\tau') = \left\langle T\left[\hat{q}(\tau)\hat{q}(\tau')\right]\right\rangle \ , \tag{4.16}$$

in which T stands for temporal ordering.

Next, we consider the quantity $G^{12}(\tau,\tau')$, the Green's function in which the first time is on the forward branch and the second time is on the backward branch in the figure (4.1):

$$G^{12}(\tau,\tau') = \int_{q(t)=q'(t)} \mathcal{D}q\mathcal{D}q' \ \exp\left(\frac{i}{\hbar}(S[q]-S[q'])\right)\rho(q(0),q'(0),0)q(\tau)q'(\tau') \ . \tag{4.17}$$

As before, we will write this in the canonical form:

$$\begin{aligned} G^{12}(\tau,\tau') = &\int dq_0 dq_0' dq_{\tau'}' dq_\tau dq(t) \left[\int_{0\le t\le\tau} \mathcal{D}q \ \exp\left(\frac{i}{\hbar}S[q]\right)\right] q(\tau) \left[\int_{\tau\le t\le t} \mathcal{D}q \ \exp\left(\frac{i}{\hbar}S[q]\right)\right] \\ &\times \left[\int_{0\le t\le\tau'} \mathcal{D}q' \ \exp\left(\frac{i}{\hbar}S[q']\right)\right] q'(\tau') \left[\int_{\tau'\le t\le t} \mathcal{D}q' \ \exp\left(-\frac{i}{\hbar}S[q']\right)\right] \\ &\times \rho(q(0),q'(0),0) \end{aligned} \tag{4.18}$$

As done for $G^{11}(\tau,\tau')$, each term inside the brackets is a matrix element of some evolution operator, hence:

$$\begin{aligned} G^{12}(\tau,\tau') = &\int dq_0 dq_0' dq_{\tau'}' dq_\tau dq(t) \ \langle q(\tau)|\hat{U}(\tau,0)|q(0)\rangle \, q(\tau) \, \langle q(t)|\hat{U}(t,\tau)|q(\tau)\rangle \\ &\times \langle q'(\tau')|\hat{U}(\tau',0)|q'(0)\rangle^* \, q'(\tau') \, \langle q'(t)|\hat{U}(t,\tau')|q'(\tau')\rangle \, \langle q(0)|\hat{\rho}(0)|q'(0)\rangle \\ = &\int dq_0 dq_0' dq_{\tau'}' dq_\tau dq(t) \ \langle q(t)|\hat{U}(t,\tau)|q(\tau)\rangle \, q(\tau) \, \langle q(\tau)|\hat{U}(\tau,0)|q(0)\rangle \\ &\times \langle q(0)|\hat{\rho}(0)|q'(0)\rangle \, \langle q'(0)|\hat{U}(0,\tau')|q'(\tau')\rangle \, q'(\tau') \, \langle q'(\tau')|\hat{U}(\tau',t)|q(t)\rangle \ . \end{aligned} \tag{4.19}$$

Using now the completeness relations, we obtain the final result:

$$\begin{aligned} G^{12}(\tau,\tau') &= \int dq(t)\ \langle q(t)|\hat{U}(t,\tau)\hat{q}\hat{U}(\tau,0)\hat{\rho}(0)\hat{U}(0,\tau')\hat{q}\hat{U}(\tau',t)|q(t)\rangle \\ &= \mathrm{Tr}\left[\hat{U}(t,\tau)\hat{q}\hat{U}(\tau,0)\hat{\rho}(0)\hat{U}(0,\tau')\hat{q}\hat{U}(\tau',t)\right] \\ &= \mathrm{Tr}\left[\hat{U}(0,\tau')\hat{q}\hat{U}(\tau',t)\hat{U}(t,\tau)\hat{q}\hat{U}(\tau,0)\hat{\rho}(0)\right] \\ &= \mathrm{Tr}\left[\hat{U}^{\dagger}(\tau')\hat{q}U(\tau')\hat{U}^{\dagger}(t)\hat{U}(t)\hat{U}^{\dagger}(\tau)\hat{q}U(\tau)\hat{\rho}(0)\right] \\ &= \mathrm{Tr}\left[\hat{q}(\tau')\hat{q}(\tau)\rho\right] = \langle\hat{q}(\tau')\hat{q}(\tau)\rangle\,. \end{aligned} \tag{4.20}$$

In the case $G^{12}(\tau,\tau')$, the primed Heisenberg operator comes out to the left, whichever time is greatest. We may think of this as a path, rather than a time, ordering.

Finally, we will develop $G^{22}(\tau,\tau')$, the Green's function where both times are on the backward branch in the figure (4.1). This function describes correlations and propagation when both times are on the backward evolution part of the contour, in which $\tau' > \tau$. As done for the previous $G^{11}(\tau,\tau')$ case:

$$G^{22}(\tau,\tau') = \mathrm{Tr}\big[\hat{q}(\tau)\hat{q}(\tau')\rho\big] = \big\langle\tilde{T}\big[q(\tau')q(\tau)\big]\big\rangle\,, \tag{4.21}$$

in which $\tilde{T}$ stands for anti-time ordering, in other words, the latest time is set to the right, since $\tau' > \tau$. This anti-time ordering property justifies the second branch as going backward concerning the first branch. Hence, the closed-time path is drawn as depicted in the figure (4.1).

In summary, the CTP formalism derives from the fact that one follows the evolution of an operator from some initial state at $t = t_0$ to some final state at a given $t > t_0$ without knowing what the proper late-time states are. We have shown that evolving an operator from t_0 to t, requires a time-ordered evolution from t_0 to t and the corresponding anti-time-ordered evolution, which can be thought of as evolution from t back to t_0. When these two integration paths are joined together, one gets the closed-time path CTP formalism.

The path integral representation which we derived for the quantum mechanics of a single particle in the appendix (A), can be easily generalized to QFT [47, 50]. However, as written before, we will stick to the Quantum Mechanics scenario since many of the relevant features are present in this scope.

As a final word before we conclude this section, there are more path possibilities, for instance, a usual procedure is to consider the initial density matrix as $\hat{\rho}(0) = \exp\left(\frac{-\beta H}{\mathcal{Z}}\right)$, which corresponds to a thermal state. In this case, the system evolves in

Euclidean time, hence, the path integral representation is defined on a time branch going from 0 to $\tau\beta$, which leads us to include a third imaginary branch in the path integral representation. For a broader discussion regarding this procedure, see the references [46, 47, 51], for instance.

4.2 Influence Functional Formalism

We need to develop a technique that allows us to average over the irrelevant degrees of freedom in order to obtain a Langevin Equation of motion for the relevant part of the system. This tool is the influence functional formalism. It gives a reduced description of the entire system focusing on the evolution of the relevant variables. The environmental details are eliminated by integrating them out via a path integral over the closed-time path contour. The influence of the environment on the dynamics of the system is totally encapsulated in the influence functional [46].

Feynman and Vernon first developed the influence functional theory by considering a system governed by the action $S[x, q]$ in which all relevant field variables, for instance, the ones whose dynamics we are interested in, are contained in the variable x, while all other variables of the system are considered collectively and denoted by $q = q_n$. The latter subsystem constitutes a background for the dynamics of the relevant variables and is interpreted as a heat bath. Consider a classical action taking the form:

$$S[x, q] = S_S[x] + S_E[q] + S_{int}[x, q] \; . \tag{4.22}$$

With the Hamiltonian $\hat{H} = \hat{H}_S + \hat{H}_E + \hat{H}_{int}$, in which $\hat{H}_S = \frac{1}{2}p^2 + V(x)$ and $\hat{H}_{int} = V_{int}(x, q)$. A priori we don't possess any information regarding the environment Hamiltonian. As we have discussed, the quantum state of the total system is described by the density matrix, hence we may write it as $\rho(xq, x'q', t)$, which depends on the system and environment, unprimed and primes variables, respectively. As we have seen in the last section, the density matrix evolves under $\hat{H}$ from an initial density matrix state $\hat{\rho}(0)$ at t=0, to $\hat{\rho}(t) = \exp\left(\frac{-it\hat{H}}{\hbar}\right)\hat{\rho}(0)\exp\left(it\hat{h}/\hbar\right)$ at given finite time t.

Recasting the path integral representation of a density matrix, we can write:

$$\begin{aligned}
\rho(xq, x'q', t) &= \langle xq, t|\hat{\rho}(t)|x'q, t\rangle \\
&= \int dq_0 dx_0 \int dq_0' dx_0' \, \langle xq, t| \, |x_0 q_0\rangle \, \langle x_0 q_0, 0| \, \rho \, |x_0' q_0', 0\rangle \, \langle x_0' q_0', 0| \, |x'q, t\rangle \\
&= \int dq_0 dq_0' dx_0 dx_0' \int_{q_0}^{q} \mathcal{D}q \int_{x_0}^{x} \mathcal{D}x \int_{q_0'}^{q'} \mathcal{D}^* q' \int_{x_0'}^{x'=x} \mathcal{D}^* x' \\
&\times \exp\big\{ i \left(S_E[q] + S_S[x] + S_{int}[xq] \right) - i \left(S_E[q'] + S_S[x'] + S_{int}[x'q'] \right) \big\} \\
&\times \langle x_i q_i, 0 | \rho(t=0) | x_i', q_i', 0 \rangle \\
&= \int dq_0 dq_0' \int_{q_0}^{q} \mathcal{D}q \int_{q_0'}^{q'} \mathcal{D}^* q' \exp\big\{ i \left(S[q] - S[q'] \right) \big\} \int dx_0 dx_0' dx \int_{x_0}^{x} \mathcal{D}x \\
&\times \int_{x_0'}^{x} \mathcal{D}^* x' exp\big(\big\{ i \left(S[x] + S[xq] \right) - i \left(S[x'] + S[x'q'] \right) \\
&\times \langle x_i q_i | \rho(t=0) | x_i', q_i' \rangle \big\} \big) \, . \qquad (4.23)
\end{aligned}$$

The relevant part is the system rather than the environment part. Hence, we don't need to evaluate the environmental contributions explicitly. Therefore, these states can be traced out to obtain the reduced density matrix describing only the system as it interacts with the environment and only computes the expectation values of system observables [46]. For this sake, we will consider that these observables are operators on the whole Hilbert space for the system taking the form $\hat{A} \otimes \mathbb{1}$, in which $\hat{A}$ is an operator in the system's Hilbert space and $\mathbb{1}$ is the unit operator on the environment Hilbert space. The tensor product of two operators $\hat{A} \otimes \hat{B}$, results in a new operator that acts on the combined space formed by taking the tensor product of the individual space, hence, $\hat{A} \otimes \hat{B}$ denotes an operator that acts on a composite system, in which $\hat{A}$ acts on the vector space of the first subsystem while leaving the second subsystem unchanged [52]. By employing the reduced density matrix ρ_r, obtained from the total density matrix $\hat{\rho}$ as a partial trace over the environmental variables, $\rho_r = \mathrm{Tr}_q \, \hat{\rho}$, we are able to compute the expectation value of the system's observables, hence:

$$\rho_r(xx', t) = \int_{-\infty}^{\infty} dq \; \rho(qx, qx', t) \, . \qquad (4.24)$$

Supposing that at $t = 0$, the system and environment are uncorrelated, then ρ_r is

given by:

$$\rho_r = \int dq \int dx_i dq_i \int dx_i' dq_i' \int_{q_i}^{q} \mathcal{D}q \int_{x_i}^{x} \mathcal{D}x \ \exp\left(i\hbar S[q,x]\right) \int_{q_i'}^{q'} \mathcal{D}q' \int_{x_i'}^{x'} \mathcal{D}x' \\ \times \exp\left(i\hbar S[q',x']\right)\rho_E(q,q_i',0)\rho_S(x_i,x_i',0) \ . \tag{4.25}$$

Defining:

$$\rho_r = \int dx_i dx_i' \mathcal{J}_r(xx',t|q_i q_i',0)\rho_s(q_i,q_i',0) \ . \tag{4.26}$$

The evolution operator for the reduced density matrix is defined by:

$$\mathcal{J}_r(xx',t|x_i x_i',0) = \int_{x_i}^{x} \mathcal{D}_x \int_{x_i'}^{x'} \mathcal{D}_{x'} \exp\left(\frac{i}{\hbar}(S[x]-S[x'])\right)\mathcal{F}[x,x'] \ . \tag{4.27}$$

It expresses the propagation of the reduced density matrix of a quantum system coupled to an environment, explicitly, is the propagator that evolves the reduced density matrix element $\rho_r(x_i,x_i',0)$ to $\rho_r(x,x',0)$. It accounts for all possible paths the system can take from the initial states to the final states, including the influence of the environment. The term $\mathcal{F}[x,x']$ is the Feynman-Vernon influence functional:

$$\begin{aligned}\mathcal{F}[x,x'] &\equiv \int dq_0 dq_0' dq \ \rho_E(q_0 q_0',0) \int_{q_0}^{q} \mathcal{D}q \int_{q_0'}^{q'} \mathcal{D}q' \\ &\quad \times \exp\left[i\left(S_E[q]+S_{int}[x,q]\right) - i\left(S_E[q']+S_{int}[x',q']\right)\right] \\ &= \exp\left(iS_{eff}[x,x']\right) \ . \end{aligned} \tag{4.28}$$

This functional describes the effect of the bath on the time evolution of the system density matrix. In the case of no system-bath coupling $H_{SB}=0 \implies \mathcal{F}=1$. In the context of CTP, the influence functional induces an explicit interaction between the two stories.

One can write $\mathcal{F}[x,x']$ in a basis independent way in terms of the propagators $\hat{U}(t)$ and $\hat{U}'(t)$ for $\hat{U}(t) \to S_E[q]+S_{int}[x,q]$ and $\hat{U}'(t) \to S_E[q']+S_{int}[x',q']$, respectively:

$$\mathcal{F}[x,x'] = \int dq dq_i dq_i' \ \rho_E(q_i q_i',0) \int_{q_i}^{q} \mathcal{D}q \ \exp\left(\frac{i}{\hbar}(S_E[q]+S_{int}[x,q])\right) \\ \times \int_{q_i'}^{q} \mathcal{D}q' \ \exp\left(\frac{-i}{\hbar}(S_E[q']+S_{int}[x',q'])\right) \ . \tag{4.29}$$

After identifying the matrix elements of the path integral terms and inserting complete

set elements for q and q_i' variables we obtain:

$$\mathcal{F}[x,x'] = \mathrm{Tr}\left[\hat{U}(t)\rho_E(0)\hat{U}'(t)^\dagger\right] \ . \tag{4.30}$$

We will conclude this section by presenting some useful properties regarding the Influence Functional. Firstly, from (4.28), after expressing the path integral terms as expectation values we may write it as:

$$\mathcal{F}[x,x'] = \int dq dq_0 dq_0' \ \rho_E(q_i,q_i',0)\,\langle q|\hat{U}(t)|q_i\rangle\,\langle q_i'|\hat{U}^\dagger(t)|q\rangle \ . \tag{4.31}$$

After inserting completion position sets for q_i, q_i' and using the trace definition, we obtain that:

$$\mathcal{F}[x,x'] = \int dq\,\langle q|\hat{U}(t)\rho_E(0)\hat{U'}^\dagger(t)|q\rangle = \mathrm{Tr}\left[\hat{U}(t)\rho_E(0)\hat{U'}^\dagger(t)\right] \ , \tag{4.32}$$

now:

$$\begin{aligned}\exp\left(\frac{i}{\hbar}S_{eff}[q,q',t]\right) &= \mathrm{Tr}\left[\hat{U}(t)\rho_E(0)\hat{U'}^\dagger(t)\right] = \mathrm{Tr}\left[\hat{U}_x(0,t)\rho_E(0)\hat{U}_{x'}^\dagger(0,t)\right] \\ &= \mathrm{Tr}\left[\hat{U}_{x'}(t,0)\hat{U}_x(0,t)\rho_E(0)\right] \ ,\end{aligned} \tag{4.33}$$

The change of notation in the evolution operator refers to the fact that they depend on both x and x' due to the term S_{int}. After integrating, this dependence does not go out after integrating. Finally, for two different stories, $\hat{U}_{x'}(t,0)\hat{U}_x(0,t)$ don't cancel each other, but when the stories are equal:

$$\exp\left(\frac{i}{\hbar}S_{eff}[x,x',t]\right) = \mathrm{Tr}[\rho_E(0)] = 1 \implies S_{eff}[x,x',t] = 0 \ . \tag{4.34}$$

Even in the presence of an external explicitly time dependence, $\hat{U}_x$ still is unitary:

$$\begin{aligned}\mathrm{Tr}\left[\hat{U}_{x'}(t,0)\hat{U}_x(0,t)\rho_E(0)\right]^* &= \mathrm{Tr}\left[\rho_E(0)\hat{U}_x{}^\dagger(0,t)\hat{U}_{x'}{}^\dagger(t,0)\right] \\ &= \mathrm{Tr}\left[\hat{U}_x(t,0)\hat{U}_{x'}(0,t)\rho_E(0)\right] \ ,\end{aligned} \tag{4.35}$$

whereas $S_{eff}[x',x,t] = -S_{eff}[x,x',t]^*$. This means that, in a functional Taylor expansion of the effective action $S_{eff}[x,x',t] = S_{eff}[X,u,t]$ in terms of the difference

variable $u = x - x'$ and the center of the mass variable $X = (x + x')/2$:

$$S_{eff}[X, u, t] = \sum_{k=1} \frac{1}{k!} \int dt_1 ... dt_k \; S^{(k)}(X, t_1, ..., t_k, t) \times u(t_1) ... u(t_k) \; . \tag{4.36}$$

One would obtain that the odd terms are real and all even terms are imaginary. Taking a variation along the diagonal, in other words, considering a situation in which x and x' are very close or even the same, for instance, $x = x'$, we obtain that $S_{eff,x}\big|_{x=x'} = -S_{eff,x'}\big|_{x=x'}$. This procedure allows one to probe local behavior or symmetries of the action. Starting with:

$$\frac{\partial S_{\text{eff}}(x, x')}{\partial x}\Big|_{x'=x} = -\frac{\partial S_{\text{eff}}[x', x]}{\partial x'}\Big|_{x'=x} \; . \tag{4.37}$$

Using the transformation of variables as defined above we obtain that:

$$\frac{\partial S_{\text{eff}}(X, u)}{\partial u}\Big|_{u=0} = \frac{\partial S_{\text{eff}}[X, u]}{\partial u}\Big|_{u=0} \tag{4.38}$$

4.3 The Linear Bath Model

This example employs the Feynman-Vernon procedure leading us to a specific effective action that will serve as a basis to proceed with the Langevin equation derivation. Let us assume that the environment action is quadratic in the q variables, the initial environment density matrix is a Gaussian (thermal) state, and the bilinear interaction term is given by:

$$S_{int} = \int dx \; x^a(t) Q_a[q(t)] \; , \tag{4.39}$$

in which $Q_a[q(t)]$ are linear combinations of the q's. Here we will need to introduce the adopted notation, in which $q(t) = q^1(t)$, $q'(t) = q^2(t)$ being replaced by $q^a(t)$, $a = 1, 2$, a singe doublet defined on a conventional path. Furthermore, we will need to introduce the usual metric tensor notation: C_{ab} and C^{ab}, the covariant and contravariant tensors, respectively. Some properties of this tensor are that $C^{ab} = (C^{-1})^{ab}$, $C_{11} = 1$, $C_{22} = -1$, and the mixed representation for this tensor $C^a_b = C^{ad} C_{db} = \delta^a_b$. Finally, the usual operations of raising and lowering indexes may be performed as $q_1 = C_{1a} q^a = q^1 = q$ and $q_2 = C_{2a} q^a = -q^2 = -q'$. For instance, a

kinetic energy term such as:

$$S[x] - S[x'] = \frac{1}{2}m \int dt\ [\dot{x}(t)^2 - \dot{x}'(t)] \ . \tag{4.40}$$

It would be re-written as:

$$S[x^a] = \frac{1}{2}m \int dt\ C_{ab}\dot{x}^a\dot{x}^b \ . \tag{4.41}$$

Note that $S[x^a]$ doesn't discriminate the contributions from either branch.

We will write the influence functional in terms of this notation $\mathcal{F}[x, x'] \to F[x^a]$, from (4.29):

$$\mathcal{F}[x, x'] = \int_{q^1(t)=q^2(t)} \mathcal{D}q^a \exp\left(\frac{i}{\hbar}(S_E[q^a] + S_{int}[x^a, q^a])\right)\rho_E(q^1(0), q^2(0), 0) \ , \tag{4.42}$$

in which the integral contains the integrations over the variables q and q' as present in (4.29). In (4.39) $Q_a[q(t)]$ are linear combinations of the many variables q that describe the environment and the initial environment density matrix is Gaussian. With these assumptions, the influence action must also be quadratic in the system's variables x and x' and the integral over the Q_a elements is a functional Fourier transform of a Gaussian, so:

$$\mathcal{F}[x, x'] = \frac{1}{2}\int dtdt'\ \ x^a(t)\mathcal{M}_{ab}(t, t')x^b(t') \ , \tag{4.43}$$

in which:

$$M_{ab}(t, t') = -i\hbar\frac{\delta^2}{\delta x^a(t)\delta x^b(t)} \exp\left(\frac{i}{\hbar}S_{eff}[x, x', t]\right)\Big|_{x^a=0} \ . \tag{4.44}$$

This matrix accounts for the bath's influence on the system's dynamics, encapsulating the environment's effects on the system. $M_{11}(t, t')$ accounts for the direct self-interaction due to the bath, in other words, how fluctuations in the first degree of freedom at time t' influence the same degree of freedom at time t. The term $M_{22}(t, t')$ is analogous but refers to the second degree of freedom. The term $M_{12}(t, t')$is a cross-term accounting for the coupled dynamics and correlations between different parts of the system due to the bath, in other words, how fluctuations in the second degree of freedom at time t' influence the first degree of freedom at time t and, $M_{21}(t, t')$ is similar to $M_{12}(t, t')$ but it describes the influence in the opposite direction.

To obtain these matrix terms one must perform the functional derivative on

$S_{eff}[x,x',t]$ with respect to $x^b(t)$ and use that $M_{ab}(t,t') = M_{ba}(t',t)$. Now, differentiating (4.42):

$$\left.\frac{\delta\mathcal{F}[x,x']}{\delta x^a(t),\delta x^b(t')}\right|_{q^a=0} = \left(\frac{i}{\hbar}\right)^2 \int_{q^1(t)=q^2(t)} \mathcal{D}q^a q_a(t) q_b(t') \ \exp\left(\frac{i}{\hbar}S_E[q^a]\right) \times \rho_E(q^1(0),q^2(0),0) \ , \tag{4.45}$$

for t,$t' \in [0,\tau]$. Now we must calculate the four elements that compose $M_{ab}(t,t')$ via (4.44). Starting with $M_{11}(t,t')$:

$$M_{11}(t,t') = (-i\hbar)\left(\frac{1}{\hbar^2}\right)\int_{q^1(t)=q^2(t)} \mathcal{D}q\mathcal{D}q' \ \exp\left(\frac{i}{\hbar}\left(S_E[q]-S_E[q']\right)\right) q_1(t)q_1(t') \times \rho_E(q(0),q'(0),0) \ , \tag{4.46}$$

but $q_1(t) = q^1(t) = q(t)$ and $q_1(t) = q^1(t) = q(t')$, so:

$$M_{11}(t,t') = \frac{i}{\hbar}\left\langle T\left[q(t)q(t')\right]\right\rangle \ . \tag{4.47}$$

Note that the expectation value is evaluated without interactions with the system. Proceeding analogously for the other terms we obtain that:

$$M_{12}(t,t') = \frac{-i}{\hbar}\left\langle q(t')q(t)\right\rangle \ , \tag{4.48}$$

$$M_{21}(t,t') = \frac{-i}{\hbar}\left\langle q(t)q(t')\right\rangle \ , \tag{4.49}$$

$$M_{22}(t,t') = \frac{i}{\hbar}\left\langle \tilde{T}\left[q(t)q(t')\right]\right\rangle \ . \tag{4.50}$$

Hence, writing $S_{eff}[x,x']$ in terms of $x(t)$ and $x'(t')$. Starting from the bilinear form of the $S_{eff}[x,x']$:

$$\begin{aligned} S_{eff}[x,x'] &= \frac{1}{2}\int dt \int dt' \ x^a(t) M_{ab}(t,t') x^b(t') \\ &= \frac{1}{2}\int dt \int dt' \left(x(t)\frac{i}{\hbar}\left\langle T\left[q(t)q(t')\right]\right\rangle x(t') - x(t)\frac{i}{\hbar}\left\langle q(t')q(t)\right\rangle x'(t') \right. \\ &\left. - x'(t)\frac{i}{\hbar}\left\langle q(t)q(t')\right\rangle x(t') + x'(t)\frac{i}{\hbar}\left\langle \tilde{T}\left[q(t)q(t')\right]\right\rangle x'(t') \right) . \end{aligned} \tag{4.51}$$

Introducing the change of variables $x = X + u/2$ and $x' = X - u/2$, and the temporal and anti-temporal orderings:

$$T\left[q(t)q(t')\right] = \theta(t-t')q(t)q(t') + \theta(t'-t)q(t')q(t)\ , \tag{4.52}$$

$$\tilde{T}\left[q(t)q(t')\right] = \theta(t-t')q(t')q(t) + \theta(t'-t)q(t)q(t')\ , \tag{4.53}$$

with $\theta(t'-t) = 1 - \theta(t-t')$. Recall that the step function has the property that if $t \geq t' \implies \theta(t-t') = 1$ and if $t < t' \implies \theta(t-t') = 0$. Combining these terms into the effective action and applying the change of variables:

$$\begin{aligned} S_{eff}[x,x'] = \frac{1}{2}\int dt \int dt' \Bigg\{ & \left(X(t) + \frac{u(t)}{2}\right)\frac{i}{\hbar}\langle T[q(t)q(t')]\rangle \left(X(t') + \frac{u(t')}{2}\right) \\ & - \left(X(t) + \frac{u(t)}{2}\right)\frac{i}{\hbar}\langle q(t')q(t)\rangle \left(X(t') - \frac{u(t')}{2}\right) \\ & - \left(X(t) - \frac{u(t)}{2}\right)\frac{i}{\hbar}\langle q(t)q(t')\rangle \left(X(t') + \frac{u(t')}{2}\right) \\ & + \left(X(t) - \frac{u(t)}{2}\right)\frac{i}{\hbar}\langle \tilde{T}[q(t)q(t')]\rangle \left(X(t') - \frac{u(t')}{2}\right)\Bigg\}\ . \end{aligned} \tag{4.54}$$

Expanding each term individually, for instance, starting with the first product term:

$$\begin{aligned} \left(X(t) + \frac{u(t)}{2}\right)\frac{i}{\hbar}\langle T[q(t)q(t')]\rangle \left(X(t') + \frac{u(t')}{2}\right) = & \\ + X(t)\frac{i}{\hbar}\langle T[q(t)q(t')]\rangle X(t') + X(t)\frac{i}{\hbar}\langle T[q(t)q(t')]\rangle \frac{u(t')}{2} & \\ + \frac{u(t)}{2}\frac{i}{\hbar}\langle T[q(t)q(t')]\rangle X(t') + \frac{u(t)}{2}\frac{i}{\hbar}\langle T[q(t)q(t')]\rangle \frac{u(t')}{2}\ . & \end{aligned} \tag{4.55}$$

The other terms are obtained analogously. Combining each expanded terms we

obtain the full expression for $S_{eff}[x, x']$:

$$\begin{aligned} S_{eff}[x,x'] = \frac{1}{2}\int dt \int dt' \Bigg[& X(t)\frac{i}{\hbar}\Big(\langle T[q(t)q(t')]\rangle - \langle q(t')q(t)\rangle - \langle q(t)q(t')\rangle \\ & + \langle \tilde{T}[q(t)q(t')]\rangle \Big) X(t') + X(t)\frac{i}{\hbar}\Big(\langle T[q(t)q(t')]\rangle + \langle q(t')q(t)\rangle - \langle q(t)q(t')\rangle \\ & - \langle \tilde{T}[q(t)q(t')]\rangle \Big)\frac{u(t')}{2} + \frac{u(t)}{2}\frac{i}{\hbar}\Big(\langle T[q(t)q(t')]\rangle - \langle q(t')q(t)\rangle + \langle q(t)q(t')\rangle \\ & - \langle \tilde{T}[q(t)q(t')]\rangle \Big) X(t') + \frac{u(t)}{2}\frac{i}{\hbar}\Big(\langle T[q(t)q(t')]\rangle + \langle q(t')q(t)\rangle + \langle q(t)q(t')\rangle \\ & + \langle \tilde{T}[q(t)q(t')]\rangle \Big)\frac{u(t')}{2} \Bigg] . \end{aligned} \tag{4.56}$$

Using the properties of the time-ordered and anti-time-ordered products, we have that the first and last terms are zero hence, after simplifying the second and third terms, we obtain that, after defining the functions $D(t, t')$ and $N(t, t')$:

$$D(t,t')X(t)u(t') = \frac{i}{\hbar}\Big(\theta(t'-t)\big[\langle q(t')q(t)\rangle - \langle q(t)q(t')\rangle\big] \Big) X(t)\frac{u(t')}{2} , \tag{4.57}$$

in which,

$$D(t,t') = \frac{i}{\hbar}\theta(t-t')\big\langle [q(t), q(t')]\big\rangle , \tag{4.58}$$

since:

$$\theta(t'-t)\big[\langle q(t')q(t)\rangle - \langle q(t)q(t')\rangle\big] = -\theta(t-t')\big\langle [q(t), q(t')]\big\rangle . \tag{4.59}$$

For the term $N(t, t')$ we obtain:

$$\frac{i}{2}N(t,t')u(t)u(t') = \frac{i}{\hbar}\big(\theta(t-t')\langle q(t)q(t')\rangle + \theta(t'-t)\langle q(t')q(t)\rangle\big)\frac{u(t)}{2}\frac{u(t')}{2} , \tag{4.60}$$

in which:

$$N(t,t') = \frac{1}{2\hbar}\big\langle \{q(t), q(t')\}\big\rangle . \tag{4.61}$$

Collecting the results:

$$D(t,t') = \frac{i}{\hbar}\big\langle\, [q(t), q(t')] \,\big\rangle \theta(t-t') \;, \tag{4.62}$$

$$N(t,t') = \frac{1}{2\hbar}\big\langle \{q(t), q(t')\} \big\rangle \;. \tag{4.63}$$

These are identified as the dissipation and noise kernels, respectively. Substituting these into the action, we get:

$$S_{eff} = \int dt \int dt' \left\{ u(t) D(t,t') X(t') + \frac{i}{2} u(t) N(t,t') u(t') \right\} \;. \tag{4.64}$$

This effective action is the basis for the Langevin equation derivation that will be performed in the next subsection.

4.4 Microscopic Langevin Equation

As written before, the Langevin description allows one to introduce dissipation and fluctuations by a separation of the entire system into relevant and irrelevant degrees of freedom, the system and the environment, respectively, in which the latter acts as a heat bath. Dissipation enters the dynamics of the system variables by ignoring details of the environment and only considering its average effect on the system: This procedure is known as coarse-graining, in which we lose the environmental information. In this procedure, the coarse-graining was performed by tracing out the density matrix over the environmental variables.

Feynman and Vernon showed that the part of the effective action involving the noise kernel can be written in terms of a stochastic force ξ acting on the particle's coordinate, allowing us in this way to obtain an equation of motion for the particle by the principle of stationary action; this equation of motion is a Langevin kind of equation. This feature was used in [45, 21, 16] to obtain a field equation for the quark condensate. The starting step is to consider the following identity:

$$\exp\left(\frac{-1}{2\hbar}\int dt dt' u(t) N(t,t') u(t')\right) = \int \mathcal{D}_\xi P[\xi] \exp\left(\frac{i}{\hbar}\int_0^\infty dt \xi u(t)\right) \;, \tag{4.65}$$

in which $P[\xi]$ is a time-independent Gaussian measure:

$$P[\xi] = \tilde{N} \exp\left(\frac{-1}{2}\int dt dt' \xi(t) N^{-1}(t,t') \xi(t')\right) \;, \tag{4.66}$$

and $\tilde{N}$ is a normalization constant and the stochastic force satisfies the additional properties $\langle \xi \rangle = 0$ and $\langle \xi(t)\xi(t') \rangle = \hbar N(t,t')$.

The procedure to obtain a Langevin equation is the following: substitute the Gaussian identity (4.65) into the path integral representation for the influence action (4.28). Then perform the x and x' integrations by the method of stationary phase. The coupled equations for the stationary paths admit solutions for $x = x'$, and the Langevin equation is the stationary condition for these solutions [46].

Recall that the Feynman-Vernon influence functional $\mathcal{F}[x,x']$ is expressed as $\mathcal{F}[x,x'] = \exp(iS_{eff}[x,x'])$. It's possible to rewrite the total influence functional as:

$$\mathcal{F}[x,x'] = \left\langle \exp\left(\frac{i}{\hbar}\int_{t_i}^{t_f} \chi(t)u(t)dt\right)\right\rangle \ , \tag{4.67}$$

To make this connection, consider the effective action term involving $u(t)$ together with the Gaussian integral representation we derived:

$$\begin{aligned}\exp\left(\frac{i}{\hbar}S_{eff}[x,x']\right) &= \int \mathcal{D}_\xi P[\xi] \exp\left(\frac{i}{\hbar}\int_0^t dt\, \xi(t)u(t)\right) \\ &\quad \times \exp\left(\frac{i}{\hbar}\int_0^t dt_1 \int_0^t dt_2\, u(t_1)D(t_1,t_2)X(t_2)\theta(t_1-t_2)\right) \\ &= \int \mathcal{D}_\xi P[\xi] \exp\left\{\frac{i}{\hbar}\int_0^t dt\, \Big(\xi(t)+\chi(t)\Big)u(t)\right\} \ , \end{aligned} \tag{4.68}$$

in which $\chi(t)$ is defined as:

$$\chi(t) = \int_0^t dt'\, D(t,t')X(t')\theta(t-t') + \xi(t) \ , \tag{4.69}$$

then:

$$\exp\left(\frac{i}{\hbar}S_{eff}[x,x']\right) = \int \mathcal{D}_\xi P[\xi] \exp\left(\frac{i}{\hbar}\int_0^t dt\, \chi(t)u(t)\right) \ . \tag{4.70}$$

The right-hand side of this expression involves an average over the noise through the probability measure $P[\xi]$, hence:

$$\mathcal{F}[x,x'] = \left\langle \exp\left(\frac{i}{\hbar}\int_{t_i}^{t_f} \chi(t)u(t)dt\right)\right\rangle \ , \tag{4.71}$$

The expression $\mathcal{F}[x,x']$ indicates that we are averaging over the noise $\chi(t)$, encapsulating the effects of stochastic fluctuations on the system's evolution. By using the

Gaussian identity (4.65) for the noise term into the influence functional, we have:

$$\mathcal{F}[x,x'] = \int \mathcal{D}_\xi P[\xi] \exp\left(\frac{i}{\hbar}\left[\int_0^t dt_1 \int_0^t dt_2\, u(t_1)D(t_1,t_2)X(t_2)\theta(t_1-t_2) + \int_0^\infty dt\, \xi(t)u(t)\right]\right), \tag{4.72}$$

combining the terms inside the exponential:

$$\begin{aligned}\mathcal{F}[x,x'] &= \int \mathcal{D}_\xi P[\xi] \exp\left\{\frac{i}{\hbar}\int_0^t dt \left(\int_0^t dt'\, u(t)D(t,t')X(t')\theta(t-t') + \xi(t)u(t)\right)\right\} \\ &= \int \mathcal{D}_\xi P[\xi] \exp\left\{\frac{i}{\hbar}\int_0^t dt\, u(t) \right. \\ &\left. \times \left(\int_0^t dt'\, D(t,t')X(t')\theta(t-t') + \xi(t)\right)\right\}. \end{aligned} \tag{4.73}$$

To evaluate this path integral, we use the method of stationary phase [46], valid in the limit where $\hbar \to 0$. The exponent is stationary when its variation with respect to $u(t)$ vanishes. This gives the stationarity condition:

$$\int_0^t dt'\, D(t,t')X(t')\theta(t-t') + \xi(t) = 0\,, \tag{4.74}$$

when $x = x'$, the action becomes:

$$S_{eff}[x,x] = \int_0^t dt_1 \int_0^t dt_2 \left(u(t_1)D(t_1,t_2)X(t_2)\theta(t_1-t_2) + \frac{i}{2}u(t_1)N(t_1,t_2)u(t_2)\right). \tag{4.75}$$

The stationary condition then reduces to a Langevin equation:

$$\frac{\delta S_{eff}[x,x]}{\delta x(t)} = 0\,, \tag{4.76}$$

coming from the stationarity condition for the effective action:

$$\int_0^t dt'\, D(t,t')X(t')\theta(t-t') + \xi(t) = 0 \Rightarrow X(t) = -\int_0^t dt'\, D^{-1}(t,t')\xi(t')\,. \tag{4.77}$$

This is the Langevin equation, which describes how the system's state $X(t)$ evolves under both deterministic forces and stochastic noise, in which $\xi(t)$ represents the stochastic noise.

To obtain the equation of motion generated by the influence action, assume that the system's Lagrangian $L(x, \dot{x}, t)$ is known from the considered action (4.2).

The effective action includes both the original action and the interaction terms due to the environment. The total effective action, considering both the system's Lagrangian and the interaction, is:

$$S_{eff}[x, x'] = S[x] + \int_{t_i}^{t_f} \left(\int_{t_i}^{t} dt' \, D(t, t') X(t') + \xi(t) \right) u(t) \, dt \, . \tag{4.78}$$

To find the equation of motion, we take the variation with respect to $x(t)$:

$$\begin{aligned} \frac{\delta S_{eff}[x, x']}{\delta x(t)} &= \frac{\delta}{\delta x(t)} \left[\int_{t_i}^{t_f} L(x, \dot{x}, t) \, dt + \int_{t_i}^{t_f} \left(\int_{t_i}^{t} dt' \, D(t, t') X(t') + \xi(t) \right) u(t) \, dt \right] \\ &= 0. \end{aligned} \tag{4.79}$$

For the Lagrangian part, the Euler-Lagrange equation is:

$$\frac{\partial L}{\partial x} - \frac{d}{dt} \frac{\partial L}{\partial \dot{x}} = 0. \tag{4.80}$$

And the variation of the interaction term with respect to $x(t)$ involves:

$$\begin{aligned} &\frac{\delta}{\delta x(t)} \int_{t_i}^{t_f} \left(\int_{t_i}^{s} dt' \, D(t, t') X(t') + \xi(t) \right) u(t) \, dt \\ &\frac{\delta}{\delta x(t)} \int_{t_i}^{s} dt' \, D(t, t') X(t') = D(s, t) \, , \end{aligned} \tag{4.81}$$

while the second part is independent of $x(t)$, so its variation is zero. Therefore, the total variation is:

$$\int_{t_i}^{t_f} u(t) D(s, t) \, dt = -\xi(t) \, . \tag{4.82}$$

Finally, combining the Euler-Lagrange equation and the variation of the interaction term, we get:

$$\frac{\partial L}{\partial x} - \frac{d}{dt} \frac{\partial L}{\partial \dot{x}} + \int_{t_i}^{t_f} dt' \, D(s, t') X(t') = -\xi(t) \tag{4.83}$$

In this chapter, we have introduced different concepts related to phase transitions and their phenomenology. In the next chapter, we will turn our attention to the main focus of this dissertation: Quantum Chromodynamics (QCD) and the effects

of strong magnetic fields on it, in which the introductory concepts developed in this chapter will be fundamental.

Chapter 5

Quark Condensate Dynamics under Magnetic Fields

"We thereby discover, in the reality of masses, an algorithmic, precise Music of the Void. It is a modern embodiment of the ancients' elusive, mystical "Music of the Spheres"."

Frank Wilczek

We start this chapter by presenting the mean-field Langevin equation for the quark condensate dynamics under the effect of strong magnetic fields derived in reference [16]. We will not rederive it here, but we will describe the main steps and approximations carried out in [16] and make contact with the detailed derivation of the Langevin equation in the previous chapter. Our task in this dissertation relates to the numerical simulation of that equation. We solve the equation for a high- to low-temperature quench scenario. More specifically, for a situation in which the temperature changes suddenly from a high-temperature value, for which the condensate is zero, to a lower temperature for which the condensate is not zero. By solving the Langevin field equation under such conditions one has access to the time scales associated with the transition from a chiral-symmetry restored phase to a chiral-symmetry broken phase.

Such a quench scenario is well known in the context of spin systems in condensed matter physics, namely: the system is subjected to a sudden change of temperature, from a temperature above critical temperature to one below it, so that the system is driven irreversibly from a spin-disordered phase toward a spin-ordered phase. The quench scenario for which we solve the Langevin equation resembles the QGP evolution in a heavy-ion collision. Of course, in the real situation, the change is not sudden, but very fast. Therefore, our quench scenario should be taken as an

idealization of the real situation. Given the resemblance to a heavy-ion situation, we include at the end of this chapter a short discussion about the time evolution of the QGP in a typical collision. The numerical results of our simulations are presented in Chapter 6.

5.1 Mean-Field Langevin Equation for the Quark Condensate

Here we present the mean-field Langevin equation for the quark condensate (σ field in the LSMq) under a strong magnetic field derived in [16]. That derivation was based on previous works not related to magnetic fields, namely [45, 20, 22, 53, 54]. We start this section by discussing the relevance and necessity of amalgamating the knowledge that we have discussed until now in this dissertation.

For the sake of investigating the magnetic field effect on the chiral condensate dynamics, we will address the dynamics with the Langevin equation, which is widely used in QFT treatments of dynamical phase transitions. For examples, see [43, 55]. For zero magnetic fields, there is a vast literature on the use of Langevin field equations in this context, for instance, refereces [56, 53, 19, 20, 57, 58, 21, 59], of which are either postulated on phenomenological grounds [53, 57, 58, 59] or derived from a microscopic model through a coarse-graining procedure [56, 19, 21]. In this dissertation, we have derived and adopted a coarse-grained Langevin equation by employing the CTP formalism.

We will turn our attention to the procedure performed in [16], in which the condensate dynamics is subject to a non-zero magnetic field and is governed by a Langevin field equation. The starting point is to address the condensate dynamics by adopting a model featuring the chiral symmetry of QCD the Lagrangian being that of the Linear-Sigma Model with quarks, in which quarks replace the nucleons of the original model [17] . The model does not describe quark confinement. Despite this, it describes many of the equilibrium, time-independent magnetic field effects on the QCD equation of state, phase structure, and chiral condensate. For the sake of readability, we will rewrite below the Lagrangian of the Linear-Sigma Model with quarks (LSMq) given in (2.90):

$$\mathcal{L} = \bar{q}[i\partial\!\!\!/ - g(\sigma + i\gamma^5 \tau \cdot \boldsymbol{\pi})]q + \frac{1}{2}\left[\partial_\mu \sigma \partial^\mu \sigma + \partial_\mu \boldsymbol{\pi} \cdot \partial^\mu \boldsymbol{\pi}\right] - U(\sigma, \boldsymbol{\pi}), \tag{5.1}$$

in which we redefined g_π as g and $U(\sigma, \boldsymbol{\pi})$ is given by

$$U(\sigma, \boldsymbol{\pi}) = \frac{\lambda}{4}\left(\sigma^2 + \boldsymbol{\pi}^2 - f_{\boldsymbol{\pi}}^2 + \frac{m_\pi^2}{\lambda}\right)^2 - f_\pi m_\pi^2\,\sigma - U_0, \tag{5.2}$$

One can fit the parameters of the model to chiral physics observables. For example, choosing $\lambda = 20$, leads to a classical sigma mass, $m_\sigma^2 = 2\lambda^2 f_\pi^2 + m_\pi^2 \approx 604$ MeV. The parameter g plays an important role in the equilibrium thermodynamics of the model. When solving the model in the mean field approximation for zero baryon chemical potential, one obtains a first-order transition at a temperature $T \simeq 123$ MeV with $g = 5.5$, a second-order transition at $T \simeq 140$ MeV with $g = 3.63$, and a crossover at $T \simeq 150$ MeV with $g = 3.3$ [45, 21]. As in [16], we restrict our study of the condensate's dynamics to the situation of a crossover. The model has also been used to study equilibrium and time-independent magnetic field effects on the QCD equation of state, phase structure, and chiral condensate. For further references, we direct the reader to [60, 61, 62].

In the derivation of the Langevin field equation in [16], the quarks are in equilibrium at some local temperature and local magnetic field. The magnetic field enters the LSMq Lagrangian by performing the substitution $\partial_\mu \to D_\mu = \partial_\mu + iqA_\mu$, in which q stands for quark or pion electric charge and A_μ is the electromagnetic vector field. In reference [16], the pion dynamics were neglected and the magnetic field was taken as a background field, not a dynamical degree of freedom. The authors in [16] argue that the pion would affect mainly the dissipation coefficient (see below) and not other dynamical properties.

The mean field Langevin equation was derived from an effective action using the closed-time path (CTP) formalism, following essentially the same steps as we have discussed in chapter (3). The magnetic field is assumed constant and taken pointing in the z-direction, and the field is assumed to be z-independent. The Langevin field equation that we solve in this dissertation is given by:

$$\frac{\partial^2\sigma(t,\boldsymbol{x})}{\partial t^2} - \nabla^2\sigma(t,\boldsymbol{x}) + \eta_{T,B}\frac{\partial\sigma(t,\boldsymbol{x})}{\partial t} + F_\sigma = \xi_{T,B}(t,\boldsymbol{x})\ , \tag{5.3}$$

where $\boldsymbol{x}$ stands for $\boldsymbol{x}_\perp = (x, y)$. In addition, F_σ is the free energy given by

$$\begin{aligned} F_\sigma &= \frac{\delta U[\sigma]}{\delta\sigma(t,x)} + g\rho_s(\sigma_0) \\ &= \lambda\sigma\left(\sigma^2 - f_{\boldsymbol{\pi}}^2 + \frac{m_\pi^2}{\lambda}\right) - f_\pi m_\pi^2 + g\rho_s^B(\sigma_0) + g\rho_s^{BT}(\sigma_0)\ , \end{aligned} \tag{5.4}$$

in which we used (5.2) for $U[\sigma]$ and the terms $\rho_s^B(\sigma_0)$ and $\rho_s^{TB}(\sigma_0)$ are contributions to the scalar density $\rho_s(\sigma_0)$; the first term depends only on B and the second on T and B:

$$\rho_s^B(\sigma_0) = -\frac{N_c}{2\pi^2}\, m_q \sum_{f=u,d} |q_f B| \left[\ln\Gamma(x_f) - \frac{1}{2}\ln 2\pi + x_f - \frac{1}{2}(2x_f - 1)\ln x_f\right] , \quad (5.5)$$

$$\rho_s^{BT}(\sigma_0) = -\frac{N_c}{\pi^2} m_q \big(|q_u B| + |q_d B|\big) \int_0^\infty dp_z \frac{n_F(E_q(p_z))}{E_q(p_z)} \quad (5.6)$$

in which $N_c = 3$ is the number of colors, q_f is equal to $2/3\,e$ for the u quark and -1/3 e for the d quark, $x_f = m_q^2/2|q_f B|$, and Γ is the Euler gamma function. The $\eta_{T,B}$ is the dissipation coefficient, which is taken as momentum independent to arrive at (5.3)) is given by:

$$\eta_{T,B} = g^2 \frac{N_c}{4\pi} \left[1 - 2n_F(m_\sigma/2)\right] \frac{1}{m_\sigma^2} (eB) \sqrt{m_\sigma^2 - 4m_q^2} \,, \quad (5.7)$$

in which, n_F is the Fermi-Dirac distribution. Note that flavor symmetry is used in the above expressions $m_u = m_d = m_q = g\sigma_0$. The quantity $\eta_{T,B}$ also controls the fluctuations as it enters in the noise correlation function:

$$\langle \xi_{T,B}(t, \boldsymbol{x})\, \xi_{T,B}(t', \boldsymbol{x}')\rangle = \eta_{T,B}\, m_\sigma \coth(m_\sigma/2T)\, \delta(t - t')\, \frac{1}{L}\, \delta(\boldsymbol{x} - \boldsymbol{x}'). \quad (5.8)$$

These quantities depend on m_σ and m_q which, in turn, depend on T and eB, implying they are not put in by hand, but calculated. The factor $1/L$ comes from the fact that the field dynamics of σ occur in the (x, y) plane (but the mass dimension of σ is still 1).

Let us briefly discuss how one arrives at this equation from the derivations by the authors of reference [16]. In chapter (3.1), we have derived a Langevin equation in the context of quantum mechanics by adopting the CTP formalism and the Feynman-Vernon procedure, which led us to a stochastic equation of motion for the coordinate of the particle. In [21, 45, 63], the derivation was done in the context of quantum field theory. The starting point is a semiclassical effective action given in terms of the $\sigma^\pm$ mean field and the quark propagators S_{++}, S_{--}, and $S_\pm$, all defined on the CTP contour discussed in chapter (3.1). Specifically, the semiclassical effective action was taken as:

$$\Gamma[\sigma, S] = \Gamma_{\rm cl}[\sigma] + i\,\mathrm{Tr}\ln S - i\,\mathrm{Tr}\left(i\not{\partial} - m_0\right) S + \Gamma_2[\sigma, S]\,, \quad (5.9)$$

where $\Gamma_2[\sigma, S]$ contains the 2PI diagrams, for which it was taken the fermion tadpole:

$$\Gamma_2[\sigma, S] = g \int_{\mathcal{C}} d^4x \, \mathrm{tr} \left[S^{++}(x,x)\sigma^+(x) + S^{--}(x,x)\sigma^-(x) \right] , \tag{5.10}$$

where $\mathcal{C}$ denotes the CTP contour and tr means trace over color, flavor, and Dirac indices. The two fields $\sigma^{\pm}(x)$ are not independent; they satisfy a boundary condition for large τ (see Fig. 4.1) for all x; there is a single mean field $\sigma(x)$ given by the equation of motion motion [46]:

$$\frac{\delta\Gamma[\sigma,S]}{\delta\sigma^+(x)}\Big|_{\sigma^+=\sigma^-=\sigma} = \frac{\delta\Gamma[\sigma,S]}{\delta\sigma^-(x)}\Big|_{\sigma^+=\sigma^-=\sigma} = 0 \, . \tag{5.11}$$

Next, quarks are integrated out by using their equation of motion obtained by varying the action w.r.t. to the components of S:

$$\frac{\delta\Gamma[\sigma,S]}{\delta S^{ab}(x,y)} = 0 \, , \tag{5.12}$$

which leads to

$$\left(i\not{\partial} - g\sigma_0(x)\right) S^{ab}(x,y) - \int_{\mathcal{C}} d^4z \, \frac{\delta\Gamma_2[\sigma,S]}{\delta S^{ac}(x,z)} \, S^{cb}(z,y) = i\delta^{ab}\delta^{(4)}(x-y) \, . \tag{5.13}$$

The above equations of motion are very difficult to solve, even numerically. A treatable approximate scheme to solve this equation is to "expand around the local equilibrium", in a sense similar to the hydrodynamic description of many-particle systems. That is, the full σ and S are written as a sum of terms with the leading contribution being the corresponding equilibrium quantities σ_0 and S_{thm} at fixed values of temperature T and magnetic field. Specifically:

$$\sigma^a(x) = \sigma_0^a(x) + \delta\sigma^a(x) \, , \tag{5.14}$$

$$S^{ab}(x,y) = S^{ab}_{\mathrm{thm}}(x,y) + \delta S^{ab}(x,y) + \delta^2 S^{ab}(x,y) + \cdots \, , \tag{5.15}$$

in which the leading terms are solutions of

$$\frac{\delta\Gamma_{\mathrm{cl}}}{\delta\sigma_0^a(x)} = -g\mathrm{Tr}S^{aa}(x,x) \, , \tag{5.16}$$

$$\left[i\not{\partial} - m_0 - g\,\sigma_0(x)\right] S^{ab}_{\mathrm{thm}}(x,y) = -i\delta^{ab}\delta^{(4)}(x-y) \, . \tag{5.17}$$

The terms $\delta S^{ab}(x,y)$ and $\delta^2 S^{ab}(x,y)$ are constructed iteratively [64, 45, 16].

Now, the variation of $\Gamma[\sigma, S]$ w.r.t. $\sigma^{\pm}$ to obtain an e.o.m. is not possible because the action is complex. The Feynman-Vernon trick is used to identify the imaginary part with a noise source coupling linearly to the field and then a real action is obtained and the variation w.r.t. σ leads to the following Langevin equation [16]:

$$\partial_\mu \partial^\mu \sigma(x) + \frac{\delta U[\sigma]}{\delta \sigma(x)} + g\rho_s(\sigma_0) - D_\sigma(x) = \xi(x)\,, \tag{5.18}$$

where $\rho_s(\sigma_0)$ is the scalar density

$$\rho_s(\sigma_0) = \mathrm{tr}\, S^{++}_{thm}(x,x)\ , \tag{5.19}$$

and $D_\sigma(x)$ is the dissipation kernel:

$$D_\sigma(x) = ig^2 \int d^4y\, \theta(x^0 - y^0)\, M(x,y)\, \sigma(y)\,, \tag{5.20}$$

$$M(x,y) = \mathrm{tr}\left[S^{+-}_{thm}(x,y) S^{-+}_{thm}(y,x) - S^{-+}_{thm}(x,y) S^{+-}_{thm}(y,x)\right]\ , \tag{5.21}$$

and, finally, the noise field $\xi(x)$ has zero mean and correlation

$$\langle \xi(x) \rangle_\xi = 0 \ \text{ and } \ \langle \xi(x)\xi(y) \rangle_\xi = N(x,y)\,, \tag{5.22}$$

where the noise kernel $N(x,y)$ is given by

$$N(x,y) = -\frac{1}{2} g^2 \mathrm{tr}\left[S^{+-}_{thm}(x,y) S^{-+}_{thm}(y,x) + S^{-+}_{thm}(x,y) S^{+-}_{thm}(y,x)\right]\ . \tag{5.23}$$

in which the noise average is a functional average with the probability distribution depending on the inverse of the $N(x,y)$ kernel:

$$P[\xi] = \exp\left[-\frac{1}{2}\int d^4x d^4y\, \xi(x) N^{-1}(x,y)\, \xi(y)\right]\ . \tag{5.24}$$

To arrive at (5.3) a series of simplifications and approximations were made in [63] in different steps. The first set of steps is the following: 1) the magnetic field is taken to be constant and lying along the z-direction, and 2) memory effects are treated in the so-called *linear harmonic approximation* [65, 19]. These simplifications will lead to a Langevin equation in momentum space with a momentum-dependent dissipation parameter $\eta(\boldsymbol{p}_\perp)$. That equation is given by equation [55] in [16], which

we do not repeat here. The second set of simplifying approximations leading to (5.3) is the following: 1) the dynamics is restricted to the plane perpendicular to the magnetic field, 2) the momentum dependence in the dissipation coefficient is neglected, and 3) a soft-mode frequency approximation is made in different places in that $E_\sigma(\boldsymbol{p}) = \sqrt{\boldsymbol{p}^2 + m_\sigma^2} \simeq m_\sigma$ to simplify integrals. Finally, by performing a Fourier transform in the resulting equation, one obtains (5.3) that we consider in this dissertation.

Before we proceed to the discussion regarding the numerical method used to solve the Langevin field equation, we present the situation we are interested in investigating and the adopted simplifications. Firstly, since the magnetic field is constant and fixed in the z-direction, we focus on the dynamics of the quark condensate in the plane (x, y)-plane, perpendicular to the magnetic field. This leads to some subtleties. First, the Laplacian in (5.3) acts only on the $\boldsymbol{x}_T = (x, y)$ coordinates. Therefore, the noise field will depend only on $\boldsymbol{x}_T$. Finally, the assumption that the magnetic field is constant may be justified since the presence of the magnetic field leads to currents due to the Faraday induction that sustains the magnetic field [66, 16].

Furthermore, we consider the σ dynamics under a temperature quench scenario: a sudden drop in the temperature drives the system out of a high-temperature phase, in which $\sigma \approx 0$, and forces the system to evolve to a lower temperature phase in which $\sigma \neq 0$. We take as lower temperature phase one around the $B = 0$ pseudocritical temperature; that is, at $t = 0$ the system is brought to one of the local maxima of the V_{eff}.

Another simplification was that we neglected the system's expansion, which is perhaps the most relevant trait of a heavy-ion collision that needs to be taken into account when simulating a real laboratory event. However, such a simulation is out of the scope of this work. As such, we do not consider the complex magnetohydrodynamics that govern the magnetic field in the medium expansion course. The magnetic field weakens as the system expands, but as discussed, it also induces electric currents that can sustain a magnetic field of sizeable strength while the system exists. This feature, to some extent, justifies the assumption of a constant magnetic field as assumed above. Finally, we do not consider reheating, energy transfer between the condensate and the background. Reheating changes the local temperature of the background and, as for zero magnetic fields, can affect the dynamics. We reserve for further studies the inclusion of the neglected effects [16].

After the introduction of the adopted model, we are finally in the position to solve numerically the expression (5.3) for the regime of long times. Furthermore, we

will also numerically explore and discuss the physics behind the magnetic damping, time scale, and scalar density. For this sake, in the next chapter, we will develop and examine numerical methods employed to simulate the dynamics of the equation (5.3).

5.2 Relativistic Heavy-Ion Collisions

Here we will not discuss in detail the characteristics involved in each step of a relativistic heavy ion collision but, point out some general aspects of the main phases that occur in an experiment. For a deeper discussion involving the phases of a collision, we refer the reader to the references [67, 68, 69, 70], for instance.

One of the most important tools to probe QCD phenomenology is due to extensive experimental work currently being done with heavy ion collisions, for example, at the Relativistic Heavy Ion Collider (RHIC) and the Large Hadron Collider (LHC). These facilities allow us to probe QCD under extreme temperatures and densities in the thermal (or hot) QCD realms. Experimentally these conditions are achieved via the high-energy collisions of heavy ions. In the past decades, a plethora of substantial data was collected at RHIC and the LHC, including the interaction of quarks and gluons at different scales, hydro-dynamics at the nucleon scale, the phase diagram of nuclear matter, properties of the Quark-Gluon Plasma (QGP) and many more properties of the rich and challenging theory of QCD [71].

Collisions of large nuclei[1] create a plasma of quarks and gluons with the properties of the early Universe, including an extraordinarily high temperature. These facilities allow us to experimentally probe the regime of QCD that lies at the intersection of nuclear physics with many-body quantum field theory, relativistic fluid dynamics, and condensed matter.

In the figure (5.1), we provide a simplified overview of the different stages that occur in heavy-ion collisions.

[1]Different types of nuclei can be used during a collision: the most common examples are Lead (Pb) and Gold (Au) which have been widely adopted at CERN and RHIC, for instance.

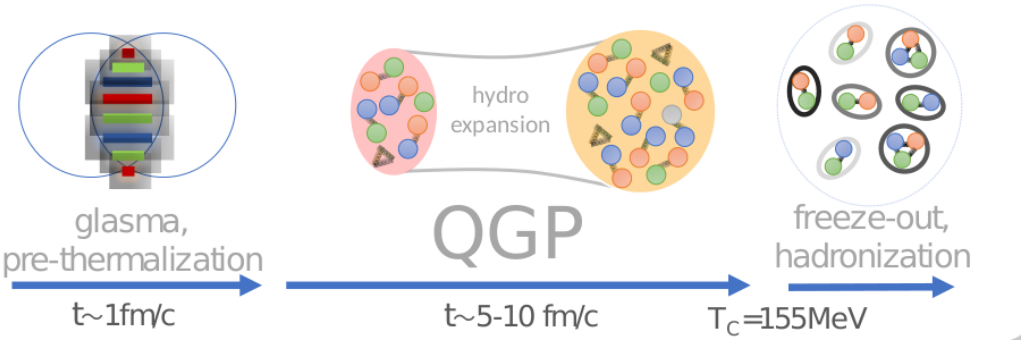

Figure 5.1: Overview of the different stages of a heavy ion collision. We also express the approximate time duration of each part of the process and the critical temperature in which we have the transition from QGP to hadronization in units of fm/c.Extracted from [72].

In heavy-ion collisions, after the pre-thermalization phase, a transition from a QGP phase to a hadron-dominant one occurs. In 2011 the search for phase transition in relativistic heavy-ion collisions started. Before that, quark-gluon plasma (QGP) at RHIC was created in Au+Au collisions at 200 GeV energy measured in the nucleon-nucleon center of mass reference frame.

Let's briefly discuss the steps involved in a relativistic heavy-ion collision based on the picture (5.1). In the first moments of the collision, when the two beams (composite of confined quarks and gluons in the hadronic matter) collide with relativistic velocity, they form a non-thermalized or pre-thermalized state with strongly interacting fields named glasma as depicted in the first picture from left to right in figure (5.1). At this moment, a significant fraction of the incoming kinetic energy is deposited in the central region leading to a high-energy-density and highly non-equilibrium state. The glasma is considered a precursor to the quark-gluon plasma (QGP) since it represents the initial, non-equilibrium stage of the collision before it thermalizes into the QGP. Before the collision, the nuclei are in a state called Color Glass Condensate (CGC): in this state, the gluon density is extremely high and when two CGC states collide, they create the glasma. For a broader discussion about this topic, we indicate the reference [70].

In the stage after the pre-thermalization, we have the formation of the Quark-Gluon Plasma (QGP) due to the fragmentation of the collided matter into a strongly interacting state of deconfined quarks and gluons. This phase occurs by providing enough kinetical energy in the collision to convert it into thermal energy. While firstly was expected to be similar to an electromagnetic plasma, by now it is well established that it is more similar to a strongly interacting fluid. Therefore, it is

often described by relativistic hydrodynamics models [68]. The transition between the pre-thermalization phase and the creation of QGP can be studied by adopting non-equilibrium methods [69] and by the QCD phase transition of deconfinement [40]. Recent analyses indicate a crossover from the hadronic phase to the quark-gluon plasma for realistic u, d, and s quark masses [10, 73]. The pseudo-critical temperature T_{pc}, which characterizes the crossover location, is around $T_c = 158.0 \pm 0.6$ MeV in agreement with the previously obtained temperature of $T_c = 156 \pm 1.5$ MeV by employing LQCD methods [25, 74]. In the crossover transition, there is no real distinction between hadronic matter and the QGP. It occurs in a small temperature interval and leads to a quick change in entropy and energy density implying large fluctuations of energy and net quark number densities[75].

An important trait in investigating relativistic heavy-ion collisions is the effect of magnetic fields which emerges in the earliest moments after the collision. These extremely strong magnetic fields, albeit with an intensity that quickly decays, are generated by the nucleons involved in the collision. The influence of this magnetic field in the formation of the quark condensate is the central topic of investigation of this dissertation.

The magnetic field created in non-central collisions in heavy ion experiments at RHIC-BNL and the LHC-CERN is possibly the highest since the epoch of the electroweak phase transition, reaching values as high as $B \approx 10^{19}$ G $(eB \approx 6m_{\pi}^2)$ for peripheral collisions at RHIC and even much higher at the LHC due to the fluctuations in the distribution of protons inside the nuclei [4, 76, 77], for instance, noncentral Pb-Pb collisions at LHC can produce fields of strengths as large as $eB = 15m_{\pi}^2$[3, 2]. The scale $eB \approx 6m_{\pi}^2$ is often used to characterize the magnetic field strength at which significant effects on chiral symmetry breaking and restoration are expected.

These magnetic fields are created due to the fact that the heavy ions are accelerated to velocities close to the speed of light. At these high speeds, the ions carry significant electric charges moving at relativistic speeds. Due to relativistic effects, the electric fields associated with the moving ions are Lorentz-contracted into thin pancake-like distributions, perpendicular to the direction of motion. When the ions collide, their electric fields interact. The highly charged ions moving at relativistic speeds can be considered as large electric currents thus, according to Ampère's Law, moving electric charges create magnetic fields. The magnetic field strength is highly dependent on the impact parameter, which is the perpendicular distance between the centers of the two colliding ions [66]. For peripheral collisions, there is a significant current due to

the sideways motion of the ions, which results in strong magnetic fields perpendicular to the trajectories, as depicted in the picture (5.2). These fields are short-lived, typically existing for only a few femtoseconds (10^{-15} s) [66, 78].

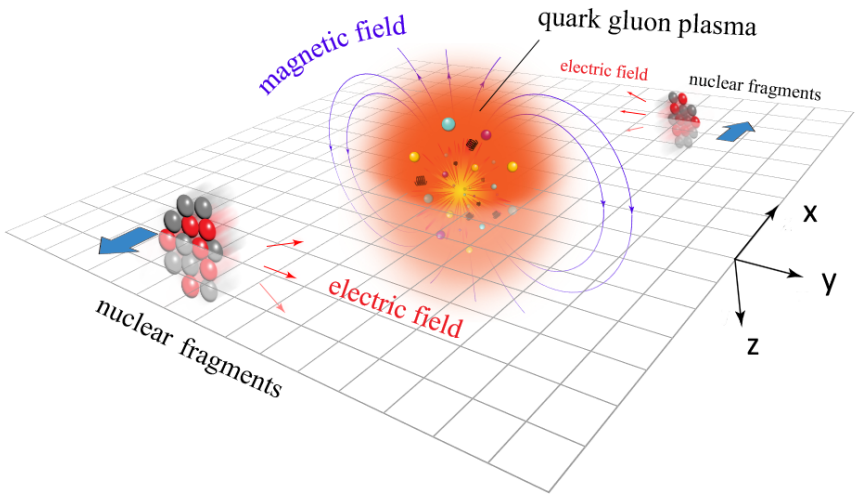

Figure 5.2: Sketch of a non-central heavy-ion collision in the lab frame. After the collision, the nucleons create a hot and dense QGP medium, and the nuclear fragments generate strong electromagnetic fields.Adapted from [66].

In the next section, we are going to present the mean-field Langevin equation that we will adopt to address the quark condensate dynamics under the effect of strong magnetic fields. The derived quantities [16] that enter the equation will also be presented and discussed.

Chapter 6

Numerical Results

6.1 Discretization of the Stochastic GLL Equation

Recall that we want to discretize the following Langevin equation:

$$\frac{\partial^2\sigma(t,\boldsymbol{x})}{\partial t^2} - \nabla^2\sigma(t,\boldsymbol{x}) + \eta_{T,B}\frac{\partial\sigma(t,\boldsymbol{x})}{\partial t} + F_\sigma = \xi_{T,B}(t,\boldsymbol{x}) \ , \tag{6.1}$$

where F_σ is given in (5.4). We stress that the discretization of the equation will be done in the transversal direction of the magnetic field and that the field σ is taken as independent of the z direction, the direction in which the magnetic field points. We will start the discretization procedure by considering $\Delta x = \frac{L}{N}$, being the spatial discrete lattice spacing, in which Δx is the spatial step taken as $\Delta x = 0.1$, L the size of a lattice's side and N the total number of points in each one of the lattice's directions. The temporal discretization is given by $\Delta t = \frac{t}{n}$, in which $n = 1000$ is the number of time steps and we have considered a simulation running from an initial time of $t = 0$ fm until $t = 10$ fm, hence the time interval is divided into pieces with size $\delta t = 0.01$. Since we are dealing with white noise, the ambiguities regarding time discretization in stochastic equations are of no concern here [23, 57]. We discretize σ on a spatial lattice, acquiring a discrete form σ_i^n, in which the term n encodes the time discretization regarded as the number of simulation steps. Consequently, one may rewrite the discretizations as $t = n\Delta t$ with $n = 0, 1, 2, \ldots$N, $x = i\Delta x$.

We solve the GLL equation by imposing periodic boundary conditions (PBC) in the spatial directions. Thus:

$$\sigma^n_{j(N+1)} = \sigma^n_{1j} \ , \tag{6.2}$$

$$\sigma^n_{i(N+1)} = \sigma^n_{i1} \ , \tag{6.3}$$

must be applied to the spatial directions of the lattice. Now we will turn our attention to discussing the discretization of the terms present in the *GLL* equation to develop an iterative method to solve it. Starting with the Laplacian, by employing the

method of finite differences, we may write the 2D Laplacian as:

$$\begin{aligned}\nabla^2\sigma_i^n &= \frac{\partial^2\sigma_i^n}{\partial^2 x} + \frac{\partial^2\sigma_i^n}{\partial^2 y} \\ &= \left[\left(\frac{\sigma^n_{(i+1)j} - \sigma^n_{ij}}{a}\right) - \left(\frac{\sigma^n_{ij} - \sigma^n_{(i-1)j}}{a}\right)\right] + \left[\left(\frac{\sigma^n_{i(j+1)} - \sigma^n_{ij}}{a}\right) - \left(\frac{\sigma^n_{ij} - \sigma^n_{i(j-1)}}{a}\right)\right] \\ &= \frac{1}{a^2}\left[\sigma^n_{(i+1)j} - 2\sigma^n_{ij} + \sigma^n_{(i-1)j} + \sigma^n_{i(j+1)} + \sigma^n_{i(j-1)} - 2\sigma^n_{ij}\right] \\ &= \frac{1}{a^2}\left[\sigma^n_{(i+1)j} + \sigma^n_{(i-1)j} + \sigma^n_{(i-1)j} + \sigma^n_{i(j+1)} - 4\sigma^n_{ij}\right] \ . \end{aligned} \tag{6.4}$$

This is a discrete expression for the Laplacian in the spatial coordinate, indexed by i and j, the lattice indexes. Note that we must impose the PBC given by eq.(6.3) in each step of the evaluation of the Laplacian. For clarity purposes, we introduce the compact notation:

$$\nabla^2\sigma^n_{ij} = (L\sigma)^n_{ij} \ . \tag{6.5}$$

Finally, we will be interested in the dynamics of the chiral quark condensate in the $\hat{i}\hat{j}$ plane, hence, the Laplacian indeed only contains the contributions of these directions while the $\hat{k}$ direction is kept constant, implying that its derivative is zero.

Following this, we will turn our attention to the time derivatives, that have been performed by the leapfrog algorithm [22, 23], given by:

$$\begin{aligned}\frac{\partial\sigma_n}{\partial t} = \dot{\sigma}_n &= \frac{1}{2}\left(\dot{\sigma}_{n+1/2} + \dot{\sigma}_{n-1/2}\right) \ , \\ \dot{\sigma}_{n+1/2} &= \frac{1}{\Delta t}\left(\sigma_{n+1} - \sigma_n\right) \ , \\ \frac{\partial^2\sigma_n}{\partial t^2} = \ddot{\sigma}_n &= \frac{1}{\Delta t}\left(\dot{\sigma}_{n+1/2} - \dot{\sigma}_{n-1/2}\right) \ ; \end{aligned} \tag{6.6}$$

Note that to employ the algorithm, one must define, before the beginning of the simulation, the fields σ^n and $\sigma^{n-\frac{1}{2}}$. In this work, we have assumed that these initial fields are random real numbers, whose values are extracted from a Gaussian function with null mean and standard deviation equal to unity. It is important to stress that these generated numbers are not actually random, but pseudorandom numbers, in other words, these numbers can be determined. To increase the randomness of the generated lattice, we have provided it with new seeds for each new round of random number generation before we initialize the random number generator. This seed [1]

[1] It's noteworthy to briefly discuss how the seed generation algorithm works: in a simplified view, the function's input is the hour from the computer's clock. The algorithm precision is in the order

is fundamental to initialize the random number generator since it is entered as the input of the Gaussian random numbers. Finally, it's important to stress that the following simulations are performed for one noise family, in other words, we have just one generator for the seeds thus, the noise family average is equal to the unity.

Using the discretized quantities derived above we obtain the following:

$$\frac{1}{\Delta t}\left(\dot{\sigma}_i^{n+1/2} - \dot{\sigma}_i^{n-1/2}\right) = \quad (L\sigma)_i^n - \eta\frac{1}{2}\left(\dot{\sigma}_i^{n+1/2} + \dot{\sigma}_i^{n-1/2}\right) - F_\sigma + \xi(T,B)\ , \quad (6.7)$$

Therefore, the equation that we must solve iteratively is:

$$\left\{1 + \frac{1}{2}\eta\Delta t\right\}\dot{\sigma}_i^{n+1/2} = \left\{1 - \frac{1}{2}\eta\Delta t\right\}\dot{\sigma}_i^{n-1/2} + (L\sigma)_i^n\,\Delta t - F_\sigma\left(\sigma_i^n\right)\Delta t + \xi(T,B)\Delta t\ , \quad (6.8)$$

or, in a more compact notation:

$$\dot{\sigma}_i^{n+1/2} = \frac{1}{\Xi}\left[\dot{\sigma}_i^{n-1/2}\Theta + (L\sigma)_i^n\,\Delta t - F_\sigma\left(\sigma_i^n\right)\Delta t + \xi(T,B)\Delta t\right]\ , \quad (6.9)$$

where

$$\Xi = 1 + \frac{1}{2}\eta_{B_T}\Delta t\ , \quad (6.10)$$

$$\Theta = 1 - \frac{1}{2}\eta_{B_T}\Delta t\ . \quad (6.11)$$

The field is updated by

$$\sigma_i^{n+1} = \sigma_i^n + \Delta t\,\dot{\sigma}_i^{n+1/2} \quad (6.12)$$

Note that to perform the leapfrog algorithm, we must keep track of the three fields simultaneously during the simulation. Since the leapfrog algorithm relies upon the method of finite differences to evaluate both time and spatial derivatives, one must investigate the stability and the convergence of the finite differences method in the scope of a stochastic simulation. This discussion was done in some detail in [22, 23].

of milliseconds.

6.2 Numerical Results

Before we present the numerical results, we will briefly discuss the programming techniques adopted in this work. The simulations performed throughout this text were written in Python due to its clean syntax. Since it's an interpreted language, in other words, the source code of a program is converted into bytecode that is then executed by the Python virtual machine, in general, is not as fast as a compiled language as C or C++. On the other hand, Python is very efficient in performing numerical calculations due to several external libraries that one may include in the workspace.

One of these external libraries is the *Numpy*, which offers optimized numerical operations on arrays and matrices. Furthermore, special mathematical functions and stable random number generators are also present in the library and were adopted in this work. Another external library employed in this work is *SciPy*, which contains modules for linear algebra, integration, special functions, Fourier Transforms, and many numerical functions.

Data plots found in the results are generated with the *Matplotlib* library for *Python*, a tool for creating static, animated, and interactive visualizations in Python. This library was chosen since *Numpy* quantities are well interpreted by the Matplotlib.

In the next subsection, we will start presenting the numerical results.

6.2.1 Dissipation Coefficient, Sigma, and Quark Masses.

We will start reproducing the results presented in [16] regarding how the temperature and magnetic field affect the values of the dissipation coefficient $\eta_{T,B}$, and the σ and the quark masses.

Table 6.1 shows the values of the dissipation coefficient $\eta_{T,B}$ for the magnetic field eB and temperature T values we use in our study. Recall that the expression for $\eta_{T,B}$ is given in (5.7). It involves $\sqrt{m_\sigma^2 - 4m_q^2}$, which means that $\eta_{T,B}$ is nonzero for $m_\sigma^2 \geq 4m_q^2$ only. This is the condition behind the physical mechanism behind the dissipation, the decay $\sigma \to q\bar{q}$. Pions will also contribute to dissipation when the condition $m_\pi^2 \geq 4m_q^2$ is satisfied. But this is not the only possible decay, there is also $\sigma \to 2\pi$. At the temperatures we consider here, the second decay is not allowed, but the first is allowed. As such, one effect one can expect when including pions is that they increase $\eta_{T,B}$.

At this point, it is interesting to compare (5.7) with the corresponding coefficient

T_{quench} [MeV]	$\eta_{T,B}$ [fm^{-1}]
$eB = 25m_\pi^2$	
50	3.13
100	2.88
$eB = 20m_\pi^2$	
50	2.55
100	2.23

Table 6.1: Values of the dissipation coefficient $\eta_{T,B}$ for values of temperature and magnetic field used to generate Fig. 6.3 to Fig. 6.9.

for zero external magnetic fields, in which case it is given by [64, 45]:

$$\eta_{T,0} = g^2 \frac{N_c}{4\pi} \left[1 - 2n_F(m_\sigma/2)\right] \frac{1}{m_\sigma^2} \left(m_\sigma^2 - 4m_q^2\right)^{3/2} . \tag{6.13}$$

Although the expression looks similar and the condition $m_\sigma^2 \geq 4m_q^2$ is the same as before, the magnetic field changes completely the temperature dependence. When the magnetic field is equal to zero, the term $m_\sigma^2 - 4m_q^2$ is positive only for temperatures larger than $T = 150$ MeV. The magnetic field increases both m_σ and m_q (magnetic catalysis), as shown in Figs. 6.1 and 6.2.

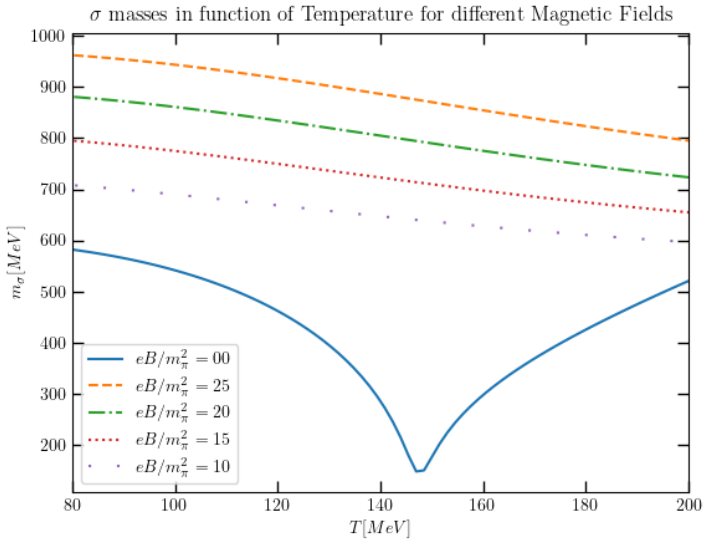

Figure 6.1: Temperature and magnetic field dependence of the σ mass for different values of the magnetic field.

Figures (6.1) and (6.2) show the temperature dependence of, respectively, the σ mass and of constituent quark masses for different values of the magnetic field.

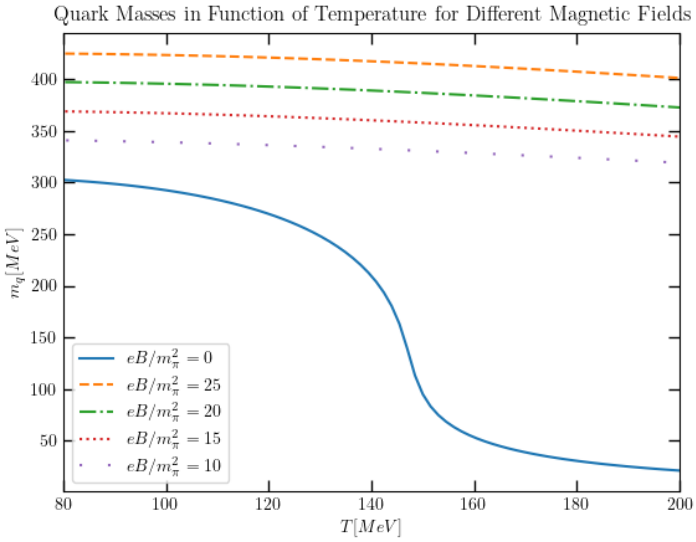

Figure 6.2: Temperature dependence of the constituent quark mass for several values of the magnetic field.

Again we obtain two different situations that depend on the presence or absence of the magnetic field. For $B = 0$ values m_σ, around $T_{pc} = 150$ MeV has its minimum value, and, for values below and above this value, m_σ increases.The quark masses possess a different behavior: for values above the pseudo-critical temperature, the quark masses are enhanced, while for values below it, the quark masses decrease. For the values of $B \neq 0$, both m_q and m_σ increase as the temperature decreases. This different behavior of the masses as a function of the magnetic field is responsible for the drastic change in the dissipation coefficient, as commented on earlier.

6.2.2 Time Evolution of Chiral Quark Condensate

We explore the dynamics of the chiral quark condensate under a magnetic field in a temperature range around the $B = 0$ crossover temperature of the model, $T_{pc} = 150$ MeV. We choose this region of temperature because of its phenomenological interest in a heavy-ion collision setting. The $B = 0$ crossover, in the mean-field approximation, occurs in parameter values $g = 3.3$ and $\lambda = 20$. The corresponding vacuum values of the σ and quark masses are $m_\sigma = 604$ MeV and $m_q = 290$ MeV. With a nonzero B, the chiral transition becomes a first-order transition, with a critical temperature close to $T_c^B = 180$ MeV; the precise value of this temperature

depends on the value of B. Since we stay away from such a critical point, these issues do not impact our results.

In this section, we present the numerical solution of the Ginzburg-Landau Langevin equation for a long time range. This is a situation different from that investigated in reference [16], which investigated the short-time dynamics. The quantity of interest in the results that we are going to present is the time dependence of the volume average of the chiral quark condensate:

$$\overline{\sigma}(t) = \frac{1}{V}\int_V d\boldsymbol{x}_\perp dz\, \sigma(\boldsymbol{x}_\perp, t) = \frac{1}{L^2}\int_{L^2} d\boldsymbol{x}_\perp\, \sigma(\boldsymbol{x}_\perp, t) \tag{6.14}$$

Recall that the field is taken to be independent of the z direction (the direction of the magnetic field) and so in the average over the volume a factor of L from the integral over z cancels an L from $V = L^3$. All simulations were performed for a spatial volume of 10^3 fm.

Initially, we simulated the dynamics for a magnetic field of $eB = 25m_\pi^2$ under a quench of $T_{quench} = 50$ MeV. The values of $\eta = 3.13$, $m_u = 426$ MeV and $m_\sigma = 973$ MeV. The results are depicted in the figure (6.3).

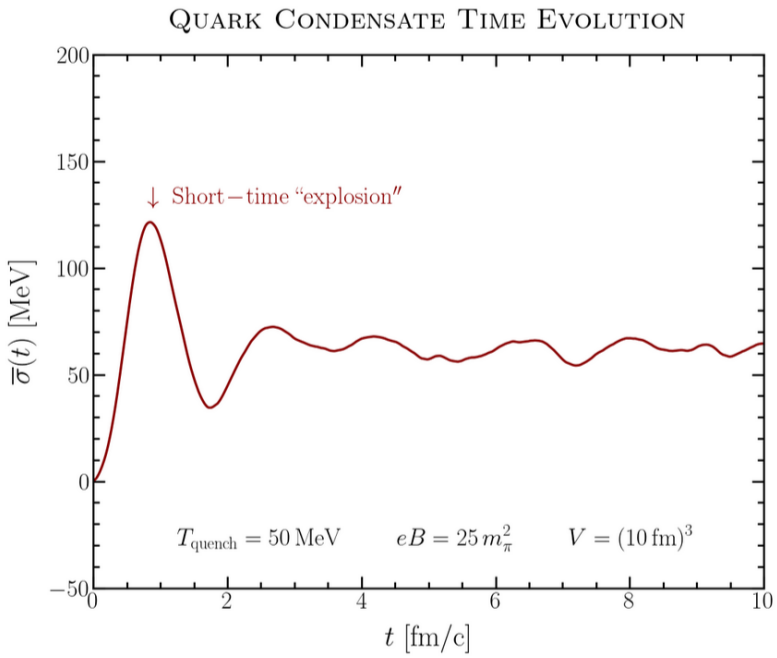

Figure 6.3: Quark condensate time evolution for a magnetic field of $eB = 25m_\pi^2$ under a quench of $T_{quench} = 50$ MeV, for which $\eta = 3.13$ fm^{-1} .

The density plots of this simulation are given in the set of pictures (6.4).

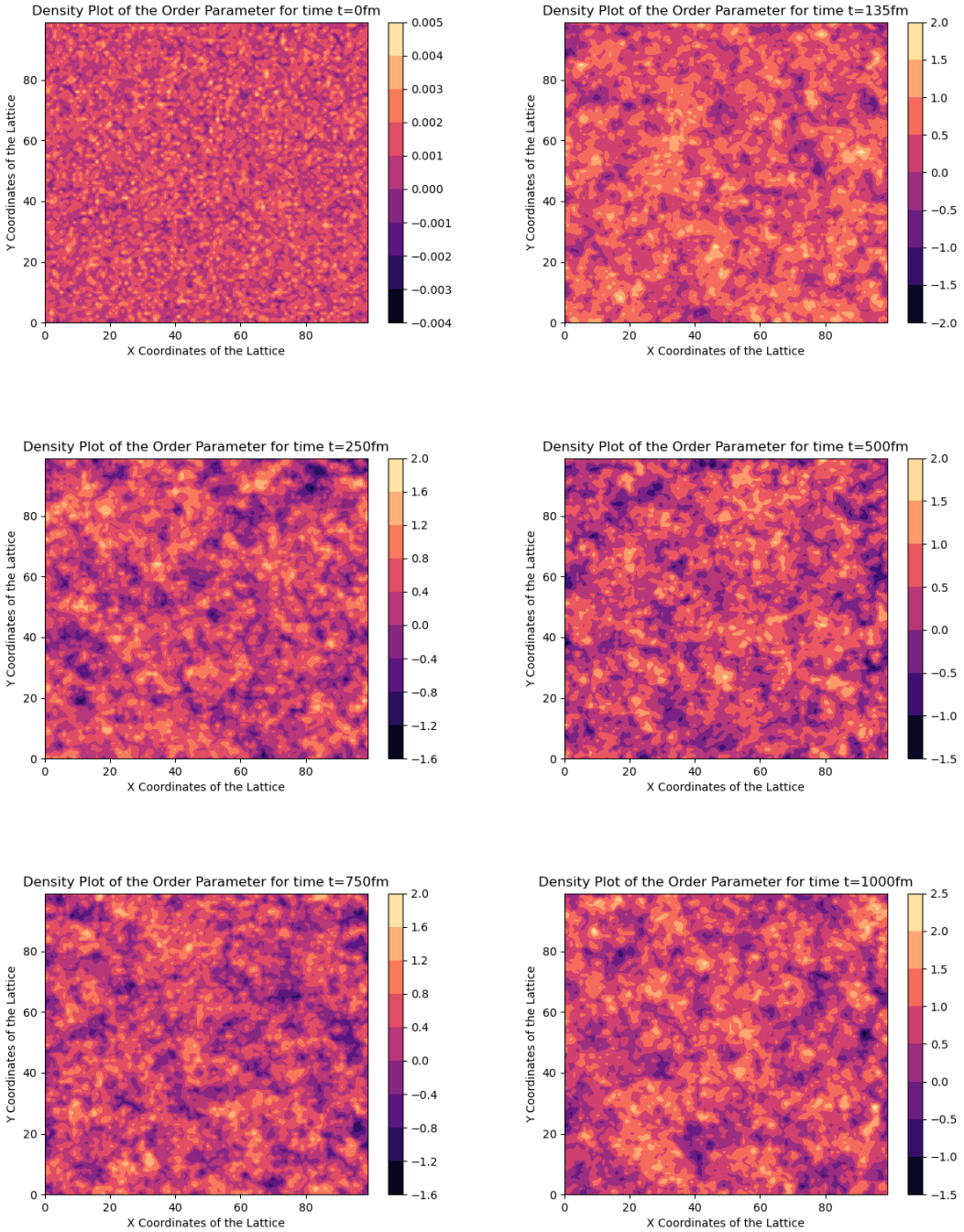

Figure 6.4: Density plot of the simulation (6.3). The axis refers to the lattice indexes in which the dynamics occur. The units of the intensity are given in MeV and the times are t = t $\times$ 10^{-2} fm. The plot for the time $t = 1.25$ fm is near the explosive peak configuration. More details in the text.

Under the same magnetic field, we performed a larger quench $T_{quench} = 100$ MeV. In this case, the values assume $\eta = 2.88$, $m_u = 424$ MeV and $m_\sigma = 944$ MeV. The results are depicted in the figure (6.5).

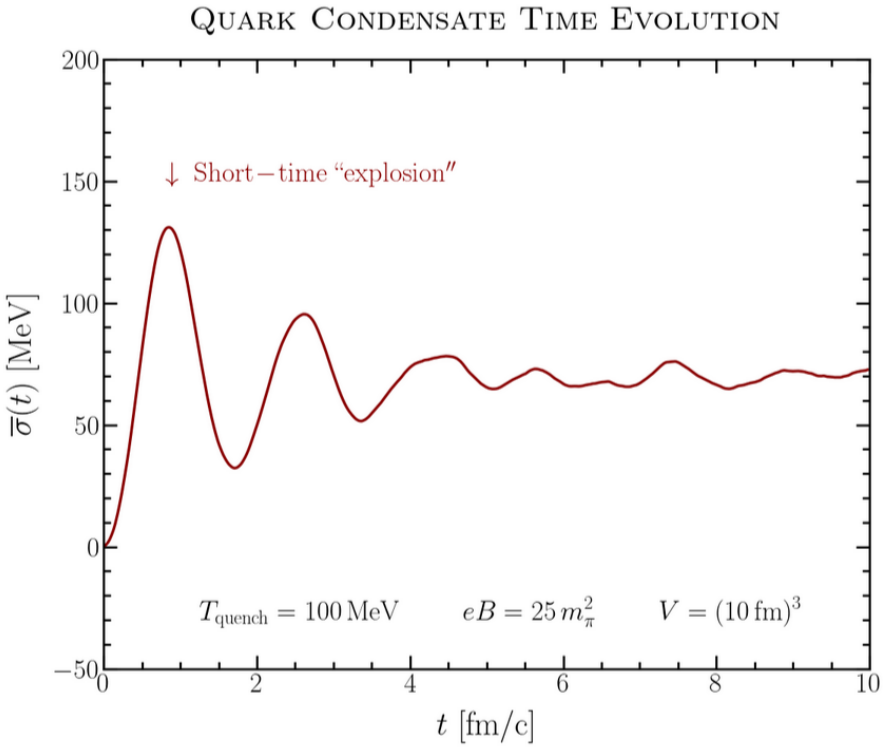

Figure 6.5: Quark condensate time evolution for a magnetic field of $eB = 25m_\pi^2$ under a quench of $T_{quench} = 100$ MeV, for which $\eta = 2.88$ fm^{-1} .

The density plots are given in the set of pictures (6.6). As discussed before, strongly interacting matter at sufficiently high temperatures undergoes a phase transition (or a crossover) to a deconfined quark-gluon plasma (QGP). Recall that, in these simulations, the chiral quark condensate started in the high-temperature phase, in which the symmetry is restored, and evolved after the temperature quench to a lower temperature stage, in which the symmetry is broken. Depending on the nature of the QCD phase transition, the process of phase conversion in the expanding QGP generated in a high-energy heavy-ion collision may proceed in several different ways [79]. Results from CERN and BNL-RHIC feature what has been called sudden hadronization [80] or explosive behavior [81] in the hadronization process of the expanding QGP favoring a fast (explosive) process. Both experiment and theory suggest that a QGP generated in a high-energy heavy ion collision expands and cools down quickly.

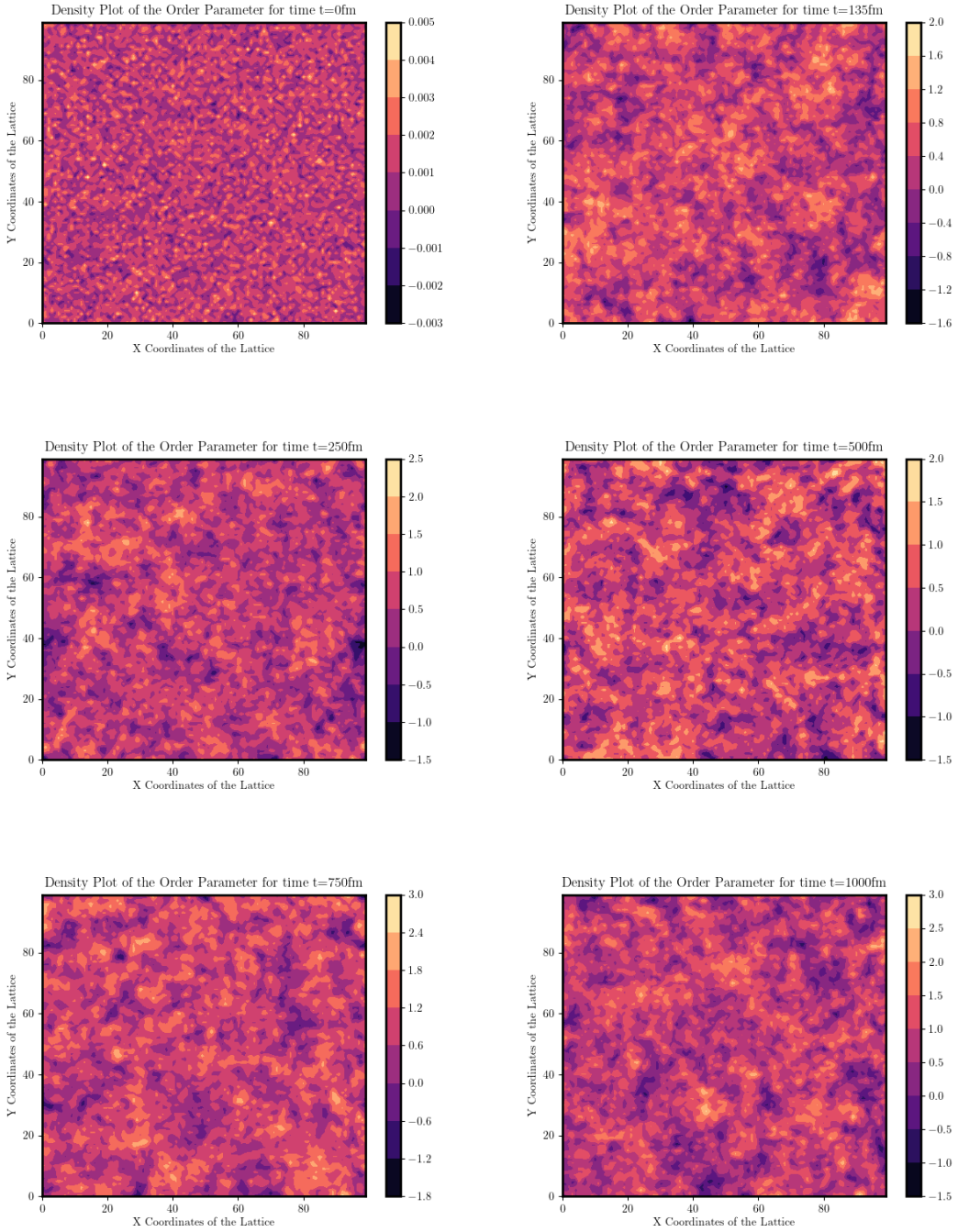

Figure 6.6: Density plot of the simulation (6.5).The axis refers to the lattice indexes in which the dynamics occur. The units of the intensity are given in MeV and the times are t = t $\times 10^{-2}$ fm/c. The plot for the time $t = 1.25$ fm/c is near the explosive peak configuration. More details in the text.

After the explosive peak, the system continues its evolution to thermalization but with differences in comparison with the no magnetic field scenario: in figures (6.3) and (6.5), the magnetic field considered is $eB = 25m_\pi^2$ with temperatures quenches

given by $T_{quench} = 50$ MeV and $T_{quench} = 100$ MeV, respectively. In these cases, the oscillatory behavior after the explosion is softer than in the cases under $eB = 20m_\pi^2$ magnetic fields as we shall see. This is because the thermomagnetic damping term, $\eta(B,T)$, is stronger, leading to faster thermalization. The effect of the damping term η on thermalization was also investigated in [79], in the context of a purely diffusive phenomenological Ginzburg-Langevin equation without the presence of magnetic fields.

From the results (6.3) and (6.5), one may see that the explosive peak is stronger in the case for $T_{quench} = 100\ MeV$ than in the case $T_{quench} = 50\ MeV$: this suggests that the temperature quench has a strong influence in the maximum value that the quark condensate achieves during its evolution. Despite this, one may check from the density plots (6.4) and (6.6) that these maximums occur at nearly equal times, in which for the strong quencher case the explosion occurs sooner than the weak quench scenario.

Finally, we proceed to the cases in which the magnetic field considered is $eB = 20m_\pi^2$ with temperatures quenches given by $T_{quench} = 50$ MeV and $T_{quench} = 100$ MeV, respectively. Starting with the former T_{quench}, $\eta = 2.55$ fm^{-1},$m_u = 398$ MeV and $m_\sigma = 894$ MeV. The picture depicts the results (6.7). The density plots are also shown in the pictures (6.8).

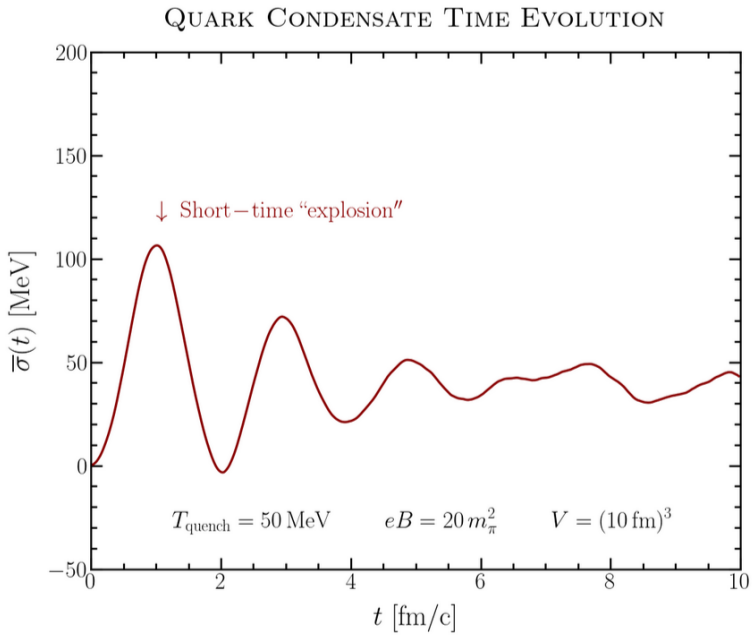

Figure 6.7: Quark condensate time evolution for a magnetic field of $eB = 20m_\pi^2$ under a quench of $T_{quench} = 50$ MeV, for which $\eta = 2.55$ fm^{-1} .

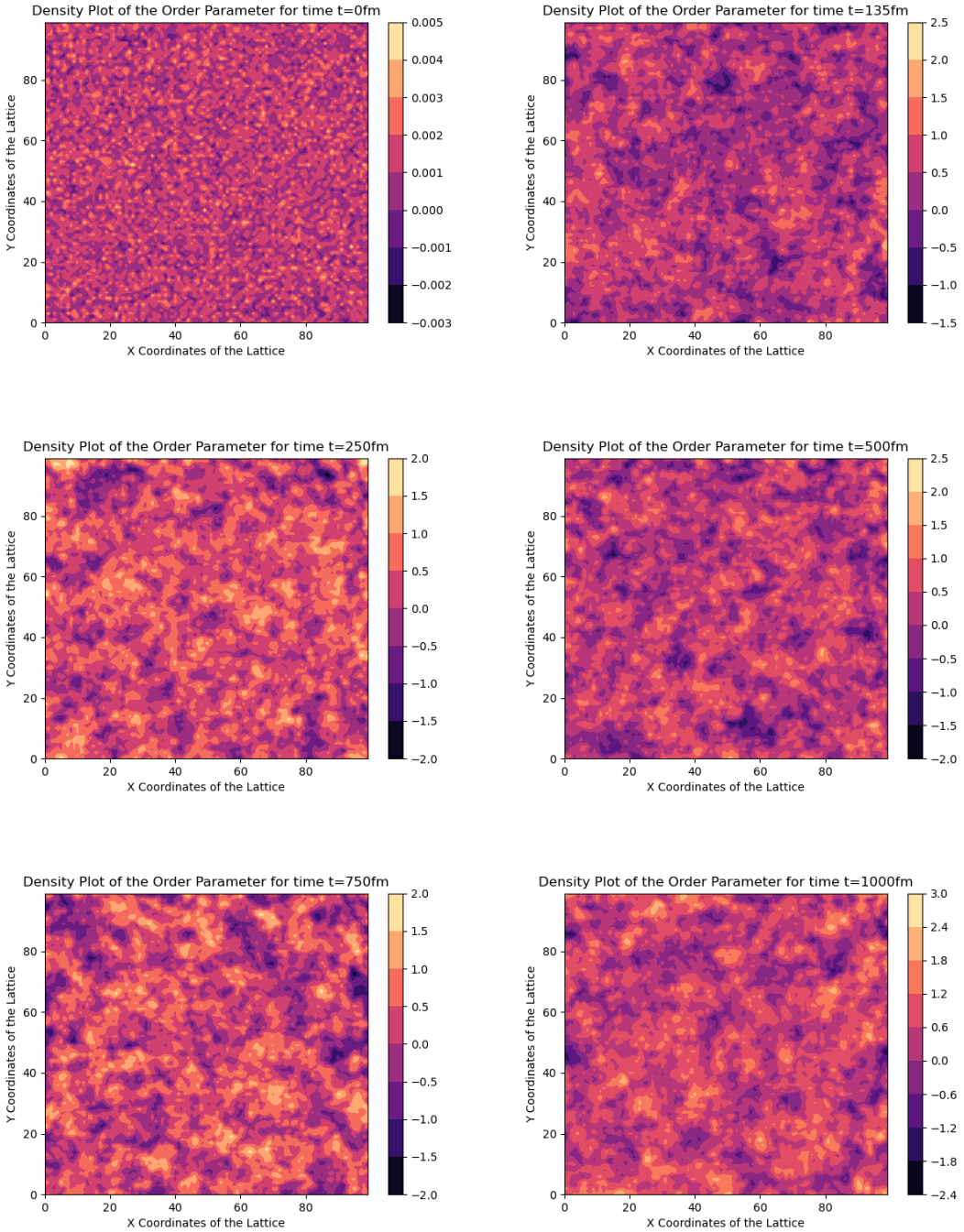

Figure 6.8: Density plot of the simulation (6.7).The axis refers to the lattice indexes in which the dynamics occur. The plot for the time $t = 1.25$ fm/c is near the explosive peak configuration. More details in the text.

While for $T_{quench} = 100$ MeV, the values are $\eta = 2.33$, $m_u = 396$ MeV and $m_\sigma = 861$ MeV with the results given in (6.9).

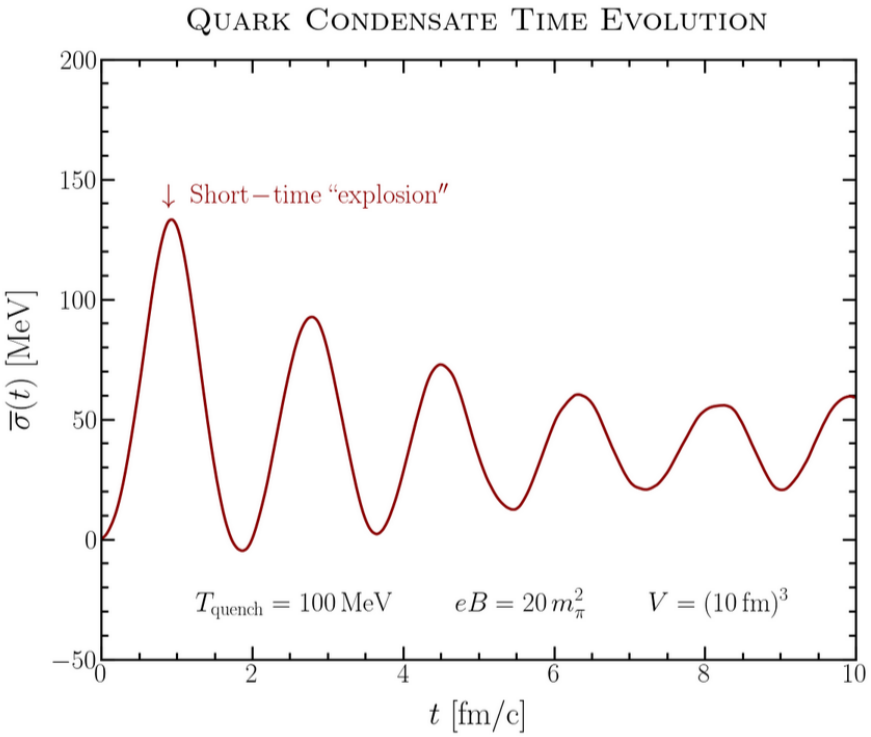

Figure 6.9: Quark condensate time evolution for a magnetic field of $eB = 20m_\pi^2$ under a quench of $T_{quench} = 100$ MeV, for which $\eta = 2.23$ fm^{-1} .

The respective density plots are given in the set of pictures (6.10). The oscillatory phenomena are due to the fact that the magnetic damping given in equation (5.7) is weaker due to its linear dependence on the strength of the field. Note that if we recall the Ginzburg-Landau-Langevin equation given in (5.3), a weaker $\eta(T, B)$ implies that it would possess a wave-equation form leading the emergence of enhanced oscillatory behavior, implying that the thermalization may take longer times than systems under stronger magnetic fields. One may see this oscillatory behavior from the density plots (6.8) and (6.10): the average of the quark condensate oscillates as time evolves leading to less homogeneous final states, especially for strong temperature quenches.

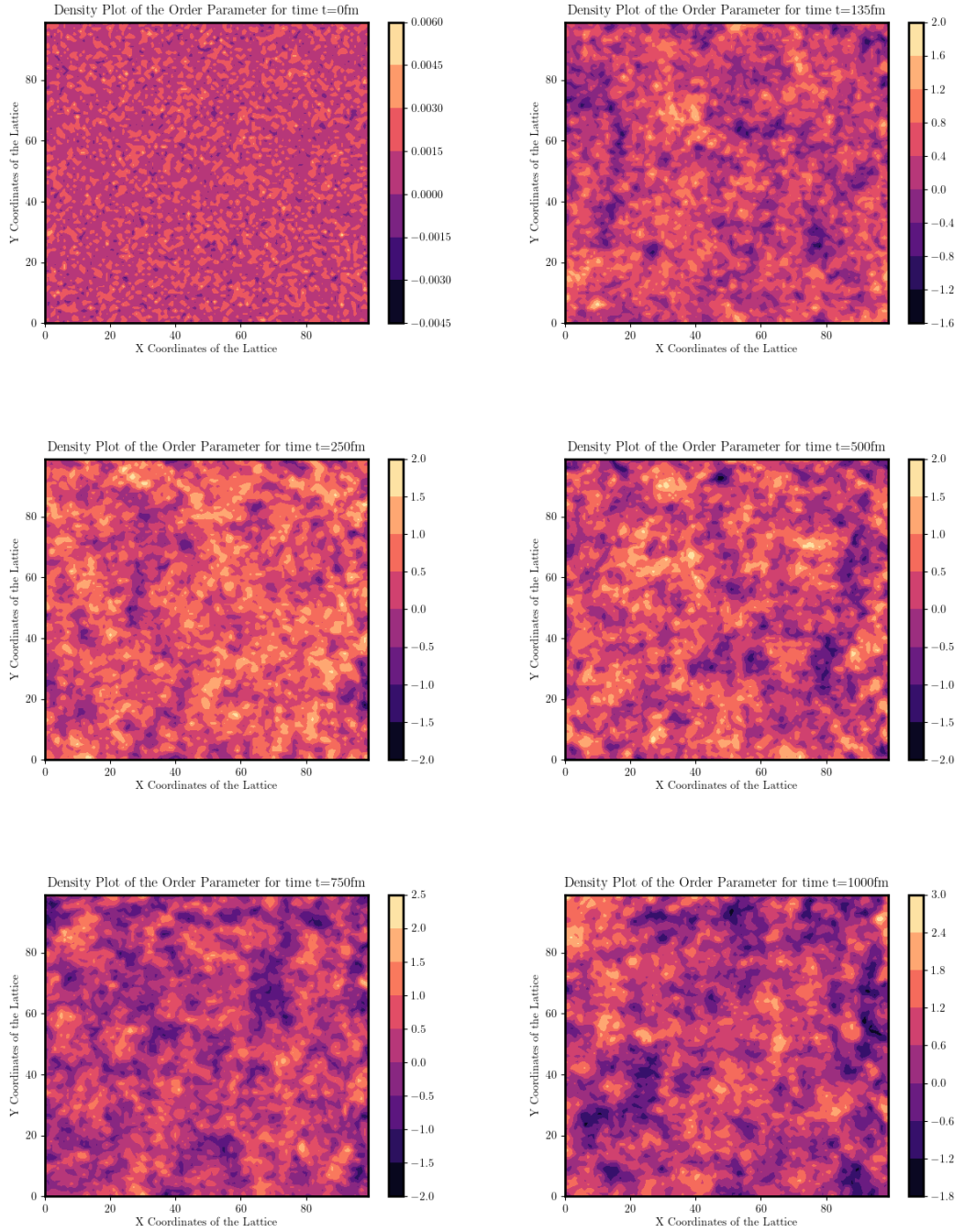

Figure 6.10: Density plot of the simulation (6.9). The axis refers to the lattice indexes in which the dynamics occur. The units of the intensity are given in MeV and the times are t $= t \times 10^{-2}$fm. The plot for the time t=1.25 fm is near the explosive peak configuration. More details in the text.

As in the preceding case for $eB = 25m_\pi^2$, one may see that the explosive peak is stronger for stronger quenches also suggesting the strong influence of the temperature quench on the condensate's maximum value and, also suggests that even by lowering

the field intensity, the explosive phenomena occurs in the same fashion as for stronger magnetic fields. Analogously, the density plots (6.8) and (6.10) also show a slight difference in the time in which these maximums occur at nearly equal times, in which for the strong quencher case the explosion occurs sooner than the weak quench scenario, as in the stronger magnetic field case.

Despite the slightness of the time difference, the different delays are not negligible since they are in the order of $t = 1$ fm/c and, this time is in the order of 10% of the total time the QGP takes to disassemble into hadrons, which average in the order of $t = 10$ fm to occur [16]. In this time interval, the temperature varies between $T_{\rm ch} \approx 150$ MeV and $T_{\rm K} \approx 100$ MeV [16], in which $T_{\rm ch}$ and $T_{\rm K}$ are respectively the chemical and kinetic freeze-out temperatures: while $T_{\rm ch}$ is a marker regarding the end of inelastic collisions, which fixes the observed hadron abundance, the latter, $T_{\rm K}$, marks the end of elastic hadron collisions leading to the disassembly of the system into hadrons [16].

6.2.3 Late-time Behavior

In this section, we address the magnetic field effects on the late-time behavior of the condensate. The aim is to understand how the magnetic field affects the relaxation of the field modes as the system equilibrates. At long times, when the field becomes close to its equilibrium value $\sigma_{\rm eq}$, the Langevin equation can be solved analytically. The equilibrium value is characterized by a homogeneous solution plus small space-time fluctuations.

We write $\sigma(t, \boldsymbol{x})$ as

$$\sigma(t, \boldsymbol{x}) = \sigma_{\rm eq} + \sigma'(t, \boldsymbol{x})\,, \tag{6.15}$$

where $\sigma_{\rm eq}$ is given by the solution of the following equation:

$$F_{\sigma_{\rm eq}} = 0 \to \left[\frac{\delta U[\sigma]}{\delta\sigma} + g\rho_s(\sigma_0)\right]_{\sigma=\sigma_{\rm eq}} = \lambda\sigma_{\rm eq}\left(\sigma_{\rm eq}^2 - v^2\right) - \epsilon + g\rho_s(\sigma_0) = 0\,, \tag{6.16}$$

where, to lighten the notation, we have restored the parameters v^2 and ϵ defined in Chapter 2, namely: $v^2 = f_\pi^2 - m_\pi^2/\lambda$ and $\epsilon = f_\pi m_\pi^2$. Close to equilibrium, since $\sigma'(t, \boldsymbol{x})$ is supposed to be small, the quadratic and cubic terms in $\sigma'(t, \boldsymbol{x})$ coming from $\delta U[\sigma]/\delta\sigma$ can be neglected and a linear equation for σ' is obtained. One can then use a spatial Fourier transform in the spatial coordinate to solve it analytically.

Defining the Fourier transformed fields $\sigma'(t,\boldsymbol{p})$ and $\xi_{T,B}(t,\boldsymbol{p})$ as

$$\begin{pmatrix}\sigma'(t,\boldsymbol{x})\\ \xi_{T,B}(t,\boldsymbol{x})\end{pmatrix} = \int \frac{d\boldsymbol{p}}{(2\pi)^2}\, e^{i\boldsymbol{p}\cdot\boldsymbol{x}} \begin{pmatrix}\sigma'(t,\boldsymbol{p})\\ \xi_{T,B}(t,\boldsymbol{p})\end{pmatrix}, \tag{6.17}$$

the momentum space linearized Langevin equation for $\sigma'(t,\boldsymbol{p})$, is given by:

$$\frac{\partial^2\sigma'(t,\boldsymbol{p})}{\partial t^2} + \eta_{T,B}\frac{\partial\sigma'(t,\boldsymbol{p})}{\partial t} + \left[\boldsymbol{p}^2 + \lambda\left(3\sigma_{\rm eq}^2 - v^2\right)\right]\sigma'(t,\boldsymbol{p}) = \xi_{T,B}(t,\boldsymbol{p})\,, \tag{6.18}$$

in which we used (6.16) and the momentum-space noise correlation is given by

$$\langle \xi_{T,B}(t,\boldsymbol{p})\,\xi_{T,B}(t',\boldsymbol{p}')\rangle = \eta_{T,B}\, m_\sigma \coth(m_\sigma/2T)\,\delta(t-t')\,\frac{1}{L}\,(2\pi)^2\delta(\boldsymbol{p}+\boldsymbol{p}'). \tag{6.19}$$

Let us first analyze the solution of (6.18) neglecting the fluctuations, i.e. for $\xi(t,\boldsymbol{p}) = 0$. Equation (6.18) is nothing more than the equation for a damped harmonic oscillator, i.e., each field momentum mode behaves as a damped harmonic oscillator. The solution can be written as

$$\sigma'(t,\boldsymbol{p}) = A_+\, e^{\omega_+(\boldsymbol{p})\,t} + A_-\, e^{\omega_-(\boldsymbol{p})\,t}\,, \tag{6.20}$$

where $\omega_\pm(\boldsymbol{p})$ are the solutions of the quadratic equation:

$$\omega^2(\boldsymbol{p}) + \eta_{T,B}\,\omega(\boldsymbol{p}) + \omega_0^2(\boldsymbol{p}) = 0 \qquad \text{with} \qquad w_0^2(\boldsymbol{p}) = \boldsymbol{p}^2 + \lambda\left(3\sigma_{\rm eq}^2 - v^2\right). \tag{6.21}$$

The solutions $\omega_\pm(\boldsymbol{p})$ of this quadratic equation are given by:

$$\begin{aligned}\omega_\pm(\boldsymbol{p}) &= -\frac{1}{2}\eta_{T,B} \pm \sqrt{\frac{1}{4}\eta_{T,B}^2 - \omega_0^2(\boldsymbol{p})}\\ &= -\frac{1}{2}\eta_{T,B} \pm \sqrt{\frac{1}{4}\eta_{T,B}^2 - \boldsymbol{p}^2 - \lambda\left(3\sigma_{\rm eq}^2 - v^2\right)}\,.\end{aligned} \tag{6.22}$$

For the values of T and eB with which we are working, the square-root argument is always negative. Therefore, the roots $\omega_\pm(\boldsymbol{p})$ acquire an imaginary part:

$$\omega_\pm(\boldsymbol{p}) = -\frac{1}{2}\eta_{T,B} \pm i\sqrt{\boldsymbol{p}^2 + \lambda\left(3\sigma_{\rm eq}^2 - v^2\right) - \frac{1}{4}\eta_{T,B}^2}\,. \tag{6.23}$$

Therefore, the relaxation of $\sigma(t,\boldsymbol{p})$ to equilibrium is accompanied by an oscillatory behavior. This damping plus oscillatory behavior is seen in the long-time behavior of

the figures above (although our analysis regards momentum-space solutions, it should be clear that the time behavior is the same in coordinate or momentum space). The effect of the magnetic field on the damping plus oscillatory behavior is clearly seen as well. Comparing e.g. Figs 6.5 and 6.9, one sees that the damping dominates and this is understood from the fact that $\eta_{T,B}$ increases with the magnetic field.

The above result does not take into account that $\sigma'(t,\boldsymbol{p})$ is a fluctuating field because we have neglected the noise field $\xi(t,\boldsymbol{p})$; because of the noise field, the $\sigma'(t,\boldsymbol{p})$ average vanishes. To see this, let us consider the noise field in the solution of (6.18). That equation is the equation of a damped harmonic oscillator in the presence of an external stochastic force. The solution is better analyzed by making a time Fourier transform so that an algebraic equation is obtained for the time Fourier transformed field $\sigma'(\omega,\boldsymbol{p})$. Defining $\sigma'(\omega,\boldsymbol{p})$ and $\xi(\omega,\boldsymbol{p})$ by

$$\begin{pmatrix}\sigma'(t,\boldsymbol{p})\\ \xi(t,\boldsymbol{p})\end{pmatrix} = \int_{-\infty}^{\infty}\frac{d\omega}{2\pi}\,e^{-i\omega t}\,\begin{pmatrix}\sigma'(\omega,\boldsymbol{p})\\ \xi(\omega,\boldsymbol{p})\end{pmatrix} \tag{6.24}$$

and replacing this into (6.18), one obtains:

$$-\omega^2\,\sigma'(\omega,\boldsymbol{p}) + i\eta_{T,B}\,\omega\,\sigma'(\omega,\boldsymbol{p}) + \omega_0^2(\boldsymbol{p})\,\sigma'(\omega,\boldsymbol{p}) = \xi(\omega,\boldsymbol{p})\,. \tag{6.25}$$

The solution for $\sigma'(\omega,\boldsymbol{p})$ can be written as:

$$\sigma'(\omega,\boldsymbol{p}) = \frac{\xi(\omega,\boldsymbol{p})}{(\omega_0^2(\boldsymbol{p})-\omega^2) + i\eta_{T,B}\,\omega}\,, \tag{6.26}$$

where the noise correlation function is given by

$$\langle \xi_{T,B}(\omega,\boldsymbol{p})\,\xi_{T,B}(\omega',\boldsymbol{p}')\rangle = \eta_{T,B}\,2\pi\delta(\omega+\omega')\,\frac{1}{L}\,(2\pi)^2\delta(\boldsymbol{p}+\boldsymbol{p}'). \tag{6.27}$$

Therefore the noise average of $\sigma'(\omega,\boldsymbol{p})$ vanishes, $\langle\sigma'(\omega,\boldsymbol{p})\rangle_\xi = 0$. Therefore, the average of $\sigma(t,\boldsymbol{p})$ for $t\to\infty$ is $\langle\sigma(t,\boldsymbol{p})\rangle_\xi = \sigma_{\rm eq}$.

Although we have not computed correlation functions, it is interesting to analyze the long-time behavior of the time-dependent correlation function that can be

computed from the solution above. Specifically:

$$
\begin{aligned}
C(t,t';\boldsymbol{p}) &\equiv \frac{1}{L}\,\langle\,\sigma'^{*}(t,\boldsymbol{p})\sigma'(t',\boldsymbol{p})\,\rangle_{\xi} = \frac{1}{L}\,\langle\,\sigma'(t,-\boldsymbol{p})\sigma'(t',\boldsymbol{p})\,\rangle_{\xi} \\
&= \frac{1}{L}\int_{-\infty}^{\infty}\frac{d\omega}{2\pi}\,e^{-i\omega t}\int_{-\infty}^{\infty}\frac{d\omega'}{2\pi}\,e^{-i\omega' t'}\,\langle\,\sigma'(\omega,-\boldsymbol{p})\,\sigma'(\omega',\boldsymbol{p})\rangle_{\xi} \\
&= \eta_{T,B}\int_{-\infty}^{\infty}\frac{d\omega}{2\pi}\,\frac{e^{-i\omega(t-t')}}{(\omega_0^2(\boldsymbol{p})-\omega^2)^2+\eta_{T,B}^2\,\omega^2}\,. \qquad (6.28)
\end{aligned}
$$

The integral can be computed analytically using the residue theorem. There are four poles in the complex plane:

$$
\begin{aligned}
\omega &= \pm i\,\frac{1}{2}\eta_{T,B} \pm \sqrt{\omega_0^2(\boldsymbol{p})-\frac{1}{4}\eta_{T,B}^2} \\
&= \pm i\,\frac{1}{2}\eta_{T,B} \pm \sqrt{\boldsymbol{p}^2+\lambda(3\sigma_{\rm eq}^2-v^2)-\frac{1}{4}\eta_{T,B}^2}\,. \qquad (6.29)
\end{aligned}
$$

Depending on $t>t'$ or $t<t'$ determines whether closing the contour on the upper half-plane or lower half-plane in the ω-imaginary plane. In any case, the final result is again oscillatory accompanied by exponentially decaying behavior. Defining $\tau=|t-t'|$, one obtains for $C(t,t';\boldsymbol{p})=C(\tau;\boldsymbol{p})$:

$$
C(\tau;\boldsymbol{p}) = \frac{e^{-(\eta_{T,B}/2)\,\tau}}{\boldsymbol{p}^2+\lambda(3\sigma_{\rm eq}^2-v^2)}\left[\cos\overline{\omega}(\boldsymbol{p})\tau+\frac{\eta_{T,B}}{2\overline{\omega}(\boldsymbol{p})}\sin\overline{\omega}(\boldsymbol{p})\tau\right], \qquad (6.30)
$$

where $\overline{\omega}(\boldsymbol{p})=\sqrt{\boldsymbol{p}^2+\lambda(3\sigma_{\rm eq}^2-v^2)-\frac{1}{4}\eta_{T,B}^2}$. Recall that the square-root argument is positive for the values of T and eB we used.

In summary, this analysis shows in a very transparent way the role played by the magnetic field on the thermalization dynamics: the more the field increases the dissipation coefficient, the larger the damping, and the system thermalizes faster. This concludes our numerical analysis of the Langevin field equation derived in [16].

Chapter 7

Conclusions and Future Prospects

Our objective in this work was to numerically investigate the time evolution of the chiral quark condensate under the effect of strong magnetic fields. The condensate dynamics was described using a Langevin field equation for the scalar field (σ) of the linear sigma model with quarks (LSMq). The Langevin equation we simulated was derived in reference [16] using the closed-time path formalism of thermal field theory. The authors started from the one-loop effective action of the model. Since the effective action develops an imaginary part coming from the decay $\sigma \to \bar{q}q$, they used the Feynman-Vernon formalism to replace the imaginary part by a noise field whose correlation is given by a dissipation coefficient and were able to derive an equation of motion for the condensate. The physics behind the dissipation coefficient is precisely the $\sigma \to \bar{q}q$ decay.

Our simulations were done for a constant magnetic field within a quench scenario in which the system's temperature suddenly changes from a high value to a lower value. We started the simulation from an initial very small condensate value (corresponding to a high temperature). As in [16], we considered the field dynamics in the plane perpendicular to the field. First, from the solution of the Lagevin field equation, we computed the volume average of the field. Our results for the volume average have shown that after a fast growth (explosion) at an early time, damped oscillations lead to the condensate toward an equilibrium value determined by the quench temperature T_{quench} and the magnetic field strength. The damping rate is determined by the dissipation coefficient. We have also made density plots, that is, plots that show the field configuration at each point in the plane perpendicular to the magnetic field. From the density plots, we obtained a visualization of the system's evolution. In these plots, one can easily see that in the explosive region, the density value of the condensate reaches a peak and, after that, the condensate starts its path to thermalization. We concluded our numerical study by analyzing the long-time behavior of the condensate evolution when the system is close to equilibrium. Close to equilibrium, one can solve the Langevin field equation analytically in momentum space. The analytical results for the condensate show in a very transparent way the

damped oscillatory behavior that we obtained in the simulations.

Finally, we will discuss some future prospects and perspectives for this work. Firstly, is possible to extend the numerical simulations here performed in two spatial dimensions to three spatial dimensions. The effects of the inclusion of the electric field in the quark condensate dynamics may also be investigated. Another possibility is to include the pion dynamics in the same approximation scheme used to arrive at 5.3; this will lead to a coupled set of Langevin field equations for σ and π, in which the $\sigma \to \pi\pi$ decay channel would contribute to the dissipation dynamics. Next, one could try to solve the momentum-space equation with momentum-dependent dissipation and noise kernels, namely equation [55] in reference [16]. This might not be so easy, as one would need to use a fast Fourier transformation method to switch back and forth between momentum and coordinate space to compute the nonlinear term coming from the derivative of the derivative of the potential $U[\sigma]$. Another more ambitious step is to couple the condensate dynamics to conserved order parameters [44] and hydrodynamic modes. Now, to eventually be useful for the phenomenology of heavy-ion collisions, one must take into account the time dependence of the magnetic field, which would lead us to consider a complex magneto-hydrodynamic problem. Finally, one should use the formalism developed in [16] at low temperatures to study the complex effect of magnetic fields on the collapse of stars that lead to a neutron star.

Appendix A

Quantum Mechanics and Path Integrals

"Feynman brought quantum field theory to the masses."

Julian Schwinger

This appendix is devoted to reviewing topics that appeared throughout this dissertation regarding quantum statistical mechanics. For a deeper discussion about it, there is a plethora of literature. We will refer the reader to some of the literature that we have followed to write this appendix: [39], [41],[82] and [52].

A.1 Quantum Mechanics Elements

Consider a quantum mechanical system described by a single degree of freedom q. The states in Hilbert space $\mathcal{H}$ are $|\alpha\rangle$ and the observables A are represented by Hermitian linear operators $\hat{A}$ in this space. We will introduce two different treatments for the dynamics of the states. Starting with the Schröndiger picture:

$$i\hbar\frac{\partial|\alpha\rangle}{\partial t} = \hat{H}|\alpha\rangle \ . \tag{A.1}$$

In this picture, observables are time-independent, while states evolve in time and the Hamiltonian operator $\hat{H}$ is associated with the observable energy.

The state vector $|\alpha\rangle$ at time t is derived from $|\alpha(t_0)\rangle$ at time t_0 by applying:

$$|\alpha(t)\rangle = U(t,t_0)|\alpha(t_0)\rangle \ , \tag{A.2}$$

in which $U(t,t_0)$ is the evolution operator possessing the properties $U^\dagger U = UU^\dagger = 1$ and $U(t,t_1)U(t_1,t_0) = U(t,t_0)$ for $t_0 \leq t_1 \leq t$. Putting (A.2) in (A.1) we obtain that:

$$i\hbar\frac{d}{dt}\left[\frac{d}{dt}U(t,t_0)\right]|\alpha(t_0)\rangle = H(t)U(t,t_0)|\alpha(t_0)\rangle \ , \tag{A.3}$$

but, since this equation must hold for any initial state, one obtains that:

$$i\hbar\frac{d}{dt}\frac{d}{dt}U(t,t_0) = H(t)U(t,t_0)\ . \tag{A.4}$$

Taking the limit $t \to t_0$:

$$i\hbar\frac{d}{dt}\frac{d}{dt}\bigg|_{t=t_0} = H(t_0)H(t)U(t,t_0)\,. \tag{A.5}$$

Naively, one would integrate this expression but since $\hat{H}$ is an operator and there's no reason to have $[H(t'), H(t'')] = 0$ we can't perform it. On the other hand, by considering a stationary state, the Hamiltonian will be independent of the choice of time origin, then:

$$U(t,t_0) = T\exp\left(\frac{-i}{\hbar}\hat{H}(t-t_0)\right)\ , \tag{A.6}$$

which depends only on $(t - t_0)$. An equivalent view for the dynamics of quantum states is provided by the Heisenberg picture, in which the states do not evolve, but observables do, according to:

$$\hat{A(t)} = U^\dagger(t)\hat{A}U(t)\ . \tag{A.7}$$

The evolution of operators in the Heisenberg picture is summarized by the Heisenberg equation:

$$\frac{d\hat{A}}{dt} = \frac{i}{\hbar}\big[\hat{H},\hat{A}\big]\ . \tag{A.8}$$

It's not hard to show that we get consistent values for expectation values of observables in either pictures $\langle\hat{A}(t)\rangle = \langle\alpha(t)|\hat{A(0)}|\alpha(t)\rangle_{Sch} = \langle\alpha(0)|\hat{A(t)}|\alpha(0)\rangle_{Hei}$.

Another useful relation is the spectral decomposition theorem: it states that $\hat{A}$ can be written as a linear combination of pairwise orthogonal projections formed from its eigenvectors, in other words, $\hat{A} = \sum_j a_j\,|v_j\rangle\,\langle v_j|$, in which $\hat{A}\,|v_j\rangle = a_j\,|v_j\rangle$ [52]. The generalization for quantum spaces with infinite dimension is valid only when $(A^\dagger)^\dagger = A^\dagger$, when A is a self-adjoint operator. We will state without proof[1]

[1]For a discussion regarding the argument that leads to this generalization see [52].

the generalized version of the spectral theorem:

$$\hat{A} = \sum_n |n\rangle\, a_n\, \langle n| + \int d\nu\, |\nu\rangle\, a(\nu)\, \langle \nu| \ , \tag{A.9}$$

in which the first term on the right accounts for the discrete part and the term on the right for the continuous part. The values of a belonging to a discrete spectrum satisfy an eigenvalue equation such as $\hat{A}\,|v_j\rangle = a_j\,|v_j\rangle$, but those of a continuous spectrum do not. It may happen that the continuous spectrum and the discrete spectrum overlap, however, for most of the operators used in quantum physics, the discrete and continuous spectra do not [52].

It's possible that some systems' states are not described by kets in the Hilbert space, hence, the quantum mechanical description of physical reality developed so far can't be considered complete. These states occur when we know that the state of the system belongs with certainty to a given class of states $|\alpha_i\rangle$, but our knowledge does not allow us to go beyond assigning a probability of occurrence p_i to each member of this class. These situations are depicted by density matrices $\rho = \sum_i \rho_i\,|\alpha_i\rangle\,\langle\alpha_i|$, in which the states are orthonormal. This is a mixed-state density operator defined as a superposition (or ensemble) of pure-state density operators. The value ρ_i is $0 \leq \rho_i \leq 1$ and represents the probability that the system is in the state $|\alpha_i\rangle$. Furthermore $\mathrm{Tr}\,\rho = 1$ with the general case being $\mathrm{Tr}\,\rho^2 \leq 1$.The interpretation of this statement is that if a measurement is performed, the total probability for the system to be found in any state of the Hilbert space must be equal to or less than unity [46],[52].

The average of any operator associated with this system may be evaluated by knowing the density matrix and, in the Schrödinger picture, it is given by:

$$\langle A\rangle(t) = \mathrm{Tr}\,\rho(t)A = \sum_i \rho_i\,\langle\alpha_i(t)|A|\alpha_i(t)\rangle \ , \tag{A.10}$$

in the Schrödinger picture. The term ρ is time-dependent, and obeys the Liouville–von Neumann equation:

$$\frac{d\rho}{dt} = -\frac{i}{\hbar}[\hat{H},\rho]\ . \tag{A.11}$$

From this expression, one may obtain that:

$$\rho(t) = e^{-iHt}\rho(0)e^{iHt}\ . \tag{A.12}$$

If the Hamiltonian is time-independent and if it commutes with $\rho(0)$, then the density matrix will be constant in time and will describe a system in equilibrium. However, in general, the system may not be in equilibrium and the Hamiltonian may have a time dependence. Hence, the density matrix may be expressed through the time evolution operator:

$$\rho(t) = U(t,0)\rho(0)U^{\dagger}(t,0) = U(t,0)\rho(0)U(0,t) \ . \tag{A.13}$$

Now, consider q is a continuous unbounded variable in which $|q\rangle$ are states in which q is well-defined and $\hat{\Pi}_a$ is the translation operator, in which:

$$\hat{\Pi}_a = \langle q| \hat{\Pi}_a |\alpha\rangle = \langle q+\alpha|\alpha\rangle \ . \tag{A.14}$$

We must have a Hermitian generator $\hat{P}$ such that $\hat{\Pi}_a = \exp(iaP\hbar)$. After considering an infinitesimal expansion of $\hat{\hat{\Pi}}_a$ in $\langle q|\hat{\hat{\Pi}}_a|\alpha\rangle$ together with (A.14) we obtain:

$$p\langle q|p\rangle = -i\hbar\frac{\partial}{\partial q}\langle q|p\rangle \ . \tag{A.15}$$

Introducing $\langle q|p\rangle = \frac{1}{\sqrt{2\pi\hbar}}e^{\frac{ipq}{\hbar}}$ such that $\int dq \langle p'|q\rangle \langle p|q\rangle = \delta(p'-p)$. Furthermore, $\hat{q}|q\rangle = q|q\rangle$ and, since the momentum and position observables do not commute we obtain the relation $[\hat{p},\hat{q}] = -i\hbar$.

A.2 Path Integrals in Quantum Mechanics

We can proceed further and develop the path integral representation of the evolution operator. For this, consider a 1D Hamiltonian of the form $\hat{H} = K(\hat{p}) + V(\hat{q})$, in which $K = \frac{\hat{p}^2}{2m}$.

We want to express the evolution operator as a sum of trajectories starting at (q,t) and ending at (q',t'). To proceed, suppose a finite time interval in which the process is occurring, in which, we are going to divide it in n pieces of equal time length so we define $n\epsilon + \epsilon = (n+1)\epsilon = t$, in which $n \to \infty$. Furthermore, since $\hat{K}$ and $\hat{V}$ do not commute, we cannot factor out the evolution operator as a product of a function of $\hat{p}$ times a function of $\hat{x}$. But by employing the Baker-Campbell-Haussdorf formula one may combine exponentials of non-commuting operators. For two operators $\hat{A}$

and $\hat{B}$, the BCH formula is typically written as:

$$e^{\hat{A}}e^{\hat{B}} = \exp\left\{\hat{A}+\hat{B}+\frac{1}{2}[\hat{A},\hat{B}]+...\right\} . \tag{A.16}$$

Using the symmetrized form of the Baker-Campbell-Haussdorf expansion firstly introduced by Feynman, for $\epsilon \to 0$ and $n \to \infty$ one may write $e^{\hat{A}+\hat{B}} = e^{\frac{\hat{A}}{2}}e^{\hat{B}}e^{\frac{\hat{A}}{2}} + \mathcal{O}(\lambda^3)$, obtaining that:

$$\langle q_j|\exp\big(-\frac{i}{\hbar}\epsilon\hat{H}\big)|q_i\rangle = \langle q_j|\exp\big(-\epsilon\frac{i}{\hbar}\frac{\hat{V}}{2}\big)\exp\big(-\epsilon\frac{i}{\hbar}\frac{\hat{P}^2}{2m}\big)\exp\big(-\epsilon\frac{i}{\hbar}\frac{\hat{V}}{2}\big)|q_i\rangle \ . \tag{A.17}$$

Using these definitions we can proceed to write the path integral representation of the evolution operator:

$$\hat{U}(t) = e^{-i\hbar t\hat{H}} = \left[\exp\big(-i\hbar\epsilon\hat{K}\big)\exp\big(-i\hbar\epsilon\hat{V}\big)\right]^{n+1} \tag{A.18}$$

Thus:

$$\begin{aligned}\langle q_{n+1}|\,\hat{U}(t)\,|q_0\rangle &= \langle q_{n+1}|\,e^{-it\hat{H}}\,|q_0\rangle \\ &= \langle q_{N+1}|\left[e^{-i\hbar\epsilon\hat{K}}e^{-i\hbar\epsilon\hat{V}}\right]^{n+1}|q_0\rangle \\ &= \langle q_{n+1}|\,e^{\frac{-i}{\hbar}\epsilon\hat{K}}e^{\frac{-i}{\hbar}\epsilon\hat{V}}...e^{\frac{-i}{\hbar}\epsilon\hat{K}}e^{\frac{-i}{\hbar}\epsilon\hat{V}}\,|q_0\rangle \ .\end{aligned} \tag{A.19}$$

Note that the last exponential may be rewritten as:

$$e^{\frac{-i}{\hbar}\epsilon\hat{V}}\,|q_0\rangle = e^{\frac{-i}{\hbar}\epsilon V(q_0)}\,|q_0\rangle \ . \tag{A.20}$$

In order to proceed, we will insert n completion relations[2] for q_n between each intermediate state:

$$\int_{-\infty}^{\infty} dq_n\,|q_n\rangle\,\langle q_n| = 1 \ . \tag{A.21}$$

Putting it on the last equation of (A.19):

$$\begin{aligned}\langle q_{n+1}|\hat{U}(t)|q_0\rangle = \int_{-\infty}^{\infty} dq_1...dq_n\,\langle q_{n+1}|\,e^{-\frac{i}{\hbar}\epsilon\hat{H}}\,|q_n\rangle \\ \times\,\langle q_n|\,e^{-i\frac{i}{\hbar}\epsilon\hat{H}}\,|q_{n-1}\rangle\,...\,\langle q_1|\,e^{-i\frac{i}{\hbar}\epsilon\hat{H}}\,|q_0\rangle \ .\end{aligned} \tag{A.22}$$

[2] the quantity is n since we have n+1 terms and we are inserting just on the intermediate states.

Each term is a matrix element for the operator $\exp\big(-\frac{i}{\hbar}\epsilon\hat{H}\big)$, so let's proceed by considering a generic term of the form:

$$\langle q_j|e^{-\frac{i}{\hbar}\epsilon\hat{H}}|q_i\rangle = \langle q_j|e^{-\frac{i}{\hbar}\epsilon\left(\frac{\hat{p}^2}{2m}+V(\hat{q})\right)}|q_i\rangle \ , \tag{A.23}$$

in which j and i are general positions between q_{n+1} and q_0 and $j > i$.

From now on, we will take $\hbar = 1$. Using the fact that $\hat{V}$ is diagonal in position space we can write:

$$\langle q_j|e^{-\frac{i\epsilon\hat{V}}{2}}e^{\frac{-i\epsilon\hat{p}^2}{2m}}e^{-\frac{i\epsilon\hat{V}}{2}}|q_i\rangle = e^{\frac{-i\epsilon\left(V(\hat{q}_j)+V(\hat{q}_i)\right)}{2}}\langle q_j|e^{\frac{-i\epsilon\hat{p}^2}{2m}}|q_i\rangle \ . \tag{A.24}$$

In order to evaluate the matrix element we must go to the momentum space in which we introduce a complete set of momentum states $\mathbb{1} = \int dp\,|p\rangle\langle p|$ obtaining the following object:

$$\langle q_j|e^{\frac{-i\epsilon\hat{p}^2}{2m}}|q_i\rangle = \int dp\,\langle q_j|e^{\frac{-i\epsilon\hat{p}^2}{2m}}|p\rangle\langle p|q_i\rangle \tag{A.25}$$

The inner product between p and q is given by [82]:

$$\langle p|q\rangle = \int \frac{1}{\sqrt{2\pi\hbar}}e^{\frac{-ipx}{\hbar}} = \langle q|p\rangle^* \tag{A.26}$$

So, after using that $\hat{p}\,|p\rangle = p\,|p\rangle$ together with the equation above, we can write:

$$\begin{aligned}\langle q_j|e^{\frac{-i\epsilon\hat{p}^2}{2m}}|q_i\rangle &= \int dp e^{\frac{-i\epsilon p^2}{2m}}\langle q_j|p\rangle\langle p|q_i\rangle \\ &= \int dp e^{\frac{-i\epsilon p^2}{2m}}\frac{1}{\sqrt{2\pi}}e^{ipq_j}\frac{1}{\sqrt{2\pi}}e^{-ipq_i} \\ &= \int dp\frac{1}{2\pi}e^{\frac{-i\epsilon p^2}{2m}}e^{ip(q_j-q_i)} \ .\end{aligned} \tag{A.27}$$

This is a Gaussian Integral given by:

$$\int dp\frac{1}{2\pi}e^{\frac{-i\epsilon p^2}{2m}}e^{ip(q_j-q_i)} = \frac{1}{2\pi}\sqrt{\frac{2m\pi}{i\epsilon}}\exp\left(\frac{im}{2\epsilon}(q_j-q_i)^2\right) \ , \tag{A.28}$$

hence the following matrix element is:

$$\langle q_j|e^{\frac{-i\epsilon\hat{p}^2}{2m}}|q_i\rangle = \frac{1}{2\pi}\sqrt{\frac{2m\pi}{i\epsilon}}\exp\left(\frac{im}{2\epsilon}(q_j-q_i)^2\right) \ , \tag{A.29}$$

leading to:

$$\begin{aligned}\langle q_j|e^{-\frac{i\epsilon\hat{V}}{2}}e^{\frac{-i\epsilon\hat{p}^2}{2m}}e^{-\frac{i\epsilon\hat{V}}{2}}|q_i\rangle &= e^{\frac{-ia(V(\hat{q_j})+V(\hat{q_i}))}{2}}e^{\frac{im}{2\epsilon}(q_j-q_i)^2}\langle q_j|e^{\frac{-i\epsilon\hat{p}^2}{2m}}|q_i\rangle \\ &= e^{\left(\frac{-i\epsilon(V(\hat{q_j})+V(\hat{q_i}))}{2}\right)}e^{\frac{im}{2\epsilon}(q_j-q_i)^2}\frac{1}{2\pi}\sqrt{\frac{2m\pi}{ia}}\ . \end{aligned} \tag{A.30}$$

Inserting the result above on each term of (A.19) we obtain the following expression:

$$\begin{aligned}\langle q_{n+1}|\hat{U}(t)|q_0\rangle &= \int_{-\infty}^{\infty}dq_{n-1}dq_{n-2}...dq_1\,\langle q_{n+1}|e^{-ia\hat{H}}\,|q_n\rangle\,...\,\langle q_1|\,e^{-ia\hat{H}}|q_0\rangle \\ &= \left(\frac{m}{2\pi i\epsilon}\right)^{\frac{n}{2}}\int_{-\infty}^{\infty}dq_{n-1}...dq_1 \\ &\times e^{\frac{-i\epsilon}{2m}\left[(q_{n+1}-q_n)^2+..+(q_{1-q})^2\right]-\epsilon\left[\frac{1}{2}V(q_{n+1})+..+\frac{1}{2}V(q)\right]}\ . \end{aligned} \tag{A.31}$$

Now we must analyze each term inside of the exponential in order to rewrite them in a more familiar way. First of all, note that for a generic pair $(q_j-q_i)^2$ we can write:

$$\begin{aligned}\frac{m}{2\epsilon}(q_j-q_i)^2 =& \frac{am}{2}\left(\frac{q_j-q_i}{\epsilon}\right)^2 \\ =& \lim_{\epsilon\to 0}\left(\frac{q_j-q_i}{a}\right) \\ =& \dot{q_i}(t_i)\ , \end{aligned} \tag{A.32}$$

in which we have used the fact that we are considering ϵ as infinitesimal and the definition of the derivative. So, for each term of the form $(q'-q_{n-1})^2+...+(q_1-q)^2$ we can rewrite as:

$$\frac{m}{2\epsilon}(q_j-q_i)^2 = \frac{m}{2}\left[\dot{q_{n-1}}^2+...+\dot{q_1}^2+\dot{q}^2\right]\ . \tag{A.33}$$

Taking the continuous limit for ϵ and recovering the fact that $\epsilon=\Delta t$ we obtain that:

$$\frac{m}{2\epsilon}(q_j-q_i)^2 = \int_{t'}^{t}dt"\frac{m}{2}(\dot{q"}_t^2)\ . \tag{A.34}$$

Note that the integrand function is in the form of kinetical energy. We will return to this fact later. Now let's devote our attention to the potential term rewriting it as:

$$\begin{aligned}\frac{1}{2}(V(q_{n+1})+...+V(q)) &= \frac{1}{2}V(q')+V(q_{n-1})+...+V(q_2)+V(q_1)+\frac{1}{2}V(q) \\ &= \frac{1}{2}(V(q')+V(q_{n-1}))+\frac{1}{2}(V(q_{n-1})+V(q_{n-2}))+\frac{1}{2}(V(q_1)+V(q))\ . \end{aligned} \tag{A.35}$$

Considering a generic pair of the form $\frac{1}{2}(V(q_j) + V(q_i))$ we will show that we can write:

$$\frac{1}{2}(V(q_j) + V(q_i)) = V(\bar{q}_i + \mathcal{O}(\epsilon^2)) \,, \tag{A.36}$$

in which $\bar{q}_i = \frac{1}{2}(q_j + q_i)$. Initially, we expand $V(q_j)$ in a Taylor Series around $\bar{q}_i$:

$$V(q_j) \approx \sum_{n=0}^{\infty} \frac{V^n \bar{q}_i}{n!}(q_j - \bar{q}_i)^n = V(\bar{q}_i) + V'(\bar{q}_i)(q_j - \bar{q}_i) + \frac{V''(\bar{q}_i)}{2}\frac{(q_j - \bar{q}_i)^2}{2} + \dots \,. \tag{A.37}$$

Doing the same for $V(q_i)$:

$$V(q_i) \approx \sum_{n=0}^{\infty} \frac{V^n \bar{q}_i}{n!}(q_i - \bar{q}_i)^n = V(\bar{q}_i) + V'(\bar{q}_i)(q_i - \bar{q}_i) + \frac{V''(\bar{q}_i)}{2}\frac{(q_i - \bar{q}_i)^2}{2} + \dots \,. \tag{A.38}$$

Note that we can write $q(t_j) = q(t_i + \epsilon) \approx q(t_i) + a\dot{q}(t_i) = q(t_i) + \mathcal{O}(\epsilon)$. Each term $(q_j - q_i)$ and $(q_i - \bar{q}_i)$ behaves as:

$$\begin{aligned} q_j - \bar{q}_i &= \frac{1}{2}(q_i - q_i + \mathcal{O}(\epsilon)) \approx \mathcal{O}(\epsilon) \\ q_i - \bar{q}_i &= \frac{1}{2}(q_i - q_i - \mathcal{O}(\epsilon)) \approx -\mathcal{O}(\epsilon) \,, \end{aligned} \tag{A.39}$$

hence, from the potential expansion:

$$\begin{aligned} \frac{1}{2}\big(V(q_j) + V_{q_i}\big) &= \frac{1}{2}2V(\bar{q}_i) + \mathcal{O}(\epsilon^2) \\ &= V(\bar{q}_i) + \mathcal{O}(\epsilon^2) \,. \end{aligned} \tag{A.40}$$

This allows us to replace each term in the potential expression as:

$$\frac{1}{2}(V(q_j) + V(q_i)) = V(\bar{q}_i + \mathcal{O}(\epsilon^2)) = \epsilon[V(q_{n-1}^{-}) + \dots + V(\bar{q}_2) + V(\bar{q}_1) + V(\bar{q}_0)] \tag{A.41}$$

And after taking the continuous limit for $\epsilon = \Delta t$:

$$\frac{1}{2}(V(q_j) + V(q_i)) = \int_t^{t'} dt'' V(q(t'')) \,. \tag{A.42}$$

Finally, we can put it all together:

$$U(q',q;t'-t)=\frac{m}{2\pi i\epsilon}^{\frac{n}{2}}\int_{-\infty}^{\infty}dq_{n-1}...dq_1\exp\left(\int_t^{t'}dt''\big(\frac{m\dot{q}^2}{2}-V(q)\big)\right). \tag{A.43}$$

Let's clean a little bit more the expression above. First of all, we define:

$$\begin{aligned}\mathcal{D}_q=&\lim_{n\to\infty;\epsilon\to 0}\frac{m}{2\pi i\epsilon}^{\frac{n}{2}}\int_{-\infty}^{\infty}dq_{n-1}...dq_1\\ =&\big(\frac{m}{2\pi i\epsilon}\big)^{\frac{n}{2}}\prod_{i=1}^{n-1}dq_i\ .\end{aligned} \tag{A.44}$$

In which we have taken a sum over all broken line paths from q' to q knowing that every continuous path can be approximated by a broken line if and only if $\epsilon\to 0$.

Finally, note that we can identify $S=\int_t^{t'}dt''(\frac{m\dot{q}^2}{2}-V(q))$ as the action, in order to write:

$$U(q',q;t'-t)=\int_{-\infty}^{\infty}\mathcal{D}_q e^{iS[q]} \tag{A.45}$$

This is the path integral in Quantum Mechanics for a Hamiltonian in 1D. We have expressed it in terms of the propagator, which we have defined before as the probability amplitude of finding the system at (q',t') since it was at (q,t) as a weighted sum of all possible paths from q to q'.

Appendix B

Partially Conserved Axial Current

The PCAC hypothesis states that the axial current is not completely conserved but is instead partially conserved. This hypothesis leads to the Goldberger–Treiman relation [34], which provides strong evidence for the underlying principles of chiral symmetry in QCD. For this appendix, we will closely follow the reference [18].

The axial current carried by a pion is given by [18]:

$$A^a_\mu = f_{\boldsymbol{\pi}} \partial_\mu \boldsymbol{\pi}^a(x) \ , \tag{B.1}$$

in which $\pi^a(x)$ is the pion field and $f_\pi = 93$ MeV is the pion decay constant, which plays a crucial role in many areas of low energy particle physics being an energy scale which determines the strength of the chiral symmetry breaking. Its value may be deduced from experimental data [83].

Considering the already derived axial current of a nucleon:

$$A^a_\mu = g_a \bar{\psi_N} \gamma_\mu \gamma_5 \frac{\boldsymbol{\tau}^a}{2} \psi_N \ , \tag{B.2}$$

in which ψ_N=(proton,neutron) is an iso-spinor representing protons and neutrons. The term $g_a = 1.25$ is due to the fact that the axial current of the nucleon is renormalized by 25%[18]. Since the nucleon has a large mass, one may not expect that its axial current is not conserved, which is the case indeed. By using the free Dirac equation for nucleons[1] one obtain that:

$$\partial^\mu A^a_\mu = g_a \bar{\psi_N} \partial^\mu \gamma_\mu \gamma_5 \frac{\boldsymbol{\tau}^a}{2} \psi_N = i g_a \bar{\psi_N} M_N \gamma_5 \frac{\boldsymbol{\tau}^a}{2} \psi_N = i g_a M_N \bar{\psi_N} \gamma_5 \frac{\boldsymbol{\tau}^a}{2} \psi_N \neq 0 \ . \tag{B.3}$$

This expression is zero only in the case of vanishing nucleon mass. However, the nucleon strongly interacts with the $\boldsymbol{\pi}$. Hence, let's assume that the total axial current is the sum of the nucleon plus the $\boldsymbol{\pi}$ contribution [18]. Using the PCAC relation

[1] $\bar{\psi_N}(i\gamma^\mu \partial_\mu - M_N)\psi_N = 0$

(B.1) and equation (B.2) we obtain:

$$A^a_\mu = f_{\boldsymbol{\pi}} \partial_\mu \boldsymbol{\pi}^a(x) + g_a \bar{\psi_N} \gamma_\mu \gamma_5 \frac{\boldsymbol{\tau}^a}{2} \psi_N \ . \tag{B.4}$$

If we require that the total current is conserved , $\partial^\mu A_\mu = 0$ we obtain:

$$\partial^\mu A^a_\mu = \partial^\mu f_\pi \partial_\mu \Psi^a(x) + \partial^\mu g_a \bar{\psi_N} \gamma_\mu \gamma_5 \frac{\boldsymbol{\tau}^a}{2} \psi_N = i g_a \bar{\psi_N} M \gamma_5 \frac{\boldsymbol{\tau}}{2} \psi_N + f_\pi \partial^\mu \partial_\mu \Psi^a = 0 \ , \tag{B.5}$$

which leads to:

$$\partial^\mu \partial_\mu \boldsymbol{\pi}^a = -\frac{i g_a M_N}{f_\pi} \bar{\psi_N} \gamma_5 \frac{\boldsymbol{\tau}}{2} \psi_N \ , \tag{B.6}$$

in which we have used (B.2). If one recalls the Klein-Gordon wave equation in natural units:

$$\frac{\partial \psi^2}{\partial^2 t} = (\nabla^2 - m^2)\psi \ , \tag{B.7}$$

and by setting $m = 0$ we see that (B.6) is the Klein-Gordon equation for a massless pion coupled to the nucleon. Thus, requiring the conservation of the total axial current leads us to the prediction that $\boldsymbol{\pi}$ should be massless. Now, if we allow a finite $\boldsymbol{\pi}$ mass, then we obtain a Klein-Gordon equation with a massive term:

$$(\partial^\mu \partial_\mu + m^2_{\boldsymbol{\pi}})\psi = -g_a i \frac{M_N}{f_\pi} \bar{\psi}_N \gamma_5 \boldsymbol{\tau} \psi_N \ . \tag{B.8}$$

With the pion-nucleon constant given by:

$$g_{\boldsymbol{\pi}NN} = g_a \frac{M_N}{f_\pi} \approx 12.6 \ . \tag{B.9}$$

This is the Goldberger-Treiman relation [34]. From pion-nucleon scattering experiments, one obtains the coupling value:

$$g^{exp}_{\boldsymbol{\pi}NN} = 13.4 \ . \tag{B.10}$$

This is in close agreement with the theoretical result (*B.9*) considering that (B.9) contains quantities extracted from the weak interaction, g_a and f_π. This close agreement is the result of an underlying approximate symmetry: chiral symmetry.

Bibliography

[1] D. Grasso and H.R. Rubinstein. **Magnetic Fields in the Early Universe**. *Physics Reports*, 348(3):163–266, 2001.

[2] J. Rafelski and B. Müller. **Magnetic Splitting of Quasimolecular Electronic States in Strong Fields**. *Physical Review Letters*, 36(10):517, 1976.

[3] D.E. Kharzeev, L.D. McLerran, and H.J. Warringa. **The Effects of Topological Charge Change in Heavy Ion Collisions:Event by Event P and CP Violation**. *Nuclear Physics A*, 803(3-4):227–253, 2008.

[4] V.V. Skokov, A. Yu Illarionov, and V.D. Toneev. **Estimate of the Magnetic Field Strength in Heavy-Ion Collisions**. *International Journal of Modern Physics A*, 24(31):5925–5932, 2009.

[5] I.A. Shovkovy. **Magnetic Catalysis: A Review**. *Strongly Interacting Matter in Magnetic Fields*, pages 13–49, 2013.

[6] K. Fukushima. **Views of the Chiral Magnetic Effect**. In *Strongly Interacting Matter in Magnetic Fields*, pages 241–259. Springer, 2013.

[7] Jens O. Andersen, William R. Naylor, and Anders Tranberg. **Phase diagram of QCD in a magnetic field: A review**. *Rev. Mod. Phys.*, 88:025001, 2016.

[8] D. Blaschke, K. Redlich, C. Sasaki, and L. Turko. ***Understanding the Origin of Matter: Perspectives in Quantum Chromodynamics***. Springer, 2022.

[9] A. Bzdak, V. Koch, and J. Liao. ***Charge-Dependent Correlations in Relativistic Heavy-Ion Collisions and the Chiral Magnetic Effect***. Springer, 2013.

[10] Y. Aoki, G. Endrodi, Z. Fodor, S.D. Katz, and K.K. Szabo. **The Order of the Quantum Chromodynamics Transition Predicted by the Standard Model of Particle Physics**. *Nature*, 443(7112):675–678, 2006.

[11] Frank Wilczek. ***The lightness of being: Mass, ether, and the unification of forces***. Basic Books, 2008.

[12] Craig D Roberts. **Empirical Consequences of Emergent Mass**. *Symmetry*, 12(9):1468, 2020.

[13] Kirill Tuchin. **Time and space dependence of the electromagnetic field in relativistic heavy-ion collisions**. *Phys. Rev. C*, 88(2):024911, 2013.

[14] Umut Gursoy, Dmitri Kharzeev, and Krishna Rajagopal. **Magnetohydrodynamics, charged currents and directed flow in heavy ion collisions**. *Phys. Rev. C*, 89(5):054905, 2014.

[15] Kirill Tuchin. **Initial value problem for magnetic fields in heavy ion collisions**. *Phys. Rev. C*, 93(1):014905, 2016.

[16] G. Krein and C. Miller. **Nonequilibrium Dynamics of the Chiral Quark Condensate under a Strong Magnetic Field**. *Symmetry*, 13(4):551, 2021.

[17] M. Gell-Mann and M. Lévy. **The Axial Vector Current in Beta Decay**. *Il Nuovo Cimento (1955-1965)*, 16(4):705–726, 1960.

[18] Volker Koch. **Introduction to chiral symmetry**. In *3rd TAPS Workshop on Electromagnetic and Mesonic Probes of Nuclear Matter*, 12 1995.

[19] Dirk H. Rischke. **Forming Disoriented Chiral Condensates Through Fluctuations**. *Phys. Rev. C*, 58:2331–2357, 1998.

[20] Z. Xu and C. Greiner. **Stochastic Treatment of Disoriented Chiral Condensates Within a Langevin Description**. *Physical Review D*, 62(3):036012, 2000.

[21] M. Nahrgang, S. Leupold, C. Herold, and M. Bleicher. **Nonequilibrium chiral fluid dynamics including dissipation and noise**. *Physical Review C*, 84(2):024912, 2011.

[22] R.L.S. Farias, N.C. Cassol-Seewald, G. Krein, and R.O. Ramos. **Nonequilibrium Dynamics of Quantum Fields**. *Nuclear Physics A*, 782(1-4):33–36, 2007.

[23] N. C. Cassol-Seewald, R. L. S. Farias, E. S. Fraga, G. Krein, and Rudnei O. Ramos. **Langevin Simulation of Scalar Fields: Additive and Multiplicative Noises and Lattice Renormalization**. *Physica A*, 391:4088–4099, 2012.

[24] P.C. Hohenberg and B.I. Halperin. **Theory of Dynamic Critical Phenomena**. *Reviews of Modern Physics*, 49(3):435, 1977.

[25] M. Arslandok, SA. Bass, AA. Baty, I. Bautista, C. Beattie, F. Becattini, R. Bellwied, Y. Berdnikov, A. Berdnikov, J. Bielcik, et al. **Hot QCD White Paper**. *arXiv preprint arXiv:2303.17254*, 2023.

[26] Franz Gross et al. **50 Years of Quantum Chromodynamics**. *Eur. Phys. J. C*, 83:1125, 2023.

[27] M.E. Peskin. ***Concepts of Elementary Particle Physics***, volume 26. Oxford University Press, 2019.

[28] F. Hanzel and A.D. Martin. **Quarks and Leptons: An introductory Course in Modern Particle Phyics**, 1984.

[29] G. Krein, A.W. Thomas, and K. Tsushima. **Nuclear-Bound Quarkonia and Heavy-Flavor Hadrons**. *Progress in Particle and Nuclear Physics*, 100:161–210, 2018.

[30] T. Appelquist and J. Carazzone. **Infrared Singularities and Massive Fields**. *Physical Review D*, 11(10):2856, 1975.

[31] A. Manohar and CT Sachrajda. **Quark Masses**. *Review of Particle Physics, J. Phys. G*, 37:075021, 2010.

[32] Rajan Gupta. **Introduction to lattice QCD: Course**. In *Les Houches Summer School in Theoretical Physics, Session 68: Probing the Standard Model of Particle Interactions*, pages 83–219, 7 1997.

[33] D. Naegels. **An Introduction to Goldstone Boson Physics and to the Coset Construction**. *arXiv preprint arXiv:2110.14504*, 2021.

[34] M. L. Goldberger and S. B. Treiman. Decay of the pi meson. *Phys. Rev.*, 110:1178–1184, 1958.

[35] K. Huang. ***Quantum Field Theory: From Operators to Path Integrals***. John Wiley & Sons, 2008.

[36] H. Leutwyler. **Symmetries of QCD**. *Nuclear Physics B-Proceedings Supplements*, 108:37–48, 2002.

[37] Craig McNeile. **Determination of Light and Strange Quark Condensates**. *PoS*, LATTICE2013:017, 2014.

[38] D. Tong. **Gauge Theory**. *Lecture notes, DAMTP Cambridge*, 10, 2018.

[39] M. Le Bellac, F. Mortessagne, and G.G. Batrouni. ***Equilibrium and Non-Equilibrium Statistical Thermodynamics***. Cambridge University Press, 2004.

[40] Jeff Greensite. ***An Introduction To The Confinement Problem***, volume 821. Springer, 2011.

[41] T. C. Chaikin, P. M.; Lubensky and T. A. Witten. ***Principles of Condensed Matter Physics***, volume 10. Cambridge University Press Cambridge, 1995.

[42] A.O. Pereira. **Transições de Fase Dinâmicas, Parâmetros de Ordem Conservados e não Conservados e a Transição de Desconfinamento na QCD.**, 2009.

[43] N. Goldenfeld. ***Lectures on Phase Transitions and the Renormalization Group***. CRC Press, 2018.

[44] Chandrodoy Chattopadhyay, Josh Ott, Thomas Schaefer, and Vladimir Skokov. **Dynamic scaling of order parameter fluctuations in model B**. *Phys. Rev. D*, 108(7):074004, 2023.

[45] M. Nahrgang. ***Nonequilibrium Phase Transitions in Chiral Fluid Dynamics Including Dissipation and Fluctuation***. PhD thesis, Frankfurt am Main, Johann Wolfgang Goethe-Univ., Diss., 2011, 2011.

[46] E.A. Calzetta and Bei-Lok B. Hu. ***Nonequilibrium Quantum Field Theory***. Cambridge University Press, 2009.

[47] M. Le Bellac. ***Thermal Field Theory***. Cambridge University Press, 2000.

[48] J.S. Schwinger. **Brownian Motion of a Quantum Oscillator**. *J. Math. Phys.*, 2:407–432, 1961.

[49] L. V. Keldysh. **Diagram Technique for Nonequilibrium Processes**. *Zh. Eksp. Teor. Fiz.*, 47:1515–1527, 1964.

[50] A. Zee. ***Quantum Field Theory In A Nutshell***, volume 7. Princeton university press, 2010.

[51] A. Das. ***Finite Temperature Field Theory***. World scientific, 1997.

[52] M. Le Bellac and G. Barton. ***Quantum and Statistical Field Theory***. Oxford University Press, 1992.

[53] T.S. Biro and C. Greiner. **Dissipation and Fluctuation at the Chiral Phase Transition**. *Physical review letters*, 79(17):3138, 1997.

[54] C. Greiner, Z. Xu, and T. S. Biro. **Stochastic disoriented chiral condensates**. In *Institute for Nuclear Theory Spring Program on Probes of Dense Matter in Ultrarelativistic Heavy Ion Collisions*, 3 1998.

[55] A. Onuki. ***Phase Transition Dynamics***. Cambridge University Press, 2002.

[56] Marcelo Gleiser and Rudnei O. Ramos. **Microphysical Approach to Nonequilibrium Dynamics of Quantum Fields**. *Phys. Rev. D*, 50:2441–2455, 1994.

[57] N.C. Cassol-Seewald, M.I.M. Copetti, and G. Krein. **Numerical Approximation of the Ginzburg-Landau Equation with Memory Effects in the Dynamics of Phase Transitions**. *Computer Physics Communications*, 179(5):297–309, 2008.

[58] A. Singh, S. Puri, and H. Mishra. **Domain Growth in Chiral Phase Transitions**. *Nuclear Physics A*, 864(1):176–202, 2011.

[59] N. Cassol-Seewald, R.L.S. Farias, G. Krein, and R.S. Marques De Carvalho. **Noise And Ultraviolet Divergences In Simulations Of Ginzburg-Landau-Langevin Type Of Equations**. *International Journal of Modern Physics C*, 23(08):1240016, 2012.

[60] J.O. Andersen and R. Khan. **Chiral Transition in a Magnetic Field and at Finite Baryon Density**. *Physical Review D*, 85(6):065026, 2012.

[61] A. Ayala, L. A. Hernández, A. J. Mizher, J.C. Rojas, and C. Villavicencio. **Chiral Transition with Magnetic Fields**. *Physical Review D*, 89(11):116017, 2014.

[62] E.S. Fraga and A.J. Mizher. **Chiral Transition in a Strong Magnetic Background**. *Physical Review D*, 78(2):025016, 2008.

[63] G. Krein. **Noise and Ultraviolet Divergences in the Dynamics of the Chiral Condensate in QCD**. In *Journal of Physics: Conference Series*, volume 378, page 012032. IOP Publishing, 2012.

[64] M. Nahrgang, S. Leupold, and M. Bleicher. **Equilibration and Relaxation Times at the Chiral Phase Transition Including Reheating**. *Physics Letters B*, 711(1):109–116, 2012.

[65] C. Greiner and B. Müller. **Classical Fields Near Thermal Equilibrium**. *Physical Review D*, 55(2):1026, 1997.

[66] M. I. Abdulhamid et al. **Observation of the electromagnetic field effect via charge-dependent directed flow in heavy-ion collisions at the Relativistic Heavy Ion Collider**. *Phys. Rev. X*, 14(1):011028, 2024.

[67] Rajeev S. Bhalerao. **Relativistic heavy-ion collisions**. In *1st Asia-Europe-Pacific School of High-Energy Physics*, pages 219–239, 2014.

[68] H. Song. **Hydrodynamic Modeling and the QGP Shear Viscosity**. *The European Physical Journal A*, 48:1–10, 2012.

[69] A. Angles-Castillo, M.C. Bañuls, A. Perez, and I. De Vega. **Prethermalization of Quantum Systems Interacting with Non-Equilibrium Environments**. *New Journal of Physics*, 22(8):083067, 2020.

[70] F. Gelis, E. Iancu, J. Jalilian-Marian, and R. Venugopalan. **The Color Glass Condensate**. *Annual Review of Nuclear and Particle Science*, 60:463–489, 2010.

[71] M.L. Mangano. **Introduction to QCD**. *High Energy Physics And Cosmology 1998-Proceedings Of The Summer School*, 15:84, 1999.

[72] M. A. Stephanov. **QCD phase diagram: An Overview**. *PoS*, LAT2006:024, 2006.

[73] C.E. DeTar and U.M. Heller. **QCD Thermodynamics from the Lattice**. *The European Physical Journal A*, 41:405–437, 2009.

[74] K. Fukushima and T. Hatsuda. **The phase diagram of dense QCD**. *Reports on Progress in Physics*, 74(1):014001, 2010.

[75] F.; Ejiri, S.; Karsch and K. Redlich. **Hadronic Fluctuations At The QCD Phase Transition**. *Physics Letters B*, 633(2-3):275–282, 2006.

[76] V. Voronyuk, V.D. Toneev, W. Cassing, E.L. Bratkovskaya, V.P. Konchakovski, and S.A. Voloshin. **Electromagnetic Field Evolution in Relativistic Heavy-Ion Collisions**. *Physical Review C*, 83(5):054911, 2011.

[77] A. Bzdak and V. Skokov. **Event-by-event fluctuations of magnetic and electric fields in heavy ion collisions**. *Physics Letters B*, 710(1):171–174, 2012.

[78] D. Kharzeev, K. Landsteiner, A. Schmitt, and H-U. Yee. ***Strongly Interacting Matter in Magnetic Fields***, volume 871. Springer, 2014.

[79] E.S. Fraga and G. Krein. **Can Dissipation Prevent Explosive Decomposition in High-Energy Heavy Ion Collisions?** *Physics Letters B*, 614(3-4):181–186, 2005.

[80] J. Rafelski and J. Letessier. **Sudden Hadronization in Relativistic Nuclear Collisions**. *Physical review letters*, 85(22):4695, 2000.

[81] Adrian Dumitru and Robert D. Pisarski. **Explosive collisions at RHIC?** *Nucl. Phys. A*, 698:444–447, 2002.

[82] J.J. Sakurai and E.D. Commins. ***Modern Quantum Mechanics, Revised Edition***. American Association of Physics Teachers, 1995.

[83] N.X. Nguyen and T.T. Vu. **Two Modes of the Pion Decay in Weak Interaction**. *VNU Journal of Science: Mathematics-Physics*, 2024.